CORA Cork Open Research Archive
Cartlann Taighde Oscailte Chorcaí

Title	Energy harvesting wireless sensor network edge device simulation tool
Authors	O'Shea, Cian
Publication date	2021
Original Citation	O'Shea, C. 2021. Energy harvesting wireless sensor network edge device simulation tool. MRes Thesis, University College Cork.
Type of publication	Masters thesis (Research)
Rights	© 2021, Cian O'Shea. - https://creativecommons.org/licenses/by-nc-nd/4.0/
Download date	2026-11-01 20:38:23
Item downloaded from	https://hdl.handle.net/10468/11308



UCC
University College Cork, Ireland
Coláiste na hOllscoile Corcaigh

Ollscoil na hÉireann

"Energy Harvesting Wireless Sensor Network Edge Device Simulation Tool"

Thesis presented by:

Cian O'Shea

For the degree of

Masters of Engineering

Supervisors: Mike Hayes, Peter Haigh

Head of Department: Dr. Jorge Oliveira





Tyndall National Institute,

University College Cork

2021

Abstract

Wireless Sensor Networks (WSN) are Internet of Things (IoT) edge devices. They are becoming widely adopted in many industries including health care, building energy management and conditional monitoring. As the scale of WSN deployments increases, the cost and complexity of battery replacement and disposal become more significant and in time may become a barrier to adoption. Harvesting ambient energies provides a pathway to reducing dependence on batteries and in the future may lead to autonomously powered sensors. This work describes a simulation tool that enables the user to predict the battery life of a wireless sensor that utilizes energy harvesting to supplement the battery power. To create this simulator, all aspects of a typical WSN edge device were modelled including, sensors, transceiver and microcontroller as well as the energy source components (batteries, photovoltaic cells, thermoelectric generators (TEG), supercapacitors and DC/DC converters). The tool allows the user to plug and play different pre characterized devices as well as add user defined devices. The goal of this simulation tool is to predict the battery lifetime of a device and determine the scope for extension using ambient energy sources.

This work was part of a larger EU multi-partner project titled “Residential Retrofit assessment platform and demonstrations for near zero energy and CO_2 emissions with optimum cost, health, comfort and environmental quality” (ReCO2ST). The ReCO2ST project has received funding from the European Union’s “Horizon 2020” research and innovation programme under the grant agreement No. 768576.

Acknowledgments

I would first like to thank Mike Hayes, Senior Program Manager, and Peter Haigh, Principal Engineer at Tyndall National Institute for their effort, time and patience these last two years coaching me along my Masters.

They were always available whenever I had a bit of trouble or a question about my research or writing. I am grateful for the opportunity and their guidance that helped me throughout my time of research and writing of this thesis. I would also like to thank John Buckley for his insight and structural inputs while writing this thesis.

Furthermore, I would like to thank Ross O'Halloran for his help and support while conducting my research. His assistance throughout the testing phase of this research was invaluable.

Finally, I must express my very profound gratitude to my parents, John and Carol, and my siblings, Kyle and Sydney, for providing me with continuous support and encouragement throughout my years of study. This accomplishment would not have been possible without them.

Declaration

I hereby declare that, except where otherwise indicated, this document is entirely my own work and has not been submitted in whole or in part to any other university.

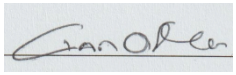
Signed:  Date: 30/04/21

Table of Contents

Abstract i
Acknowledgments ii
Declaration iii
List of Figures vii
List of Tables ix
Abbreviations x
1 Introduction 1
1.1 Project Motivation: 1
1.2 Energy Harvesting: 3
1.2.1 PV: 4
1.2.2 TEG: 5
1.3 Energy Storage Unit: 6
1.4 Power Management: 7
1.5 Project aims and objectives: 8
1.6 Report Structure: 8
2 Literature Review 10
2.1 Introduction: 10
2.2 Wireless Sensor Network: 10
2.3 Energy Harvesting Unit: 12
2.3.1 PV Cell: 12
2.3.1.1 Perturb & Observe: 14
2.3.1.2 Fractional Open-Circuit Voltage: 16
2.3.2 Thermoelectric Generator: 18
2.3.2.1 Step-up Converter: 20
2.3.2.2 Maximum Power Point Tracker for TEGs: 23
2.4 Energy Storage Unit: 26
2.4.1 Supercapacitor: 26
2.4.1.1 Charge / Discharge: 28
2.4.2 Batteries: 30
2.4.3 Batteries vs Supercapacitor: 31

2.5 Ultra-Low Powered DC-DC Converters: 33
2.6 Simulators: 34
2.7 Literature Review Conclusion: 36
3 System Architecture 38
3.1 Introduction 38
3.2 Data Structure 39
3.3 PV Cell 40
3.3.1 Introduction 40
3.3.2 Characterization 40
3.3.2.1 Test Setup 40
3.3.2.2 SLMD600H10L 41
3.3.2.3 AM-1801CA 44
3.4 TEG 47
3.4.1 Introduction 47
3.4.2 Characterization 47
3.4.2.1 Test Setup 47
3.4.2.2 TG12-4-01LS 49
3.4.2.3 MCPE1-12706AC-S 52
3.4.2.4 MPPT for TEG 53
3.5 Energy Storage Unit 55
3.5.1 Introduction 55
3.5.2 Characterization 55
3.5.2.1 Equivalent Series Resistance 55
3.5.2.2 Leakage Current 57
3.5.2.3 Charge 57
3.5.2.4 Batteries 59
3.6 Power Management 61
3.6.1 Introduction 61
3.6.2 DC-DC Converter 61
3.7 Sensor 66
3.7.1 Introduction 66
3.7.2 Characterization 66
3.8 Summary 68

4 Measurement vs. Simulation 69
4.1 Introduction 69
4.2 Comparison 69
4.3 Governing Energy Equation 73
4.4 Results 76
5 Conclusions & Future Work 79
Appendix 81
References 91

List of Figures

Figure 1: Energy Harvesting WSN 4
Figure 2: Photovoltaic Cell 5
Figure 3: TEG 6
Figure 4: Report Structure 9
Figure 5: WSN 11
Figure 6: PV Cell I-V Curve & P-V Curve 12
Figure 7: PV Cell Test Setup 13
Figure 8: Change of Output Power for different light levels 14
Figure 9: P&O Algorithm 15
Figure 10: FOCV Algorithm 17
Figure 11: Seebeck Effect 19
Figure 12: TEG WSN 20
Figure 13: Boost Converter Diagram 20
Figure 14: Stage 1 of Gruber boost converter 21
Figure 15: Stage 2 Gruber boost converter 22
Figure 16: Analog Devices LTC3108 schematic 23
Figure 17: TEG I-V Curve & P-V Curve 24
Figure 18: Buck-Boost converter schematic 25
Figure 19: Capacitor diagram 27
Figure 20: Capacitor RC charging circuit 28
Figure 21: Capacitor charging voltage over time 29
Figure 22: Capacitor discharging voltage over time 30
Figure 23: Specific Energy & Specific Power of different energy storage devices 31
Figure 24: RoWBUsT GUI 36
Figure 25: ReCO2ST GUI 38
Figure 26: Circuit Setup 41
Figure 27: I-V & P-V Curve at 2000 Lux 42
Figure 28: IV Curves for different Lux values 43
Figure 29: MPP for different Lux values 44
Figure 30: I-V & P-V Curve at 2000 Lux 45
Figure 31: TEG Test Circuit 48
Figure 32: Lab Setup 49

Figure 33: I-V & P-V Curve for TG12-4-01LS *50*
Figure 34: IV Curve for varying temperature differences *51*
Figure 35: MPP for varying temperature differences *52*
Figure 36: TEG I-V & P-V Curve *53*
Figure 37: ESR effect or real-world test *56*
Figure 38: Charge Circuit *58*
Figure 39: Charge Comparison between Real-World and Simulation *59*
Figure 42: TPS63020 Block Diagram *62*
Figure 43: TPS63020 - Efficiency vs. Output Current *63*
Figure 44: TPS63020 Max Output Current vs. Input Voltage *64*
Figure 45: Full WSN *66*
Figure 46: LoPy4 Pycom Device *69*
Figure 47: Bluno V2.0 ..... *7070*
Figure 48: TPS63020evm-487 ..... *711*
Figure 49: Test Circuit *7171*
Figure 50: Lab Setup Circuit *722*
Figure 51: Circuit - Equation Block Diagram *722*
Figure 52: Efficiency vs Output Current *774*
Figure 53: Real-World vs. Simulation *777*
Figure 54: ReCO2ST GUI *81*
Figure 55: ReCO2ST GUI buttons *82*
Figure 56: Select Device Load *82*
Figure 57: Select Energy Harvesting Device *833*
Figure 58: Select Energy Harvesting Conditions *844*
Figure 59: Select Energy Storage Devices *855*
Figure 60: Select DC-DC Converter *866*
Figure 61: Dynamic Simulation Conditions *877*
Figure 62: Battery vs. EH Lifetime *877*
Figure 63: Using EH Indicator *888*
Figure 64: Using Battery Indicator *888*
Figure 65: Dynamic Simulation *899*
Figure 66: Simulation Results *9090*

List of Tables

Table 1: Internet of Things projection 2
Table 2: Comparison of different PV Cell types 18
Table 3: Comparison of different Energy Storage devices 32
Table 4: List of different WSN simulators 35
Table 5: Results from IV curve 42
Table 6: Data Template for SLMD600H10L 43
Table 7: Results from IV curve 45
Table 8: Results from IV curve 50
Table 9: Data Template for TG12-4-01LS 51
Table 10: Results from IV curve 53
Table 11: Data Template for PowerStor supercapacitor 57
Table 12: Battery Capacity 60
Table 13: Data Template for TPS63020 Efficiency 63
Table 14: Data Template for TPS63020 65
Table 15: Efficiency for different Input Voltages 744
Table 16: Input Power at different efficiencies 755
Table 17: Charge Time Comparison 777
Table 18: Discharge Time Comparison 788

Abbreviations

A	Amps
BEM	Building Energy Management
C	Capacitance
E	Energy
EH	Energy Harvesting
ESR	Equivalent Series Resistance
ESU	Energy Storage Unit
FOCV	Fractional Open-Circuit Voltage
GUI	Graphical User Interface
I	Current
$\mathbf{I_{MPP}}$	Maximum Power Point Current
IoT	Internet of Things
$\mathbf{I_{SC}}$	Short-Circuit Current
m	milli
MPPT	Maximum Power Point Tracking
$\boldsymbol{\eta}$	Efficiency
P	Power
PV	Photovoltaic
P&O	Perturb and Observe
RC	Resistor-Capacitor
TEG	Thermoelectric Generator
µ	micro
V	Voltage
$\mathbf{V_{MPP}}$	Maximum Power Point Voltage
WSN	Wireless Sensor Network
$\mathbf{V_{OC}}$	Open-Circuit Voltage

$\mathbf{V_{sc}}$	Supercapacitor Voltage
W	Watts

1 Introduction

1.1 Project Motivation:

With the ever increasing push to have a more energy efficient environment, commercial and residential buildings are now expected to meet better and higher standards of energy efficiency. The introduction of energy harvesting into building energy management (BEM) systems is seen as a necessary requirement in order to accomplish these goals. The Irish government recently passed legislation with a "Nearly Zero Energy Building" standard. This legislation mandates that all commercial buildings built after 31st December 2018 will require renewable energy sources to power at least 20% of the primary energy use. Under this regulation, all new residential buildings will also require a renewable energy ratio of 20% [1].

According to the United States Department of Energy and the European Commission, building energy consumption accounts for roughly 40% of total energy consumption across the U.S and Europe [2][3]. With the ability to harvest ambient energies, wireless sensor networks (WSNs) can be used to monitor lighting, temperature, carbon dioxide levels, humidity and airflow resulting in a more informed and energy efficient BEM.

WSNs are a series of dispersed nodes equipped with one or more sensors that can monitor the environment and communicate the sensor data. The accumulation of these devices is known as the "Internet of Things" (IoT).

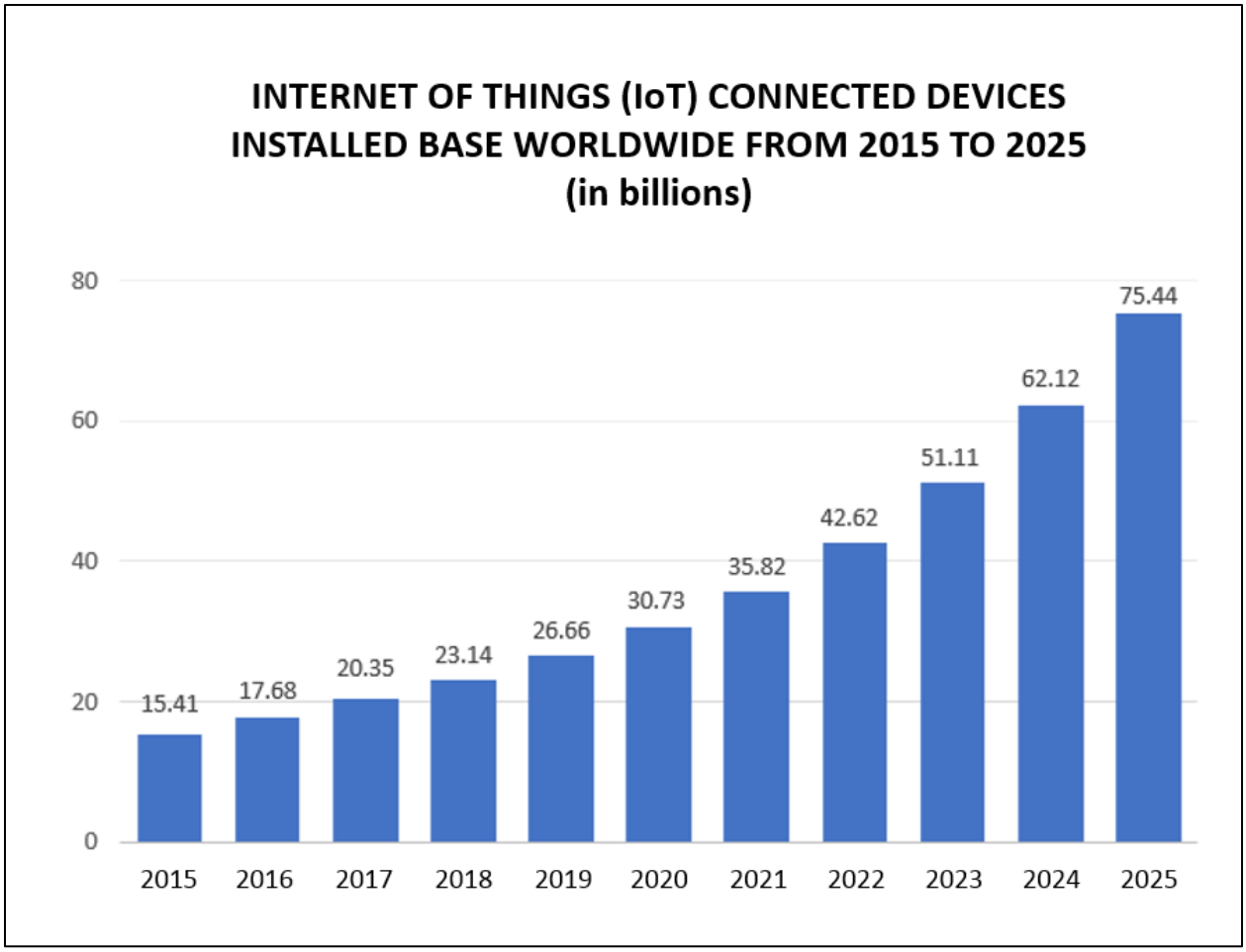


Table 1: Internet of Things projection [4]

IoT devices are growing at an exponential rate. According to a Statista report, by 2025, there will be over 75 billion IoT devices worldwide. One of the biggest challenges that IoT devices face is battery life. With so many devices globally, device battery replacement is already set to be a major impediment to scaling and ongoing reliable operation. According to the United States Environmental Protection Agency, roughly 90% of batteries are recycled [5]. By 2025, that already leaves 7.5 billion batteries filling landfills and polluting the earth with the number dramatically increasing thereafter. Combine this with the environmental cost of mining the material used and the monetary cost of producing so many batteries, it is clear that renewable energy will become an even more desirable form of technology. In addition to environmental costs, the maintenance cost of replacing each individual battery will encourage the adoption of renewable energy. The simulation tool presented in this thesis enables a non-expert user to select from a range of

different components to potentially extend the battery life of the IoT devices offering more cost effective, environmentally friendly and energy efficient solutions.

1.2 Energy Harvesting:

The ability to harvest energy from external sources can be dated back to a time where people used windmills and waterwheels. In modern times, electrical energy is the most dominant form of energy. Energy harvesting can be seen in everyday objects such as road signs and calculators. Having the ability to harvest ambient energy and then convert it to electrical energy efficiently, would not only prove to be beneficial to people who live in remote areas but would also have potential cost saving measures for large scale WSN deployments by not having to replace batteries multiple times throughout the sensors lifetime. Energy harvesting also helps the population as a whole, as moving to renewable energy sources positively impacts the environment.

Energy harvesting comprises collecting ambient energy from the environment and either converting it into device ready electrical energy or storing it. The environment has readily available ambient energy sources. Using such energy reduces the use of batteries or the need for mains electricity resulting in a more environmentally friendly system. Energy harvesting can be a very beneficial source of energy for WSNs. Depending on the type of device and its power requirements, small ambient energy sources have the capability of supplying power to low-power devices. However, even if the ambient energy cannot completely power the device, energy harvesting can still be used to extend battery life.

An energy harvesting circuit requires three main elements, energy harvesting transducers, energy storage devices and power management. The energy harvester converts the ambient energy into usable electrical energy. The energy storage device such as a battery or supercapacitor stores the collected energy. The power management efficiently controls the generation, storage and use of power and includes functions such as Maximum Power Point Trackers (MPPTs) and DC/DC converters. MPPTs ensure that the maximum possible power is

being transferred to the circuit from the EH transducer at any given time while the DC-DC converter converts a source of direct current from one voltage level to another. These components allow the EH devices to efficiently transfer power to the load or the storage device through impedance matching.

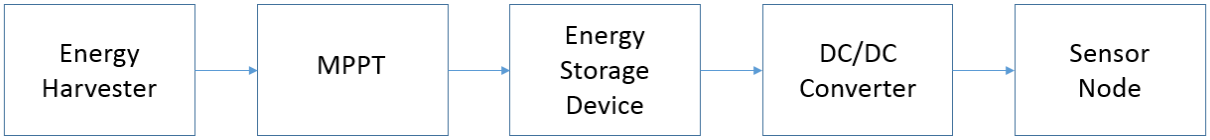


Figure 1: Energy Harvesting WSN

There are a number of different types of energy sources used in energy harvesting, such as vibration, light, thermal, kinetic and RF energy. The two types of energy harvesting components included in this tool are photovoltaic cells (PV) and thermoelectric generators (TEG). PV cells were selected as the obvious choice in an office environment to power wall mounted sensors. TEGs can be utilized to harvest waste energy from heaters, engines, furnaces, radiators, etc., or even exploit temperature gradients e.g. between a window and the ambient air.

1.2.1 PV:

The photovoltaic effect was first discovered in 1839. This effect occurs when light is absorbed by a material creating an electrical voltage. The first ever PV cell to use this effect operated with an energy conversion rate of 1-2%. Modern PV cells mostly use silicon to create this effect with an efficiency of ≈ 20%**.** However, some technologies can operate as efficiently as ≈ 45% [6]. With silicon based PV cells, two thin slices of silicon are put together. The slices are then "doped" (process in which other materials are added to the silicon in order to give it a positive or negative electrical charge). When light hits the PV cell, a photon knocks an electron free. These moving electrons can now be converted to usable electricity [7].



Figure 2: Photovoltaic Cell

[8]

Figure 2 shows a typical PV cell. PV cells are used for a whole range of different applications and sizes from commercial and residential buildings, to calculators and children's toys. Indoor light levels fluctuate considerably and cannot produce as much solar energy as outdoor light, therefore PV cells on their own are generally unable to power electric circuits reliably, and because of this, these circuits are often powered from a secondary battery or super-capacitor that is re-charged by the PV Cell.

1.2.2 TEG:

The Seebeck effect is a phenomenon in which a voltage difference is produced between two dissimilar conductors or semiconductor plates when at different temperatures. When heat is applied to one side of the TEG electrons flow more easily to the colder side resulting in electrical current flow. The output power of the device is a function of the size and temperature difference between the plates. Usually when TEGs are considered for energy harvesting, multiple parts are used in series. This is because a temperature gradient of 1 degree between the two plates creates only a few microvolts. This type of energy harvester is most useful on a physical heat source such as engines, heaters or the back of a large PV panel. Modern vehicle engines lose up to 65% [9] of their energy to heat. If TEGs are connected to the engine, some of that wasted energy could be

harvested and recycled. However, there are some challenges in trying to keep the cool side of the component cold. This can be done through the use of heat sinks. Heat sinks work by transferring the heat generated by the component to a fluid medium, often air or liquid coolant. The size dimensions of the heat sink are entirely dependent on the size of the component and the heat generated. Figure 3 shows a thermoelectric generator.

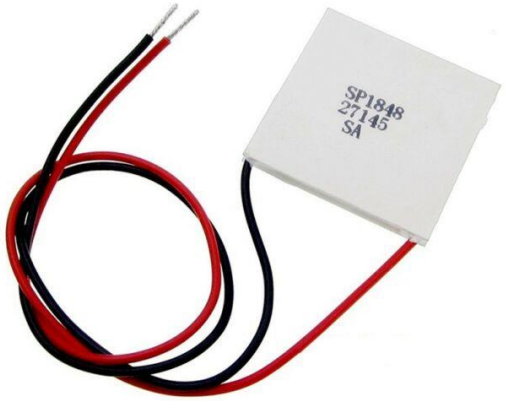


Figure 3: TEG [10]

1.3 Energy Storage Unit:

The energy storage devices most commonly used in energy harvesting systems are supercapacitors and rechargeable batteries. There are typically two types of batteries, primary and secondary. Secondary batteries can be recharged multiple times whilst primary batteries are single use storage devices. The main problems with rechargeable batteries is that they can be quite expensive, they have a limited number of charge/discharge cycles, have a higher leakage current and, if they are left idle for too long, the maximum charge available is reduced.

Capacitors consist of two conductors separated by an insulator which stores electrical energy. Supercapacitors are different to regular capacitors because supercapacitors do not use the conventional solid dielectric, instead, they use electrostatic double-layer capacitance or electrochemical pseudocapacitance. Another difference is that supercapacitors have larger

plates with a smaller distance between those plates. Supercapacitors have as much as 10x the power density of rechargeable batteries, however, their energy density is only around one tenth of comparable size rechargeable batteries [11]. Energy density is the amount of energy in a given volume whereas, power density is the amount of power in a given volume. These differences result in batteries being able to store more energy in the same amount of space, however, the supercapacitor can give off energy more quickly. This also allows the supercapacitor to recharge much quicker than a battery. This is why supercapacitors can be very beneficial when using EH devices to power a WSN.

Supercapacitors are much easier to charge than rechargeable batteries as they only require a charge current and over voltage protection as opposed to rechargeable batteries which requires constant-voltage and constant-current [12]. Because most energy harvesting WSNs use low-power energy harvesters, supercapacitors are an ideal storage device, however for long term devices, an additional primary battery is sometimes required due to leakage current in the supercapacitor over time and to assist with cold-start, re-starts, prolonged absence of ambient energies, etc. A more detailed discussion on energy storage devices is provided in table 3 in chapter 2.

1.4 Power Management:

Harvesting from these types of ambient energies is still difficult as each of these require an additional power conversion circuit to efficiently harvest, store and convert that energy into usable electrical energy. Power management is a key element in designing energy harvesting systems. In this thesis, the main focus will be on two types of power management, maximum power point tracking (MPPT) and DC/DC converters.

MPPT, as the name suggests, is a technique that dynamically adjusts the load impedance to ensure the device is operating at its maximum output power. There are a number of different MPPT algorithms, which will be discussed later. Some of these require a microcontroller to maintain tracking, for example “Perturb & Observe”, however these have the draw-back that the

microcontroller requires power thus reducing overall system efficiency. Other techniques such as “FOCV” (Fraction Open Circuit Voltage) are simpler to implement as they do not require complex algorithms running in a microcontroller. They do not track as accurately, but often prove to have the best system efficiency taking the microcontroller power consumption into account.

1.5 Project aims and objectives:

The software application discussed in this thesis is an energy harvesting simulation tool for applications using battery powered sensors. The main objective of this project is to create a piece of software that can accurately simulate a real-life WSN node that uses an energy harvesting system.

This software tool enables people to optimize energy harvested powered end nodes, by easily identifying the optimized selection of key system blocks (Power Management IC, Energy Storage, etc.) as a function of battery life. The user can determine if the available ambient energy can usefully extend battery life, without necessarily understanding the underlying complexities. In addition it can also be used by circuit designers to understand the impact of various power system blocks on overall battery life.

This tool will encourage the use of ambient energies, whether that is in applications that would greatly benefit from the reduction of batteries used or expanding what is possible in hard to reach areas such as medical implants.

1.6 Report Structure:

This thesis will first present a literature review of the current knowledge and findings regarding WSNs that utilize EH methods, Energy Harvesting Wireless Sensor Networks (EH-WSNs). Chapter 3 will discuss the system architecture of the simulation tool. It will also show the data templates and structure for gathering and characterizing components in a way that the software can easily read and process.

Each section in this chapter examines all of the different components that create an EH-WSN. It will encompass how each of the EH devices, ES devices, power management components and loads were tested, characterised and loaded onto the system.

Chapter 4 shows a comparison between a real-world test and software simulation, showing the accuracy of the tool and explaining the equations used to predict the lifetime of the device.

Chapter 5 then concludes the thesis by discussing the findings and proposing several possible directions for future work.

The overall layout structure of the thesis can be found in figure 4.

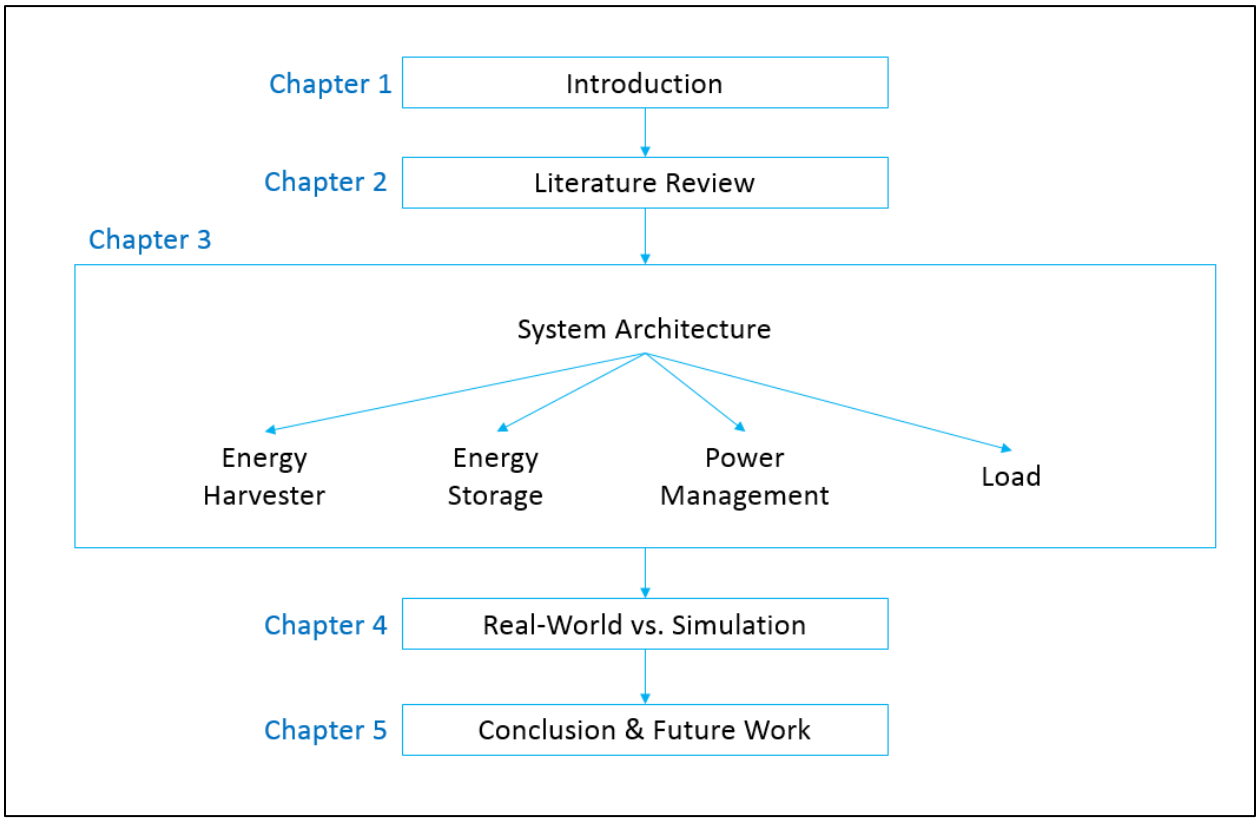


Figure 4: Report Structure

2 Literature Review

2.1 Introduction:

The main focus of this thesis is to create a simulation tool for energy harvesting wireless sensor networks. This work focuses on two of the main types of energy sources commonly used in wireless sensor networks, light and thermal energy.

This chapter will review the current scientific research of energy harvesting technologies, energy storage devices and wireless sensors networks and is divided in 6 sections. The first section will discuss the different types of sensors commonly associated with wireless sensor networks. The second section will present different types of energy harvesting technology and ways of extracting the maximum possible energy. The third section will layout the different types of energy storage. The fourth section will discuss the DC-DC converters used for power matching a WSN node circuit. The fifth section will present the different types of WSN simulators currently available and what they offer to users. The final section will draw conclusions from the information shown in this literature review chapter and illustrate the importance of this tool.

2.2 Wireless Sensor Network:

Wireless sensor networks (WSNs) consist of nodes that monitor and transmit data. Each node is wirelessly connected to a central device that collects and records the incoming data. WSNs typically monitor, but are not limited to, environmental conditions such as temperature, air, water quality, light and sound levels. WSNs can be versatile so the type of data depends on the application, and ranges from single byte temperature data at low duty cycles to video streaming.

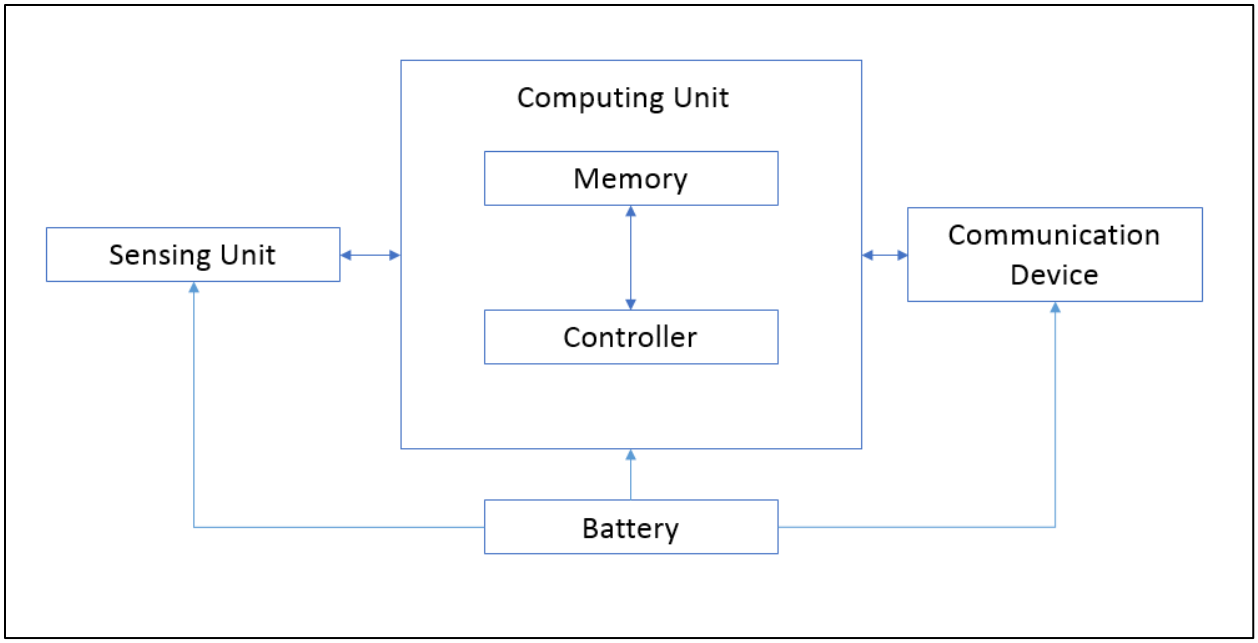


Figure 5: WSN [13]

Figure 5 shows a typical block diagram of a wireless sensor node. The "Sensing Unit" block contains the sensor (thermometer, lux meter, IR sensor, etc.) that transfers the sensor data to the microcontroller, which stores that data until it is ready to be transmitted to the main node. Each node in the network is powered by its own power source. In most cases it is a non-rechargeable battery.

WSNs have a wide range of applications. As discussed in the introduction, they can be valuable in building energy management systems [14], but they are also widely used in other areas such as body sensors for medical applications [15], tracking and localizations [16], aircraft monitoring [17], vehicle monitoring [18], agriculture [19], and generic sensor networks [20].

With the focus of this thesis encompassing EH, the power source block is the most important one. The number of nodes in a network can vary from a few to a few thousand. Having batteries in each of these nodes is costly and time consuming to replace.

In recent years there has been a major effort to enhance the capabilities of WSNs such as reducing the power required and creating more energy aware sensor nodes [21] [22] [23]. With the lifetime limitations that accompany the use of batteries, WSN deployments can now

introduce the use of energy harvesting to offset some of those problems. However, the introduction of energy harvesting into these systems introduces various design questions such as "what is the best energy harvesting technology to use?", "what type of energy storage is best suited?", "what is the best way to manage this harvested power?"

This literature review will discuss these questions and compare the results of this thesis with the current scientific research.

2.3 Energy Harvesting Unit:

With the growing number of WSNs in operation and growing desire for more power, WSNs need to look beyond batteries to extend their lifetime. In this section, two of the most popular methods of energy harvesting [24] will be presented along with the different methods of power management.

2.3.1 PV Cell:

A PV cell is a semiconductor device that converts solar energy into electrical energy. When photons collide with the atoms in the material, they transfer their energy to the loose electrons in the PV cell creating electrical current. The electrical output properties can be characterized by an I-V curve [25].

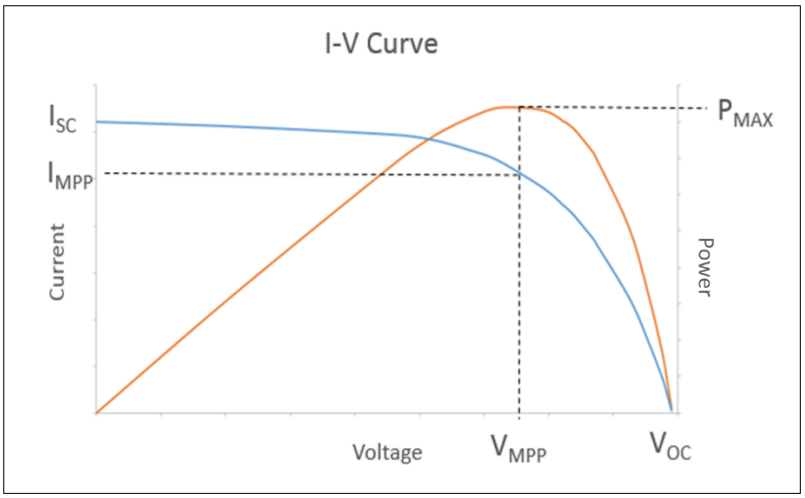


Figure 6: PV Cell I-V Curve & P-V Curve

The I-V curve shown in figure 6 is a graphical representation of the relationship between the current sourced by the photovoltaic cell and the voltage produced. In order to acquire this graph, the open-circuit voltage (Voc) and the short-circuit current (Isc) must be found. When the PV cell is disconnected from any load and currently operating as an open-circuit, the voltage across the device is at its maximum while the current is at its minimum. When the PV cell is then short-circuited, the opposite occurs where the current is at its maximum and the voltage at its minimum. One way of finding the values that connect these two points is to attach a voltmeter and ammeter to the PV cell circuit shown in figure 7. Supply the PV cell with a known Lux value and vary the load on the circuit. Figure 6 also shows a P-V curve (Power-Voltage), which is obtained by multiplying the current and voltage values. This curve is used to find the maximum power point in the device.

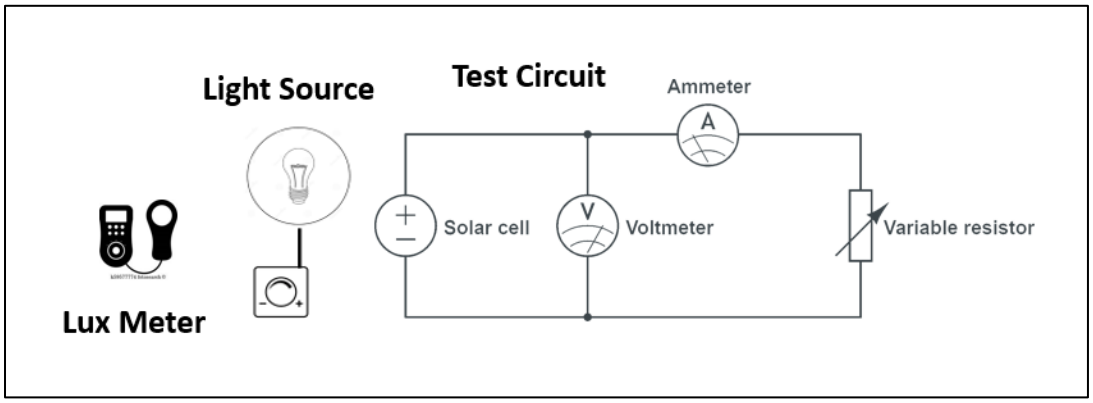


Figure 7: PV Cell Test Setup

Looking at the P-V curve shown in figure 6, the maximum power point can be seen as the point at which the voltage and current in the circuit are producing the maximum possible power. Due to the varying environmental conditions associated with harvesting ambient energy, a maximum power point tracker (MPPT) is necessary to increase the efficiency of the PV cell and maintain a stable output power by matching the load to the source for maximum power transfer. An MPPT circuit needs to be dynamic because as the light changes or the temperature on the components

changes, the impedance of the PV cell also changes, thus requiring the matching circuit to be able to adapt to such changes.

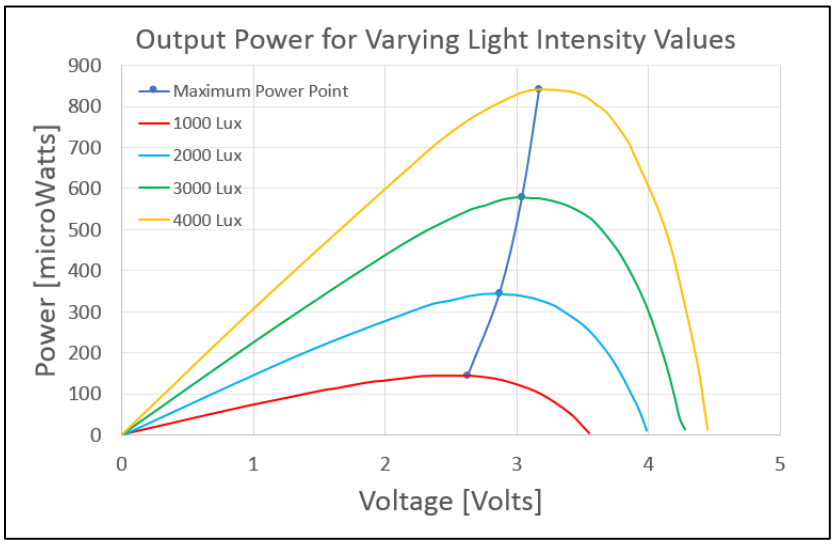


Figure 8: Change of Output Power for different light levels

However, there are multiple types of MPPT controllers, each having their own advantages and disadvantages depending on the type of application [27].

According to current research the "perturb and observe" and other "hill climbing" methods [26] are considered to be the most efficient in obtaining the maximum power point [28]. In this section, two types of MPPTs will be compared, "Perturb & Observe" (P&O) and "Fractional Open-Circuit Voltage" (FOCV).

2.3.1.1 Perturb & Observe:

Different MPPTs use different algorithms with the same goal to automatically find the voltage and current that delivers the maximum available power produced by the PV cell. The P&O algorithm can be explained using the flowchart in figure 9. This method measures both the voltage and the current of the PV cell. The controller then modifies the operating voltage or current of the cell until the maximum output power is achieved [29]. As an example, if the operating voltage of the cell increased the resulting output power is increased, then the

controller will repeatedly increase the operating voltage until the output power begins to decrease. Once this happens the controller will then decrease the operating voltage. The algorithm will then oscillate around the maximum output power until it stabilizes [30]. The algorithm can be modified to change the step size of the controller. Reducing the step size can help the MPPT be more accurate, however, the more steps that the tracker is using to find the MPP, the more power it consumes. This is the biggest drawback of using P&O as the MPPT.

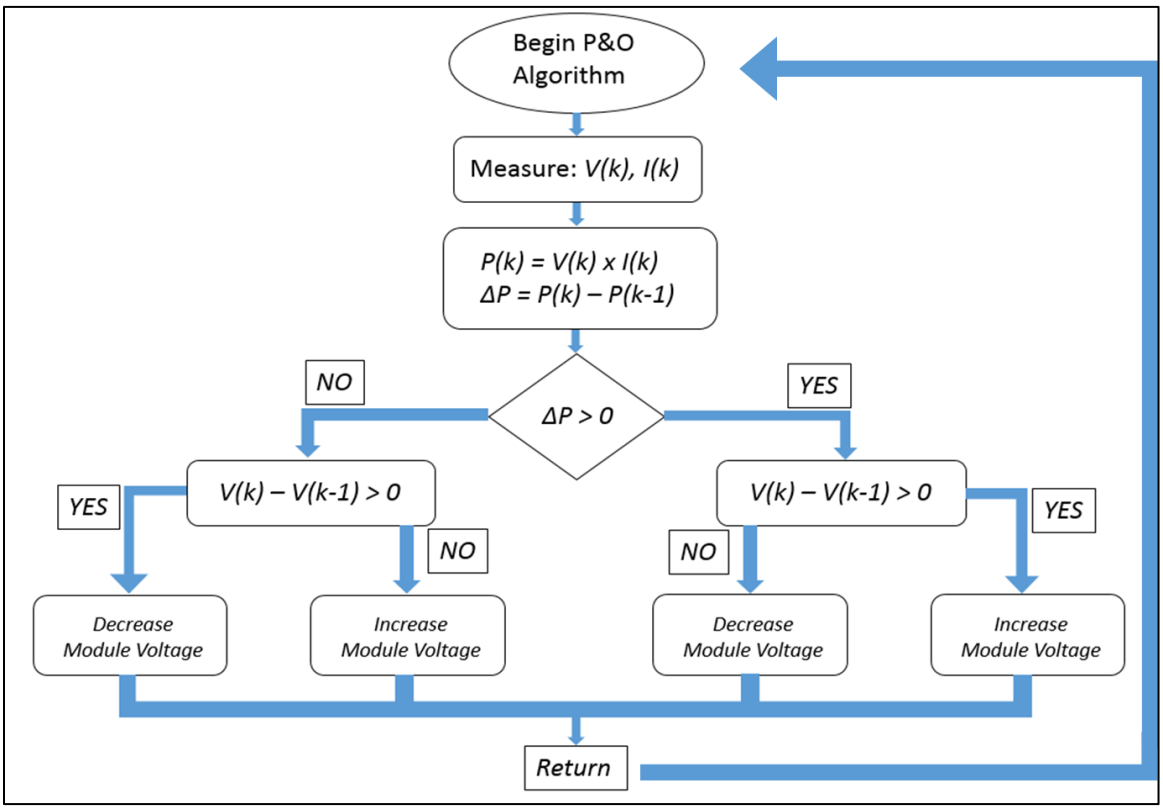


Figure 9: P&O Algorithm

An example of this algorithm is shown in figure 9 and works by measuring the voltage and current at some time "k". The power is then calculated from these values and compared with the previous measurement. If the power value is greater at time "k", this makes ΔP greater than 0. The voltage at "k" and "k-1" is then compared and the results determine whether to increase or decrease the module voltage. These steps are then repeated to ensure the maximum power is sent to the load.

While this algorithm is widely used for higher power applications, it typically consumes far too much power (10-100mW) rendering it unusable for sub-mW WSN applications that use small-scale indoor PV cells [31].

2.3.1.2 Fractional Open-Circuit Voltage:

The fractional open-circuit voltage method is based on the fact that the voltage of the PV cell at the maximum power point is approximately linearly proportional to the open-circuit voltage. The equation used in finding the maximum power point voltage is as follows:

$$V_{MPP} \approx K_1 * V_{OC} \quad (1)$$

Where K_1 is the proportional constant for the voltage factor and V_{OC} is the open-circuit voltage. This constant typically has a value range from 0.7-0.9 depending on the overall characteristics of the PV cell [32] [33]. This value can usually be found in the component's datasheet. Due to this voltage factor remaining nearly constant for change in light levels and temperature, the measured open-circuit voltage allows for an accurate value of the maximum power point voltage [33]. The current level at the maximum power point can be calculated using equation 2.

$$I_{MPP} \approx K_2 * I_{SC} \quad (2)$$

Where K_2 ranges from 0.78-0.92 [34] and I_{SC} is the short circuit current. These values can be used to find the maximum power point when the environment surrounding the PV cell shifts.

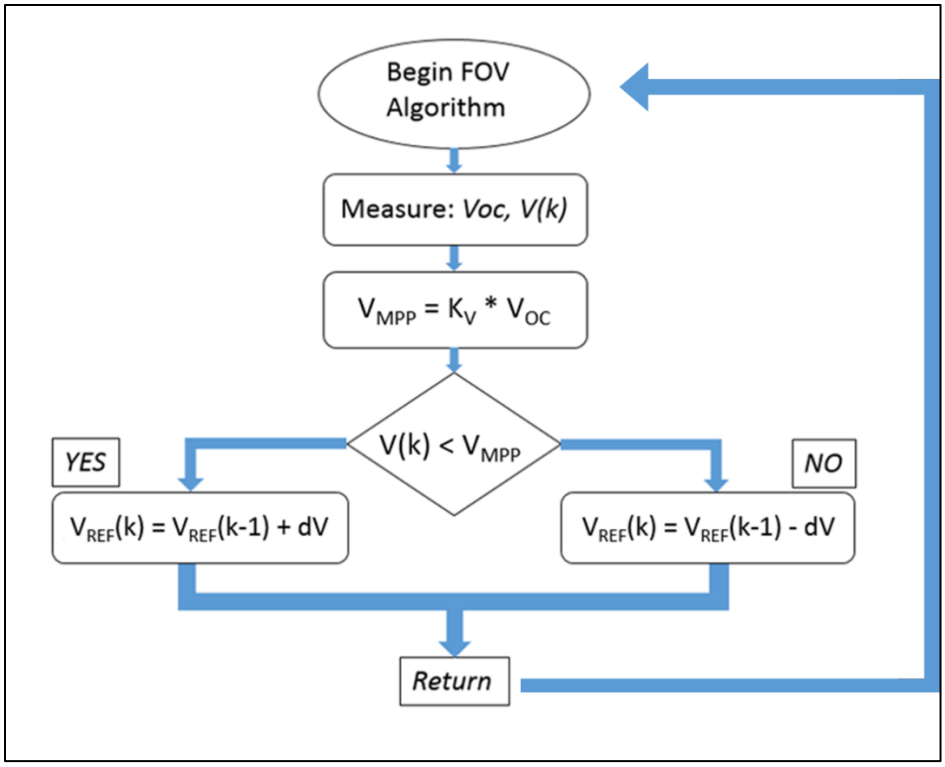


Figure 10: FOCV Algorithm [35]

An example of the FOCV algorithm is shown in figure 10 and begins by measuring the voltage generated by the device and the open-circuit voltage. The open-circuit voltage is then multiplied by a constant K_V to determine the MPP voltage. This reference voltage is compared to the measured supply voltage and depending on the outcome, the load impedance is changed to either increase or decrease the voltage across the load to match the MPP reference voltage.

In order for this algorithm to work an additional switch needs to be added to the system to periodically interrupt its normal operation. The load is disconnected as the open-circuit voltage is measured. This measurement is stored in a hold circuit to act as Vref on the control loop [36]. The frequency and duration of the measurement process has a direct effect on the accuracy of the estimated maximum power point voltage. Higher frequencies provide more accurate open-circuit voltage values but increase power consumption of the MPPT circuit [33].

As the popularity of solar power increases more and more funding is generated with the goal of improving the efficiency of PV cells while reducing overall production costs. A number of factors

limit the efficiency of the PV cell which reduces the amount of output power generated by these cells, such as, light intensity, cell size, cell type and temperature.

PV Cell Type	***Efficiency rate***	***Advantages***	***Disadvantages***	***Cost***	***Indoor Light***
Monocrystalline PV cells (Mono-SI)	~20%	High efficiency rate; optimized for commercial use; high lifetime value	Expensive	€€€	✓
Polycrystalline PV cells (p-Si)	~15%	Lower price	Sensitive to high temperatures; Lower lifespan & slightly less space efficiency	€€	✓✓
Thin-Film: Amorphous Silicon PV cells (A-SI)	~7-10%	Relatively low costs; easy to produce & flexible	Shorter warranties & lifespan	€	✓✓✓

Table 2: Comparison of different PV Cell types [37]

2.3.2 Thermoelectric Generator:

When considering deployment for a WSN, light may not be an available ambient source of energy for a particular location. Other forms of ambient energy sources need to be considered. Another popular energy harvester for WSN are TEGs. These devices are ideal when operating in locations such as mechanical rooms that contain devices such as boilers, water pumps, and heat exchange units. The temperatures radiating from these large scale devices sometimes contain enough energy to be harvested by TEGs and converted to usable levels of electricity. Smaller temperature gradients can also be used, from electronic goods to temperature gradients at walls or windows.

Thermoelectric generators work by taking advantage of the Seebeck effect which directly converts temperature difference into electricity. The typical structure of a TEG module is illustrated in figure 11. When heat is applied to one of the two conductors, the temperature of electrons close to the surface begins to rise and flow towards the cooler surface creating current

flow. When a temperature difference exists on the multiple P-N junctions, a potential voltage difference between the hot and cold surfaces occurs [38].

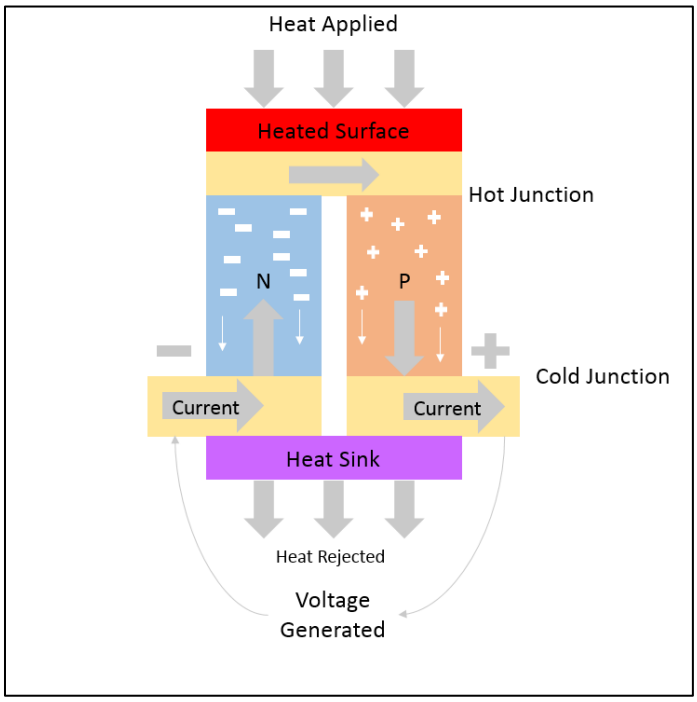


Figure 11: Seebeck Effect [38]

However, depending on the power requirements of a WSN, a single TEG device may not have the capabilities to harvest enough energy to the power the device. In this case, multiple TEGs can be connected in series in order to generate high voltage levels or a step-up DC/DC converter can be used.

The main design issues when considering a TEG for WSN are types of material, and the number and size of TEG devices. Most TEGs have the ability to output a voltage level in the range of 10mV to several hundred millivolts [39]. Depending on the number of TEGs used, an ultra-low voltage step-up DC/DC may be used. A conventional TEG-based WSN is illustrated in figure 12.

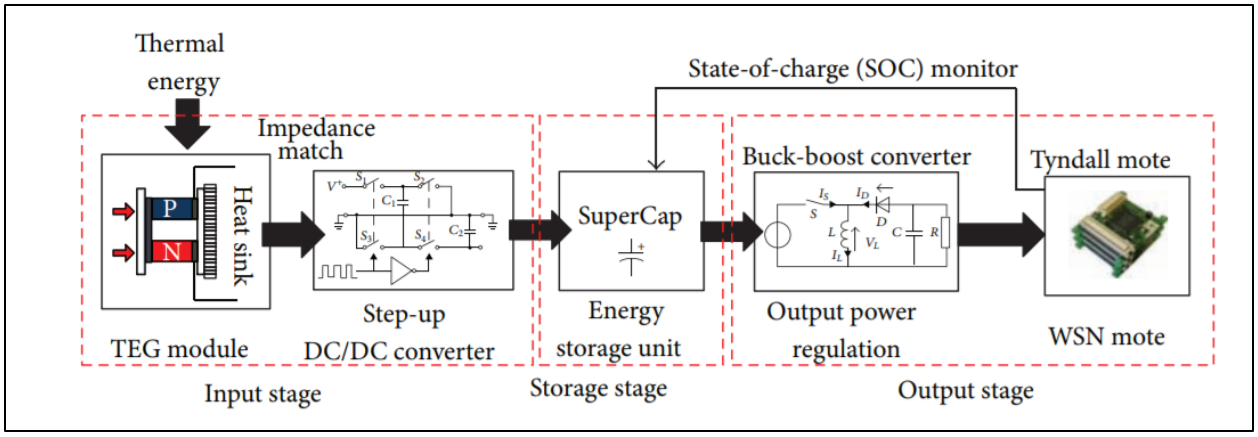


Figure 12: TEG WSN [39]

2.3.2.1 Step-up Converter:

J.M Gruber and S. Mathis presented a new boost converter for TEG devices that could output 3.6V with increased efficiency at low input voltages of a few 10mV [40]. Their prototype operates at an input voltage level of roughly 15mV with an efficiency of 45%. When the input voltage is increased to 120mV, the efficiency rises to 74%. A block diagram of the boost converter can be found in figure 13.

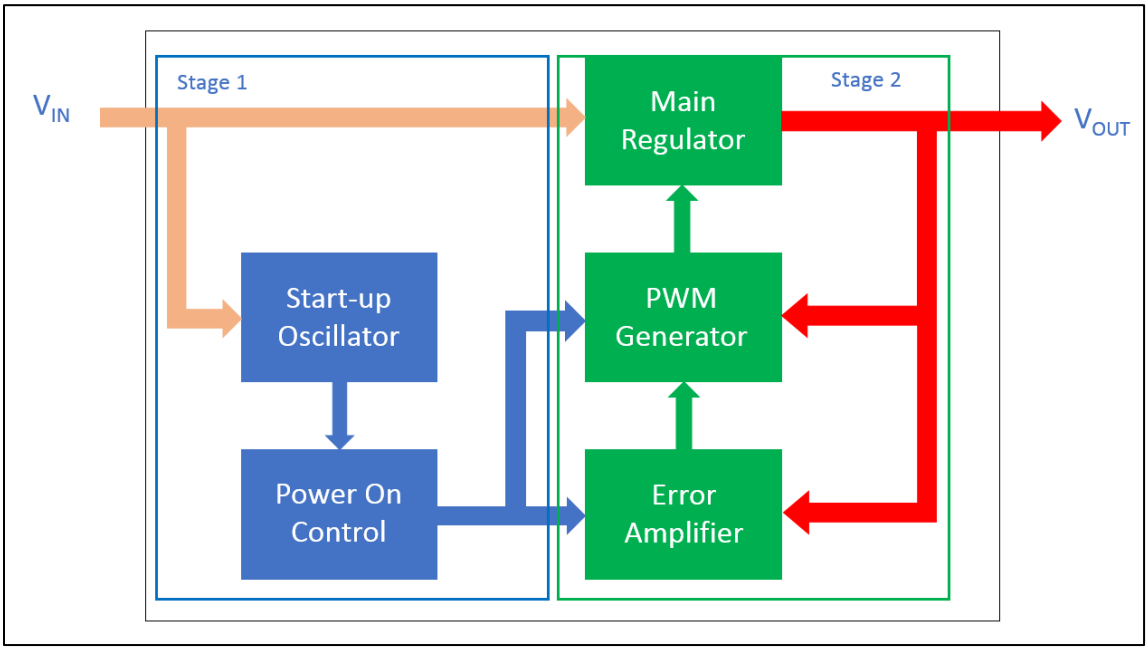


Figure 13: Boost Converter Diagram [40]

The converter has two separate stages. Stage 1 allows for a cold start with an operating input voltage of 36mV. The circuit in stage 1 contains a self-resonant oscillator connected to a voltage doubler. The voltage doubler charges capacitors from the input voltage and then switches these charges to ideally double the voltage produced at the output.

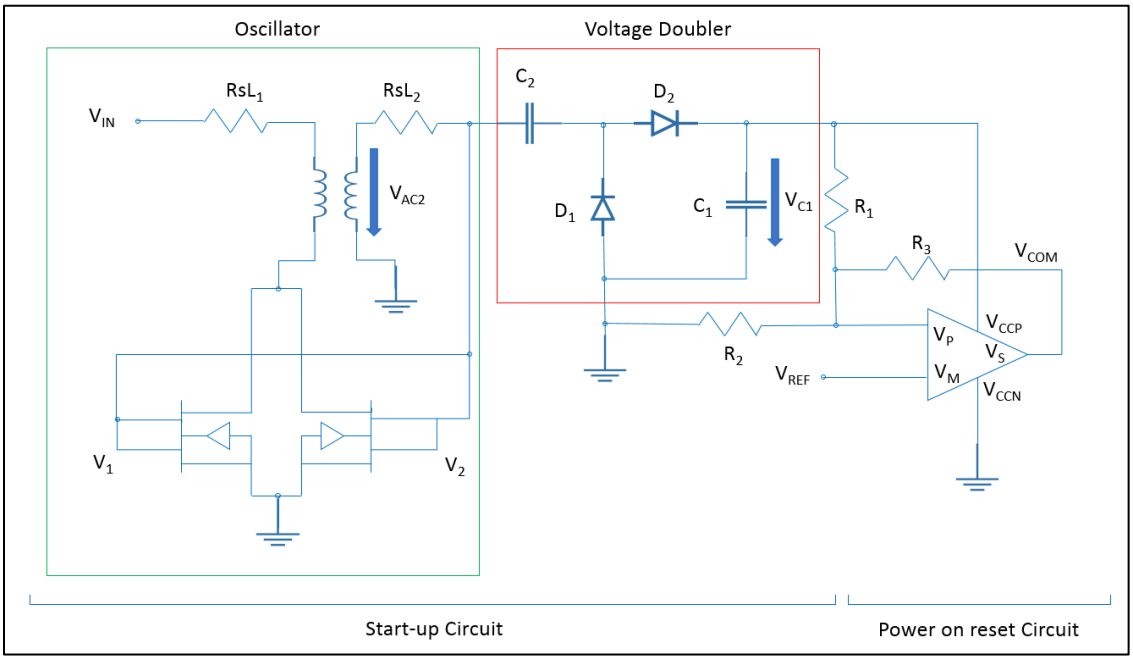


Figure 14: Stage 1 of Gruber boost converter [40]

The circuit in stage 2 contains the main converter, a triangle wave generator, comparator and an error amplifier. A pulse width modulated signal is generated on the N-FET V1 when the main regulator control blocks are switched on. This then turns on the main regulator and allows current to flow through the inductor and charge the output capacitor.

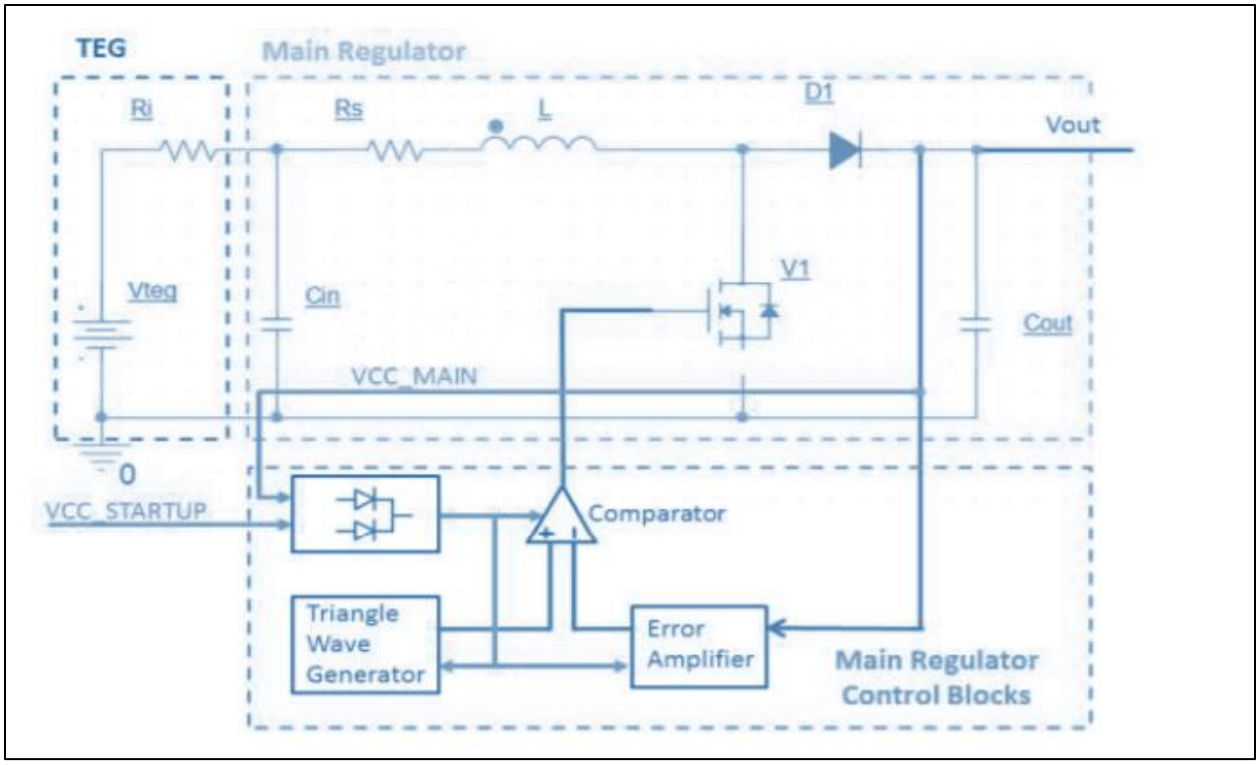


Figure 15: Stage 2 Gruber boost converter [40]

From their measured results, their prototype reaches a high efficiency at 15mV which is ideal for low voltage TEG devices. The converter can start directly from a 36mV input voltage while delivering an output voltage of 3.6V. When the prototype was tested at a 3K temperature difference, the step-up converter delivered 802µW while operating with an efficiency of 62% [40].

For commercial-off-the-shelf boost converters, Linear Technology offer an ultra-low voltage boost converter, LTC3108 [41]. This integrated circuit uses a normally-on MOSFET and a resonant oscillator scheme with a small external step-up transformer. With an additional external charge pump capacitor coupled to the oscillator and a rectifier, this device can provide an output voltage anywhere from 2.35V – 5V.

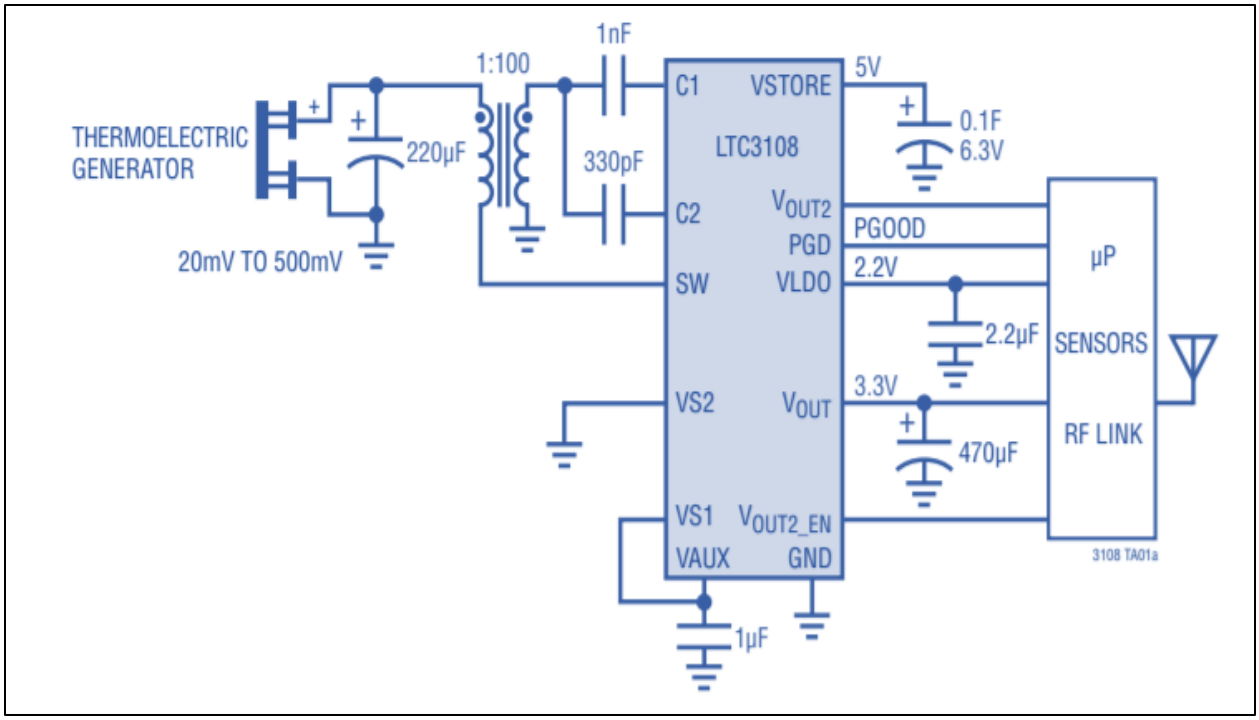


Figure 16: Analog Devices LTC3108 schematic [41]

Taking the results from the datasheet, it can be seen that the main disadvantage with this converter is its efficiency. The LTC3108 has a peak efficiency of 40% at 70mV which then decreases to 10% at an input voltage of 250mV [40]. Compared to the Gruber-Mathis design, the LTC3108 falls behind in efficiency.

2.3.2.2 Maximum Power Point Tracker for TEGs:

The magnitude of a TEG's open-circuit voltage is directly proportional to the temperature difference. Similar to photovoltaic cells, the most conventional MPPT method is P&O [42] [43]. The main difference in using these algorithms for PV systems is that, for PV systems the relationship between the cell's voltage and current levels are logarithmic, while for TEGs, the relationship is linear.

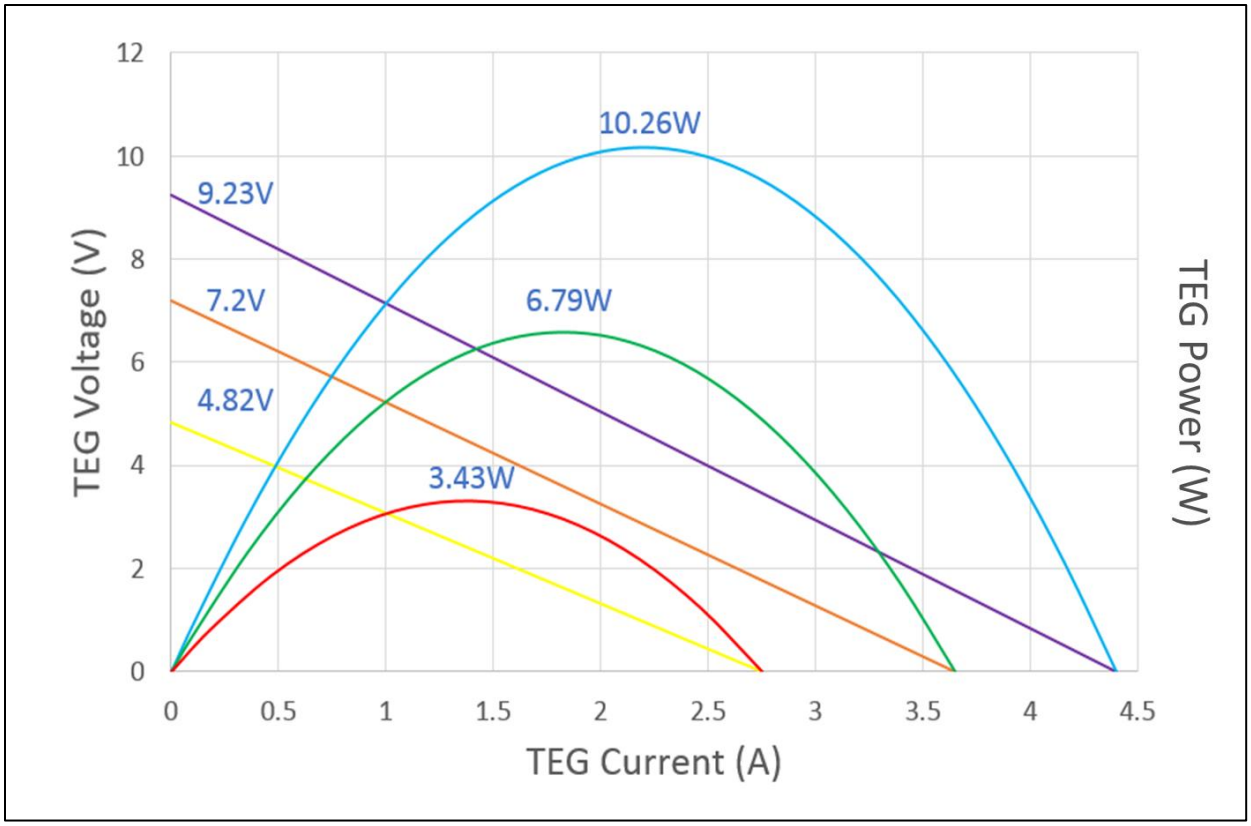


Figure 17: TEG I-V Curve & P-V Curve [44]

From figure 17, the maximum power values can be obtained by the following equations:

$$V_{MPP} \approx \frac{V_{OC}}{2} \tag{3}$$

$$I_{MPP} \approx \frac{I_{SC}}{2} \tag{4}$$

The FOCV method for MPPT is the favored approach when it comes to obtaining the maximum power from sub-mW harvesters. However, while measuring the open-circuit voltage and the short-circuit current during operation, no energy flows through the system because the converter needs to be disconnected. A paper written by Andrea Montecucco and Andrew Knox proposes a measurement technique that measures during the normal switching of the converter, with a "minimal reduction in collection efficiency" [44]. A schematic of their proposed circuit can be found in figure 18.

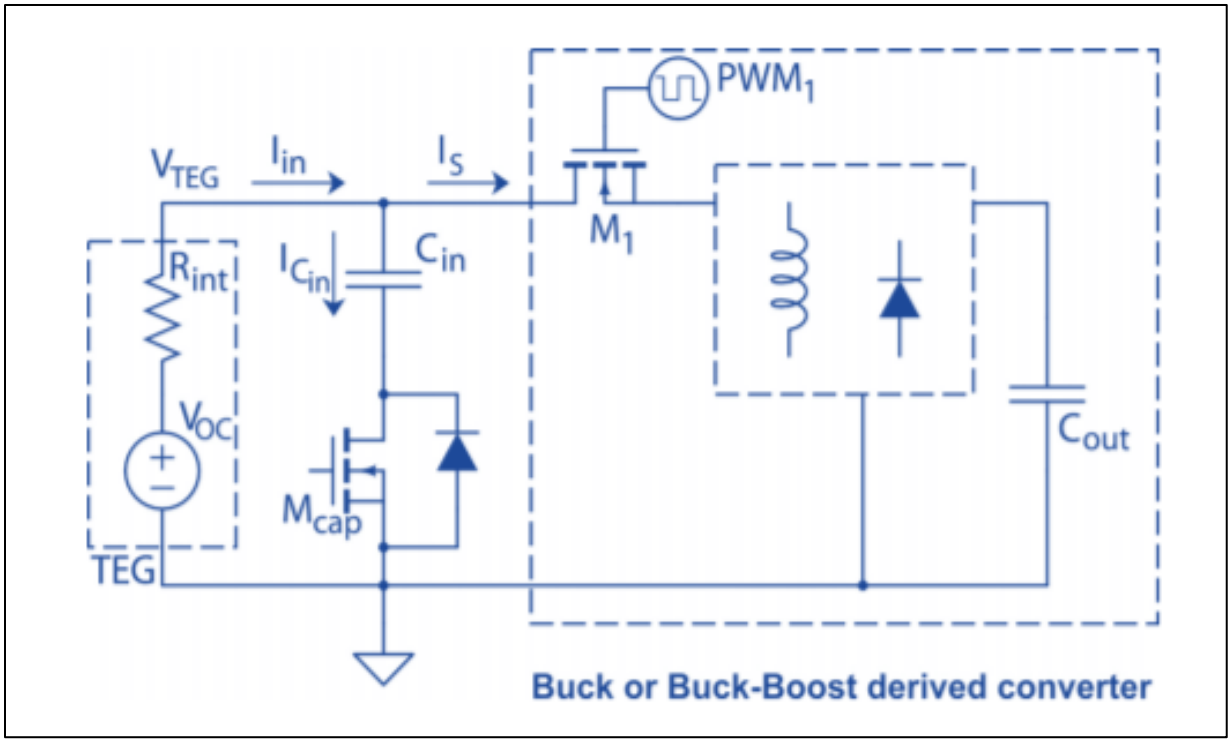


Figure 18: Buck-Boost converter schematic [44]

Under normal operating conditions of the system, Mcap is closed and Cin adds to the input current required by the converter. When the system needs to measure the open-circuit voltage, Mcap is opened and the TEG is disconnected from the rest of the system. During this time, the current is unable to flow through Cin, causing the terminals of the TEG to rise to the open-circuit voltage level. This typically takes tens of nanoseconds [43]. A microcontroller is timed to measure the voltage level of the TEG. This process can take between 0.1 s and 1 s [44] which is faster than disconnecting the converter until the voltage in Cin reaches the open-circuit voltage (typical method of measuring Voc). While using a Buck-Boost converter with an efficiency of 93%, their method can harvest close to 100% of the maximum power [44].

2.4 Energy Storage Unit:

WSNs provide an elegant solution to the problems encountered when tackling mass scale monitoring. The elimination of wires and the need for grid connected devices opens up the possibility of monitoring harsh or hostile environments where wired networks can't be deployed. However, energy storage in WSNs is the biggest hurdle to overcome when discussing cost and maintenance fees due to many networks having nodes in the thousands. Even with a suitable energy harvesting device, an energy storage unit (ESU) is essential in order for a sensor to operate and provide a continuous and reliable stream of data when ambient energy can no longer be harvested. The two types of storage devices that will be discussed in this section are supercapacitors and batteries.

2.4.1 Supercapacitor:

Depending on the types of sensors used and the type of data required, power requirements for WSNs can be different. Supercapacitors, also known as ultracapacitors or double-layer electrolytic capacitors, are commonly used in energy harvested WSNs as they have a higher power density than batteries and can operate without the need for additional charging circuitry. They also have a long operational lifetime, with charging and discharging of the device having little to no effect [45]. Inside the capacitor are terminals connected to two metal plates. The plates are separated by a thin layer of separator. One side is then filled with an electrolyte. This setup allows for what's called "electrical double layers" [46].

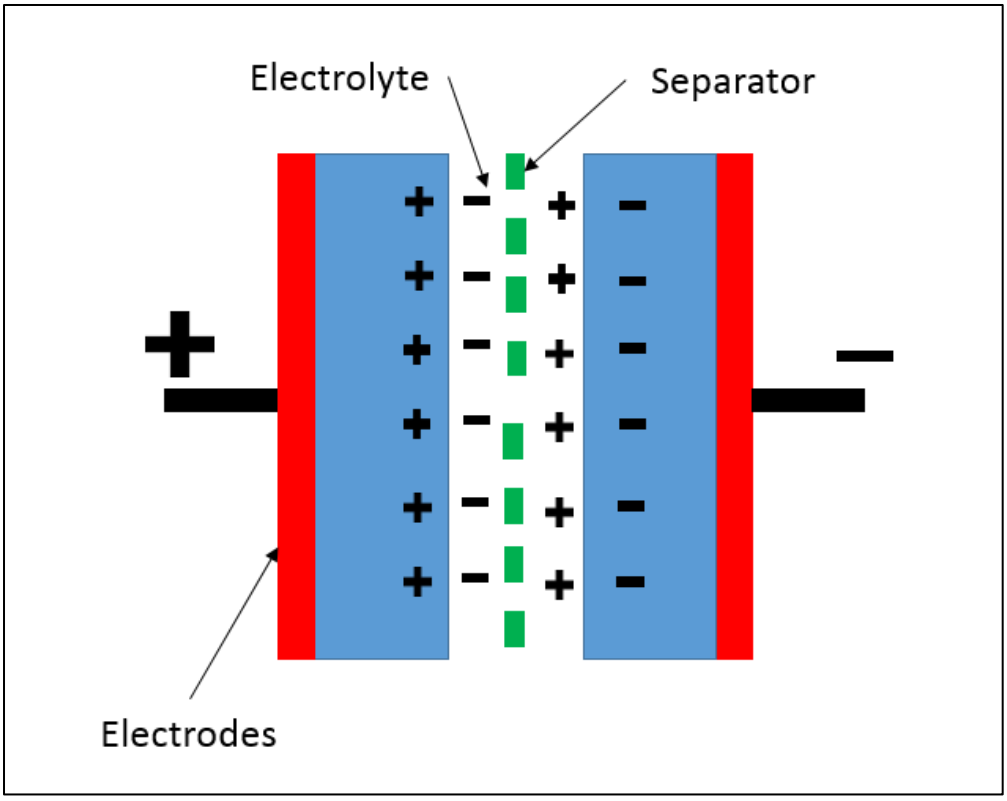


Figure 19: Capacitor diagram

The supercapacitors charge and discharge process is entirely electrostatic, meaning no chemical reactions occur inside the supercapacitor [47]. Due to this fact, the charge and discharge cycle should run indefinitely. Many supercapacitor datasheets provide charge cycle values of 100s of thousands. Commercial-off-the-shelf supercapacitors usually claim a lifetime of between 10-20 years under normal operating conditions [48].

Supercapacitors possess orders of magnitude higher energy density than conventional capacitors. Using a porous activated carbon electrode allows supercapacitors to achieve a high surface area. They also have quite a low equivalent series resistance (ESR) compared to batteries. Lower ESR means less energy is wasted through losses such as heat. Supercapacitors can provide much higher power density level because of such a low internal resistance. Supercapacitors have a much higher capacitance rating that conventional capacitors. The capacitance of a supercapacitor ranges from 1 mF to hundreds of Farads.

The capacitance of a capacitor is given by the following equation:

$$C = \frac{k\,\varepsilon\,A}{d} \tag{5}$$

Where k is the relative permittivity, ε is the permittivity of free space, A is the surface area of the plates and d is the distance between the plates. What gives the supercapacitor such a high capacitance value is its large plate surface area and reduced distance between them.

To find the energy stored in a capacitor, the following equation is used, where V is the voltage:

$$E = \frac{CV^2}{2} \tag{6}$$

2.4.1.1 Charge / Discharge:

One of the key benefits of using supercapacitor technology is its ability to charge and discharge a large number of time and charging times can be as little as a few seconds. A capacitor charging circuit can be represented as follows:

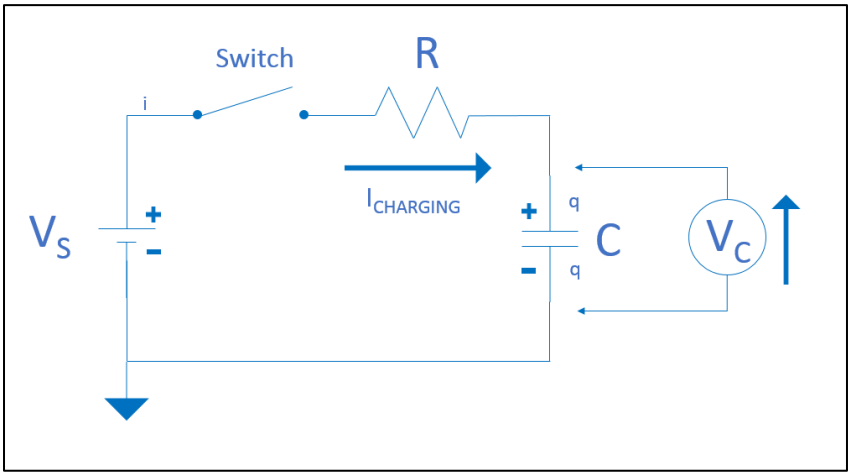


Figure 20: Capacitor RC charging circuit

The equation used to calculate the voltage across a supercapacitor is given by:

$$V_C = V_s \left(1 - e^{\left(-\frac{t}{RC}\right)}\right) \quad (7)$$

Where V_C is the voltage across the capacitor, V_S is the supply voltage, t is the elapsed time and RC is the time constant given by the resistor value and the capacitance of the supercapacitor.

Hence, the voltage across the supercapacitor over time is demonstrated in figure 21.

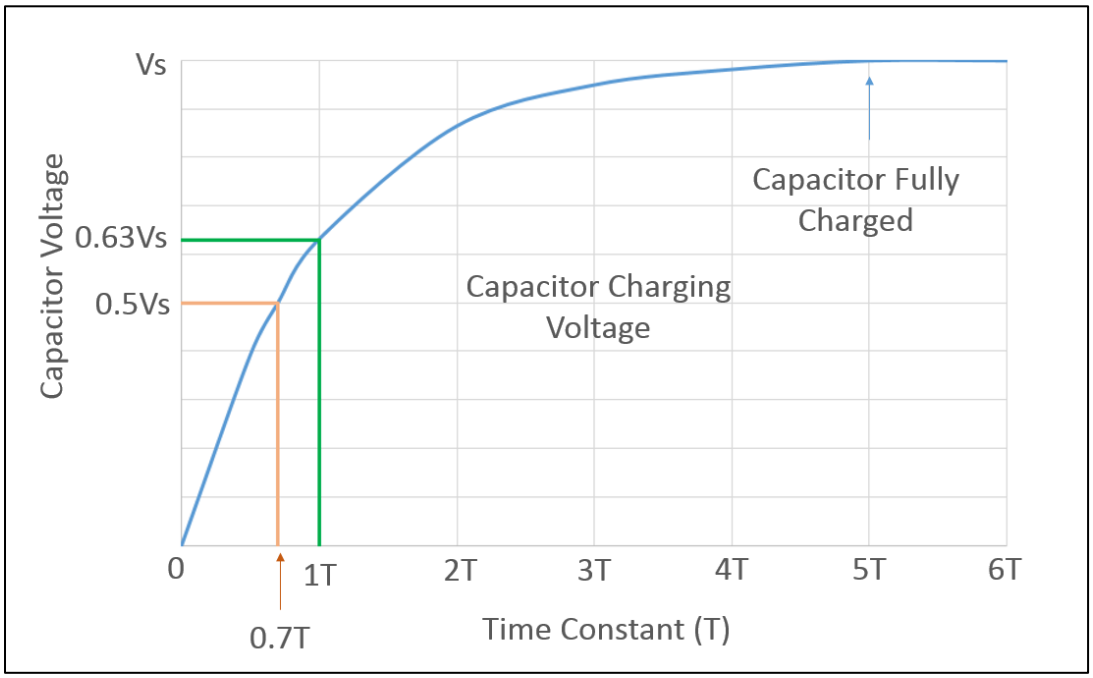


Figure 21: Capacitor charging voltage over time

To calculate the capacitor voltage when discharging, this equation is used:

$$V_C = V_s \left(e^{\left(-\frac{t}{RC}\right)}\right) \quad (8)$$

Similar to the charging graph that slopes upwards, requiring more and more time to increase in voltage, the discharge graph has a steep initial downward curve. The supercapacitor loses voltage quite quickly in the beginning but slows down the lower the voltage level becomes.

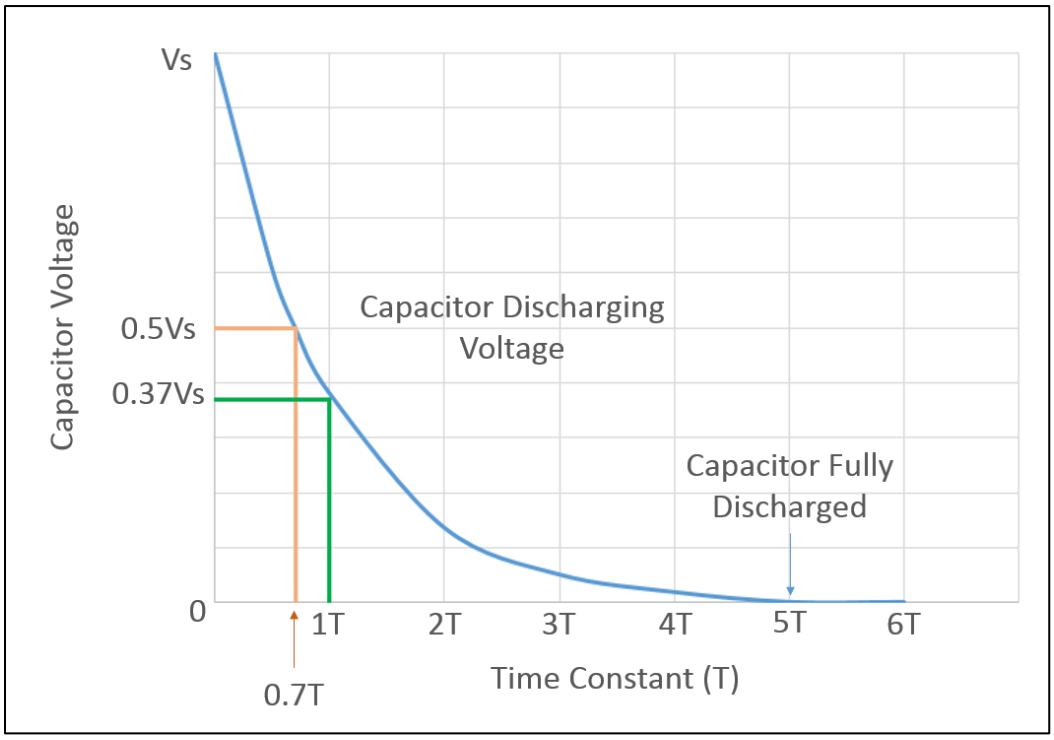


Figure 22: Capacitor discharging voltage over time

2.4.2 Batteries:

When it comes to WSNs, using batteries to power nodes can be very challenging, as batteries have a finite amount of charge and, if using a rechargeable battery a limited number of charge cycles. With a lot of WSNs begin deployed in harsh, hostile or difficult to reach environments, having to change batteries multiple times throughout the nodes lifetime can be extremely difficult and expensive, especially if it is a large-scale network. This section will show some current understanding of batteries used in WSNs with the main focus on powering nodes using a battery-supercapacitor hybrid model.

2.4.3 Batteries vs Supercapacitor:

A comparison between supercapacitors and batteries is shown in table 3. The main difference between the two types of energy storage devices are energy and power density. A supercapacitor has a much higher power density than a battery but has a considerably lower energy density [49].

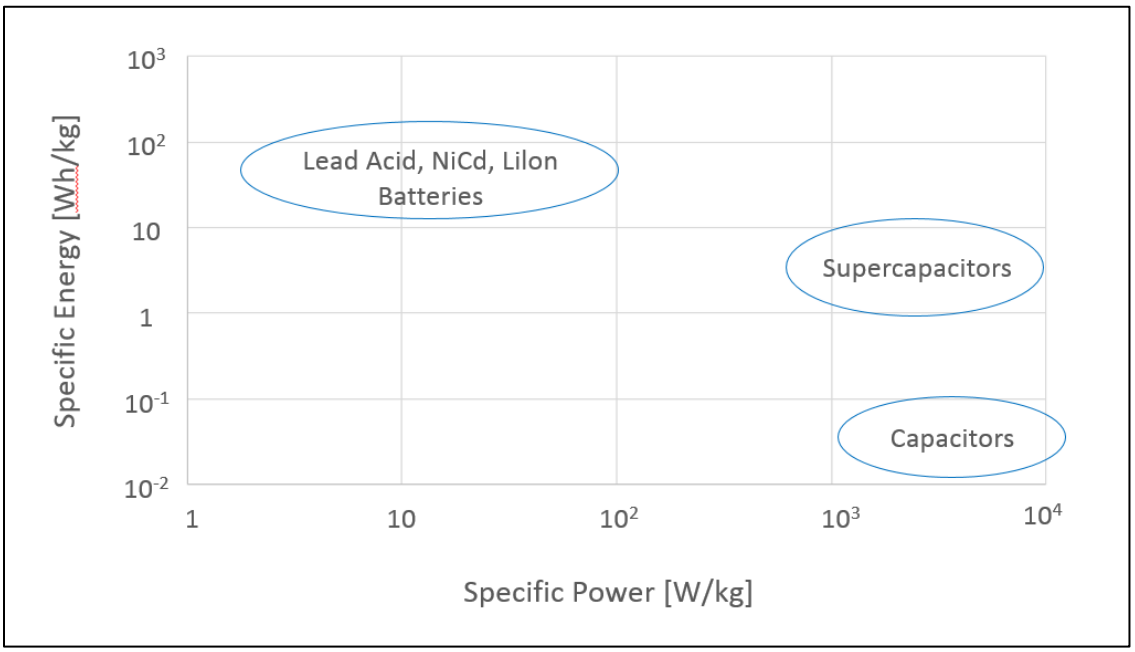


Figure 23: Specific Energy & Specific Power of different energy storage devices [50]

The specific energy is given by:

$$Specific\ Energy = \frac{V\ I\ t}{m} \tag{9}$$

Where V is the voltage, I is the current, t is time and m is mass in kg.

The specific power is given by:

$$Specific\ Power = \frac{V\ I}{m} \tag{10}$$

There has been a lot of research into using battery technology with WSNs. Table 3 is a list of comparisons between different battery and supercapacitor types.

	Maxwell UltraCap P270 SuperCap [65]	Cap-xx H206 SuperCap [66]	Infinite Power Solutions MEC-202 TFB [67]	Energizer CA-5L Battery [68]	Tadiran TLI Battery [69]
Type	Supercapacitor	Supercapacitor	Thin Film Battery	Li-ion Rechargeable Battery	Li-ion Rechargeable Battery
Charge Cycles	> 500,000	> 1 million	> 100,000	< 1,000	5,000
Lifetime	> 10 years	> 15 years	> 10 years	5 years	> 25 years
Voltage Rating	2.5 V	5.5 V	4.1 V	3.7 V	3.6 V
Capacity	10.3 J (3.3F)	9.1 J (0.6F)	36 J (2.2mAh)	15000 J (1120mAh)	15500 J (1200mAh)
Form Factor	Dia: 10mm L: 21.5mm	W: 39mm L: 14mm H: 2.4mm	W: 50mm L: 25mm H: 0.2mm	W: 45mm L: 32mm H: 8.1mm	Dia: 14.5mm L: 50.1mm
Energy Density	6.1 J/cm^3	6.9 J/cm^3	145 J/cm^3	1300 J/cm^3	1900 J/cm^3
Self-Discharge	Max. 30µA	Max. 10µA	Max. 1µA	< 1% per month	< 0.1% per month
ESR	290mΩ	70mΩ	50-75Ω	50-200mΩ	250mΩ
Operation Temperature	-20 ~ 70°C	-40 ~ 85°C	-20 ~ 70°C	-20 ~ 70°C	-40 ~ 85°C
Unit Cost	$2.50	$12	$5	$15	$50
Comment	Low cost SOTA SuperCap	Low leakage current SuperCap	SOTA thin film battery	Low cost rechargeable battery	SOTA long lifetime battery

Table 3: Comparison of different Energy Storage devices [51]

Table 3 compares state of the art supercapacitors, thin-film, rechargeable and non-rechargeable batteries. This data shows that supercapacitors have longer lifetimes than both rechargeable and non-rechargeable batteries when under normal operating conditions. The supercapacitors also have a significantly higher number of charge cycles compared to the batteries. However, the supercapacitors do have a much higher leakage current which requires them to be recharged more often. The ESR values in the supercapacitor is much lower than the thin film battery. Unsurprisingly, the batteries do have a much higher energy density which was shown in figure 23. From this data, a battery's lifetime could be extended by utilizing a supercapacitor to deliver transient power to the WSN. Fewer pulses of power drawn from the battery enables it to operate more efficiently and increases the number of charge cycles possible.

While there are constant upgrades to current technology, reducing the power consumption required by WSNs [52] and improving the efficiency of the radio transmitting and receiving [53], it still seems that currently the optimum method of powering a WSN which is cost effective and more environmentally friendly is to use a supercapacitor-battery hybrid model [54] [55].

2.5 Ultra-Low Powered DC-DC Converters:

The sensor in a WSN node requires a constant voltage level when in operation, meaning that the voltage received from the ESU needs to stay at a constant level. As the voltage in the ESU is constantly changing, an additional component to the circuit is required for continuous operation. This is a where a DC-DC converter is used. The purpose of a DC-DC converter is maintaining a constant voltage on the output regardless of the voltage on the input. These components are more important with supercapacitors than batteries. In a normal operating WSN the charge levels in the supercapacitor or battery are constantly changing. Hence, an ultra-low powered DC-DC converter is required to interface the energy storage unit with the load. Depending on the size of the load and the energy storage unit, different types of DC-DC converters can be used. These types include buck, boost and buck-boost. The goal of a buck converter is to reduce the input voltage to a lower constant output voltage, while the boost converter does the opposite. The buck-boost converter has the ability to perform both of these actions depending the input voltage and the required output voltage.

For WSNs that require low power, quiescent current is a huge factor when deciding on which model of DC-DC converter to choose from. Texas Instruments offer ultra-low powered DC-DC converters with quiescent currents ranging from several hundred nanoamps to several microamps [56].

2.6 Simulators:

Simulation tools to aid in the improvement of WSN are increasingly being used to test new applications and protocols. A paper written by Harsh Sundani et al. [57] documented a survey completed by his team on currently available simulation tools. WSNs can be very environment and application specific, meaning that it is very difficult to create an application that fits all. When designing a simulator, a whole range of factors need to be considered such as, sensor type, environment, number of nodes, type of transceiver/receiver and what type of protocols to use. They created an extensive survey and comparison of the most popular WSN simulators [57]. These simulators can be incredibly powerful. Castalia for example, has the ability to represent different sensing devices (e.g. temperature, light, pressure, acceleration), while (J)Prowler focuses on modelling all levels of the communication channel and the application. However, since each simulator has its own main area of focus, this results in limitations in the simulator. A sample list of the simulator's programming language, key features and limitations can be found in table 4.

While these simulators are designed for WSNs, they don't take into account the use of energy harvesters. There are a significant number of papers dedicated to modelling and simulating of energy harvesting components. Yunus Emre Yagan et al. took a PV cell unit and mathematically modelled it and simulated its behavior under different conditions in Matlab/Simulink [58]. Alexander Korotkov et al. simulated the behavior of TEGs using the ANSYS Workbench software platform [59]. There are also simulators of supercapacitors and other energy storage devices [60] that can be incredibly accurate. However, all of these simulators are separate entities and do not have the capability to interact with each other. A simulation tool that closely follows the work that will be presented in this thesis is titled RoWBUsT [61].

Simulator	Programming language/ Platform	Key Features	Limitations
SENS [70]	C++	• Platform-independent. • Users can assemble application-specific environments. • Defines an environment as a grid of interchangeable tiles.	• Not accurately simulate a MAC protocol. • Provides support for sensors, actuators, and physical phenomena only for sound.
Castalia [71]	C++	• Physical process modeling, sensing device bias and noise, node clock drift, and several MAC and routing protocols implemented. • Highly tunable MAC protocol and a flexible parametric physical process model.	• Not a sensor specific platform. • Not useful if one would like to test code compiled for a specific sensor node platform.
SENSE [72]	C++	• Balanced consideration of modeling methodology and simulation efficiency. • Memory-efficient, fast, extensible, and reusable.	• Not accurate evaluation of WSN research. • Lacks a comprehensive set of models. • Absence of a visualization tool
(J)Prowler [73]	Matlab / Java	• Probabilistic wireless sensor network simulators. • (J)Prowler provides an accurate radio model.	• Provides only one MAC protocol, the default MAC protocol of TinyOS.

Table 4: List of different WSN simulators

RoWBUsT is a tool that was designed to get high efficiency in terms of quality of service and energy harvesting in commercial buildings. The RoWBUsT simulation tool has hard coded

components in its software. The tool simulates the lifetime of a TelosB mote and allows a user to determine the duty cycle of the mote, the size of the PV cell attached to it, the power management IC, the size of the supercapacitor storing the energy and the length of time that the simulation can run for.

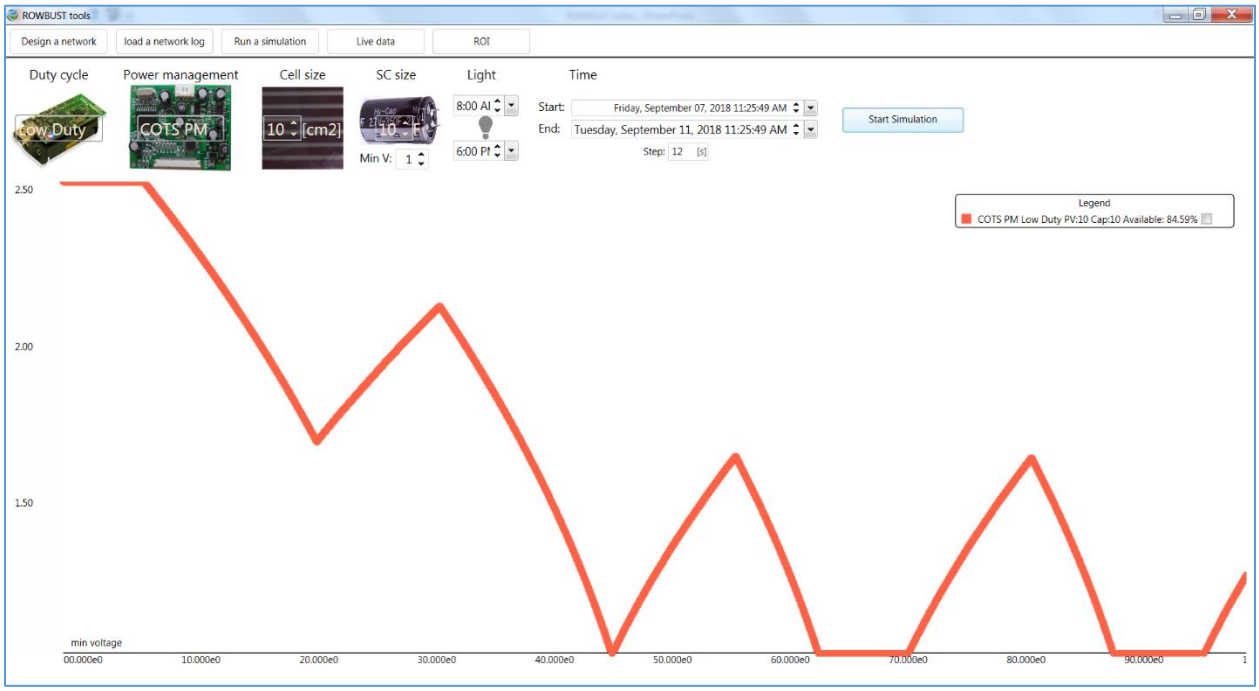


Figure 24: RoWBUsT GUI

Once the components have been selected, a graph presents the data in the form of the voltage level in the supercapacitor over time for the length of the simulation. The components can then be modified until the desired outcome has been achieved.

2.7 Literature Review Conclusion:

After reviewing the current literature surrounding EH-WSN, it is clear that a lot of advancements have been achieved in this field over recent years. The further development of photovoltaic cells and thermoelectric generators is allowing for a much broader range of use cases for these components. PV and TEG components are constantly improving their efficiencies. Especially with

the use of lower powered MPPT, the power conversion to the energy storage devices is becoming more and more efficient. With renewable energy expanding into all types of industries, the effort and capital spent trying to improve energy storage devices are increasing. With houses, buildings and vehicles all trying to be more and more renewable energy dependent, the energy density of these storage devices is constantly increasing. While harvesting energy and storing it are important, how that energy is transferred throughout the circuit has the potential to vastly increase the efficiency of WSN. The J.M. Gruber and S. Mathis DC-DC converter show that while industry standard DC-DC converter are still acceptable components in any WSN, new technology being developed will exceedingly improve the level of efficiency that energy converters have.

Reviewing the current simulators that revolve around WSN, the problem that is most prevalent is that they take a very narrow view and very application or device specific approach to simulating a WSN. The ReCO2ST tool presented in the following chapters, allows for a “plug and play” approach. Uniquely, the tool described in this work allows the user to define their own system components to undertake bespoke simulations specific for their application. Once the data templates provided with the software are completed properly, any PV, TEG, supercapacitor, DC-DC converter or sensor node can be simulated.

As the desire and need for EH-WSN increases, a simulation tool that has the capability to simulate the lifetime of a sensor with different components will become much more beneficial to reduce the use of batteries and allow WSN to operate for longer periods of time and in harsher environments.

3 System Architecture

3.1 Introduction

The simulation tool outlined in this section was built using ElectronJS (JavaScript library), HTML and CSS. The software has multiple components already built into the system but the main feature that this simulation tool offers is the ability to add new components to the system. The application performs a simulation with the data provided by the user, which simulates the difference in the sensor node's lifetime between being powered by batteries versus utilizing energy harvesting methods to extend the battery life. Figure 25 presents the "home" screen of the Graphical User Interface (GUI). Each button at the top opens up a window for the user to modify the simulation inputs.

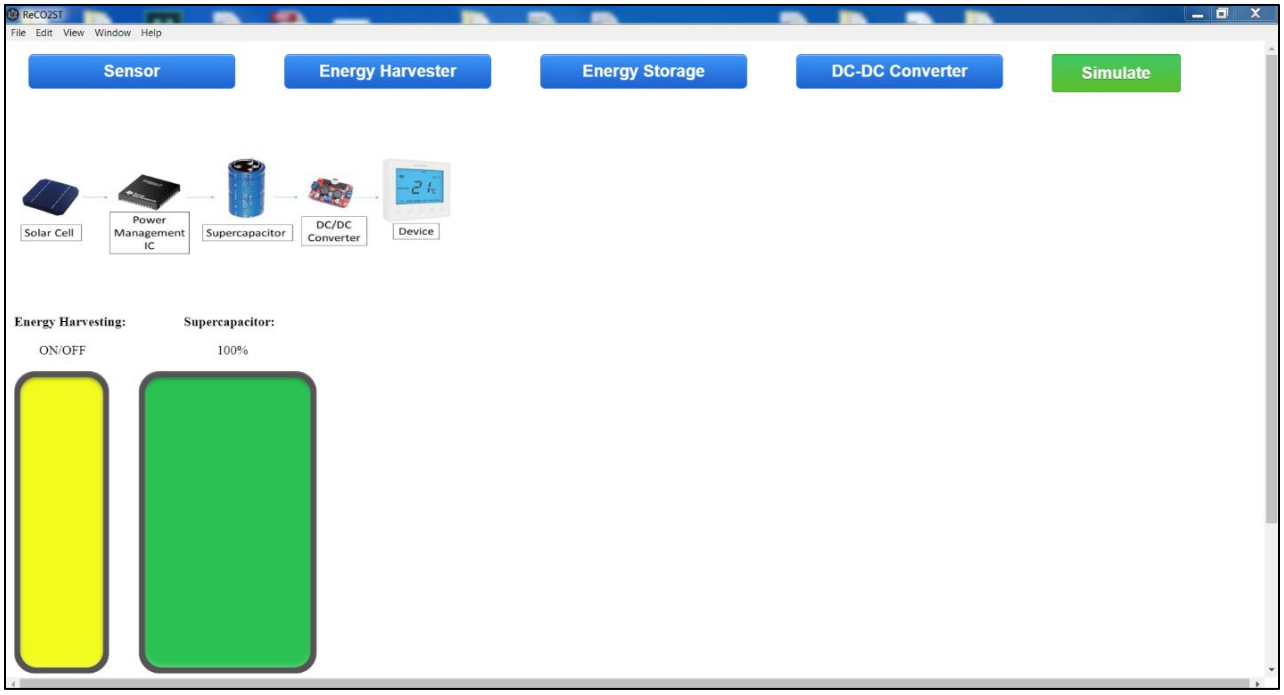


Figure 25: ReCO2ST GUI

The simulation then presents a dynamic line graph of the voltage level in the energy storage device over a 1 week period. For seamless power to the load, the voltage in the supercapacitor needs to stay above a given threshold. Once the simulation is complete, it can then be run for an unlimited number of times, comparing different component type and sizes. This feature allows the user to find the optimum power management setup for their device, whether they want to extend the battery's lifetime or eliminate the need for batteries all together.

3.2 Data Structure

To reliably provide power to low-power sensor networks, certain building blocks are required. At sub-mW levels, ambient energy harvesting methods, such as photovoltaic cells and thermoelectric generators, become more feasible. Due to the varying environmental conditions associated with harvesting ambient energies, a maximum power point tracker (MPPT) is necessary to optimize the efficiency of the energy harvester for a given set of conditions by matching the load to the source.

Energy storage devices such as supercapacitors and rechargeable batteries are used to power the device when the ambient energy is not available. As the voltage on the storage device is changing on an ongoing basis depending on charge/depletion stage, a DC-DC converter is necessary to maintain a stable output voltage to the load.

With the goal of this software to provide reliable lifetime calculations for WSNs, it needs to be able to take data from all sorts of components. To accurately use different components and determine their performance, it is essential that they are characterized in a uniform and standardized manner and under conditions that reflect real-life operating scenarios. By doing this, an extensive array of components can be catalogued and stored in the software for comparison and to determine their viability for different applications.

For each component type available in this software there is an accompanying data template to be completed with characterized data from which the simulation tool can then read and add to the software to compare with other components.

3.3 PV Cell

3.3.1 Introduction

In this section, the method used to characterize the photovoltaic cells is presented, demonstrating the test setup and the results for the different material types and lights levels. A description of how the MPPT is used in this simulation is also be explained. The results are then used to complete a data template that is fed into the simulation tool to be simulated for different EH-WSN parameters.

Two types of photovoltaic cells were characterized. A monocrystalline PV cell, SLMD600H10L [74], manufactured by IXOLAR^{TM} and an amorphous PV cell, AM-1801CA [75], manufactured by SANYO. These types of PV cells are most suited for indoor light levels.

3.3.2 Characterization

3.3.2.1 Test Setup

Both PV cells were characterized under the same conditions using the same test equipment and lighting levels. Figure 26 presents the test setup with a circuit diagram and equipment used.

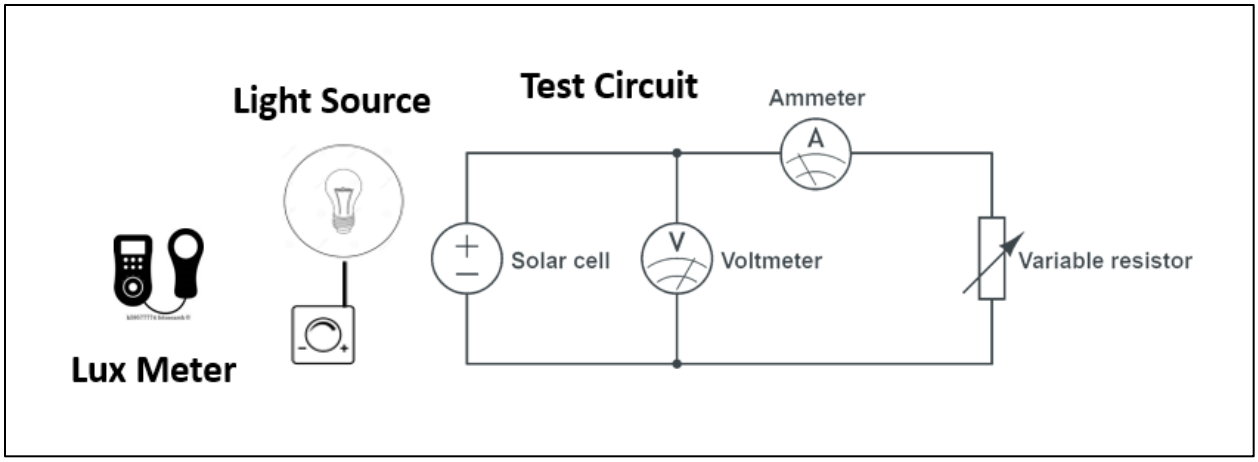


Figure 26: Circuit Setup

The goal of this test setup was creating I-V & P-V curves for each PV cell while under different lighting levels and different indoor light sources. To do this each PV cell was connected to a variable resistor. To ensure accuracy when measuring light levels, the circuit was placed in a box with a lamp pointing directly at the PV cell. The box blocked out all other light sources. A Lux meter was placed beside the PV cell to ensure the light level measured was the same as that on the PV cell. An ammeter and a voltmeter were each attached to the circuit measuring current and voltage respectively. To achieve an I-V curve, the resistor was constantly varied, measuring the voltage and current level at different intervals creating a sloped graph as shown previously. The output power was then calculated from these values and a MPP was found. When testing these PV cells, the light intensity levels ranged from 375 lux to 5000 lux using fluorescent, incandescent and LED lights. For each light level, an I-V curve was documented allowing for a P-V curve to be created to calculate the MPP of the PV cell for each lux level.

3.3.2.2 SLMD600H10L

Using the circuit presented above, the following graph was obtained using a fluorescent light source at 2000 lux.

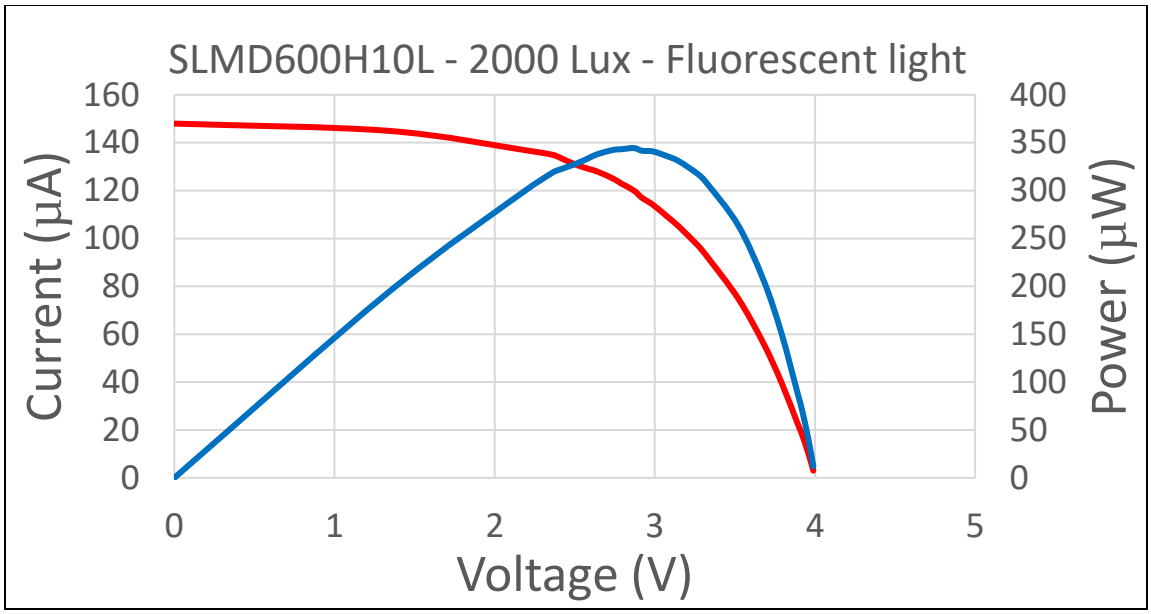


Figure 27: I-V & P-V Curve at 2000 Lux

Voltage	***Power***	***Current***
V	µW	µA
0.0015	0.222	148
1.33	192.85	145
2.18	298.66	137
2.36	318.6	135
2.4	321.6	134
2.5	327.5	131
2.59	334.11	129
2.64	337.92	128
2.74	342.5	125
2.79	343.17	123
2.87	344.4	120
2.92	341.64	117

Voltage	***Power***	***Current***
V	µW	µA
2.99	340.86	114
3.08	335.72	109
3.15	330.75	105
3.27	317.19	97
3.32	308.76	93
3.52	264	75
3.68	206.08	56
3.79	151.6	40
3.89	89.47	23
3.92	70.56	18
3.96	39.6	10
3.99	11.97	3

Table 5: Results from IV curve

From these results, the MPP can be found at 344.4 µW with 2.87 V and 120 µA being the component's voltage and current levels respectively at this MPP. Depending on what conditions the user envisages this method can be used for a range of different light intensity levels. Once all of the data is collected, the data template that accompanies the software can be filled out which is then be fed into the software to be run in a simulation.

Part Number :	SLMD600H10L		
Size :	7.7 cm^2		
Type :	Monocrystalline		
Voltage	Current	Power	Illuminance
V	µA	µW	Lux
1.94	20	38.8	375
2.07	29	60.03	500
2.63	55	144.65	1000
2.87	120	344.4	2000
3.04	190	577.6	3000
3.17	265	840.05	4000

Table 6: Data Template for SLMD600H10L

Table 6 shows the data that was measured using the SLMD600H10L component for a range of different light intensity levels. At each lux level, the MPP can be obtained and provided to the software.

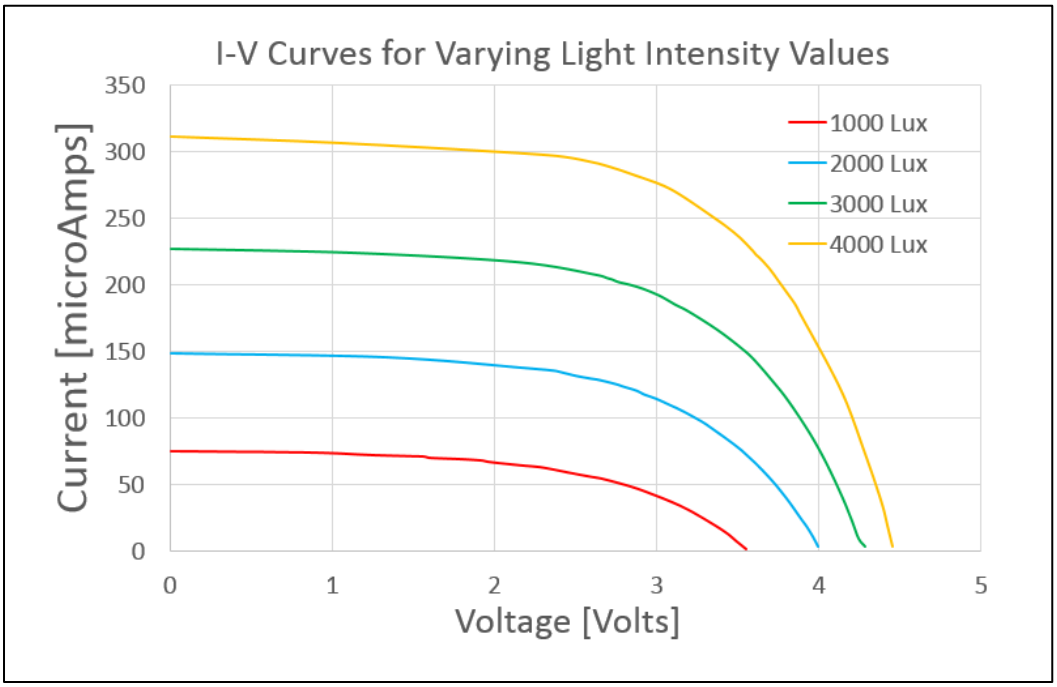


Figure 28: IV Curves for different Lux values

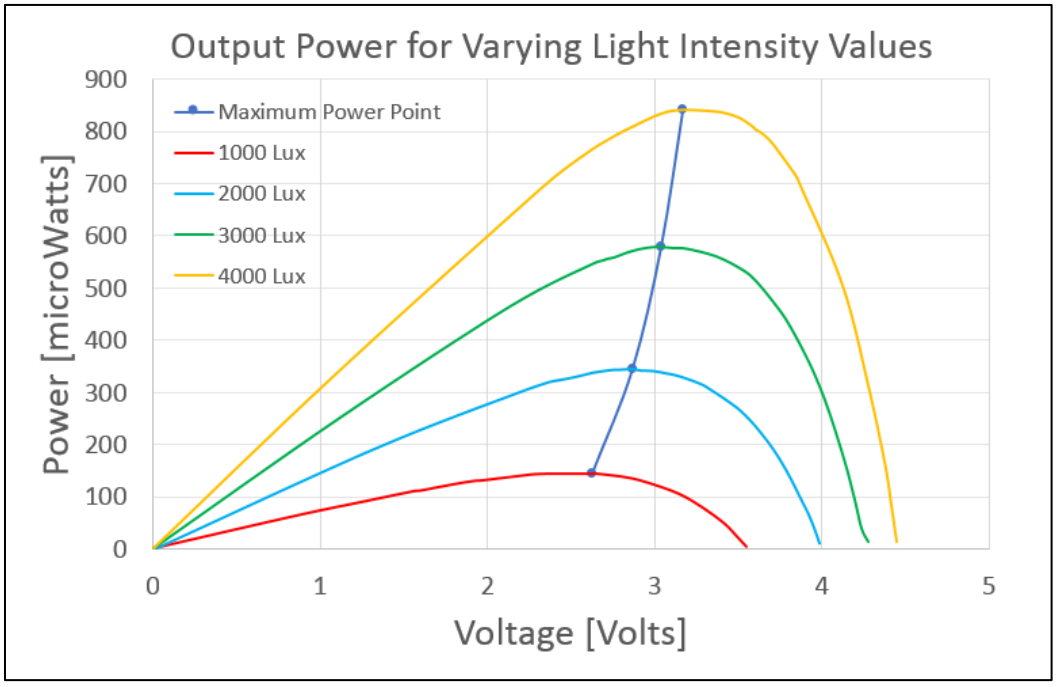


Figure 29: MPP for different Lux values

Figure 28 shows how different lux levels can affect the current generated by the PV cell while figure 29 presents the maximum output power of the PV cell for each lux value.

3.3.2.3 AM-1801CA

Similarly to the SLMD600H10L, the amorphous PV cell was characterized under the same conditions. From figure 30, it can be seen that for indoor levels amorphous PV cells can produce more power than monocrystalline PV cells. With amorphous PV cells being easy to produce and have to ability to produce more power than monocrystalline PV cells, it makes them the better choice for indoor applications.

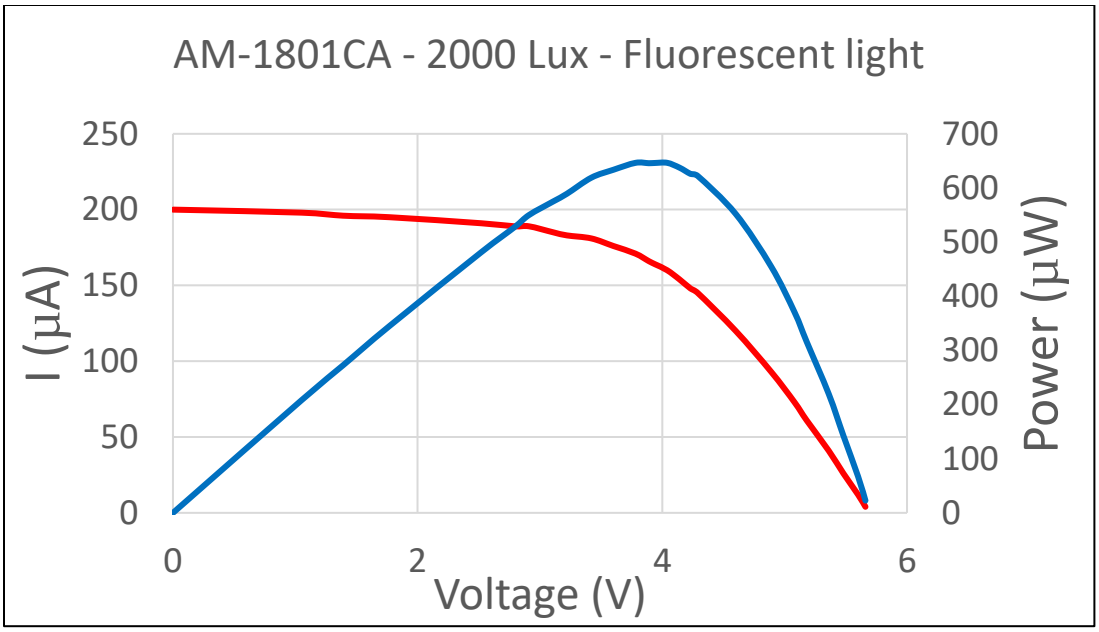


Figure 30: I-V & P-V Curve at 2000 Lux

Voltage	***Power***	***Current***
V	µW	µA
0.002	0.4	200
1.05	207.9	198
1.39	272.44	196
1.77	345.15	195
2.52	481.32	191
2.79	527.31	189
2.91	549.99	189
3.11	575.35	185
3.22	589.26	183
3.42	619.02	181
3.6	633.6	176
3.78	646.38	171
3.89	645.74	166

Voltage	***Power***	***Current***
V	µW	µA
3.94	646.16	164
4.04	646.4	160
4.14	637.56	154
4.23	626.04	148
4.29	622.05	145
4.6	552	120
4.89	454.77	93
5.08	370.84	73
5.18	315.98	61
5.36	219.76	41
5.48	142.48	26
5.6	67.2	12
5.66	22.64	4

Table 7: Results from IV curve (AM-1801CA)

In this simulation tool, the MPPT used is the FOCV method. This method was chosen due to its practicality and efficiency for low-power sensor networks. As mentioned in the literature review, the following equations are used to accurately simulate an MPPT connected to a PV cell where the value for K_1 ranges from 0.7-0.9 and K_2 ranges from 0.78-0.92 depending on the overall characteristics of the PV cell.

$$V_{MPP} \approx K_1 * V_{OC} \tag{11}$$

$$I_{MPP} \approx K_2 * I_{SC} \tag{12}$$

From [26], [33] and [36] it was concluded that the FOCV method was the best fit for low-power sensor networks with an accuracy rating of 96%, which is the value used in this simulation tool. Using the data gathered from the 2000 lux test on the amorphous PV cell, the MPP was 646.38 µW.

$$MPP_{CHARACTERIZED} * 0.96 \approx MPP_{SIMULATION} \tag{13}$$

$$646.38\ \mu W * 0.96 \approx 620.52\ \mu W \tag{14}$$

Using the template provided by the software, voltage, current and component size are all required values. For voltage, this allows the simulation to accurately predict the charge time of the supercapacitor which is heavily dependent on the incoming voltage of the EH device. The software allows the user to manipulate the size of the components. When characterizing a PV cell, the current increases linearly with the total area size of the cell. The simulation tool can then accurately predict the output current of a PV cell for varying sizes even if a PV cell with that particular size was not specifically characterized.

3.4 TEG

3.4.1 Introduction

Thermoelectric generators can be useful in generating power in applications where a lot of thermal energy is wasted. TEGs can be used to convert some of this energy into reusable electrical power. Applications like BEM can find great benefit in the use of TEGs, as residential and commercial buildings can provide a number of areas in which thermal energy is wasted, from low temperature gradients on walls and windows to high temperature gradients on radiators, water heaters and hot water pipes. TEGs can also be installed in wearable devices, vehicles, and industrial factories. If TEGs are installed in these areas, the wasted thermal energy can be captured and used to continuously power a WSN node.

This section will discuss how TEGs can be characterized, showing two different TEGs, how the simulation tool is able to read that data and what the simulation tool does with that data to accurately simulate power generated for a WSN. For varying degrees of temperature gradient, a Marlow Industries, Inc. TEG, TG12-4-01LS [76] and a Multicomp TEG, MCPE1-12706AC-S [77] were characterized and implemented into the software.

To fully utilize the low-voltage that is harvested by TEGs, either multiple TEGs are used in series or a boost converter can be used to raise the output voltage level of the device to allow it to power a WSN node.

3.4.2 Characterization

3.4.2.1 Test Setup

Similar to a PV cell, a TEG is also characterised using I-V and P-V curves to obtain a maximum power point. The circuit shown in figure 31, was used to characterize both TEGs. The aim of this characterisation was to see if a data template could be created where accurate WSN power results could be simulated for any TEG device that followed that data template.

For this test the temperature is only controlled on the hot side of the TEG which was placed atop a hot plate which could be varied in temperature while the cold side was attached to a heat sink for the purposes of maintaining a steady temperature difference between the two sides. To accurately read the temperature of each side of the TEG, thermocouples were attached to an Arduino which relayed the current temperature to a computer. For each temperature difference value a variable resistor was used to characterise an I-V curve, with a voltmeter and ammeter attached to the circuit. These results were then used to create a P-V curve.

A thermocouple, similar to a TEG, produces a temperature dependent voltage due to the thermoelectric effect. For a given thermocouple each voltage reading can be interpreted as a temperature reading allowing for constant temperature reading of both sides of the TEG. Figure 32 shows the lab equipment used to characterize each TEG.

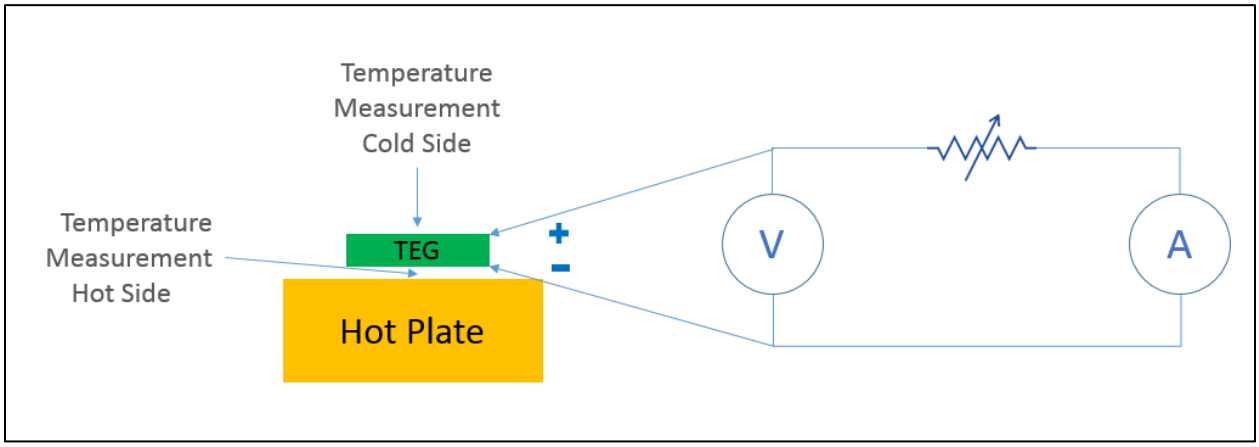


Figure 31: TEG Test Circuit

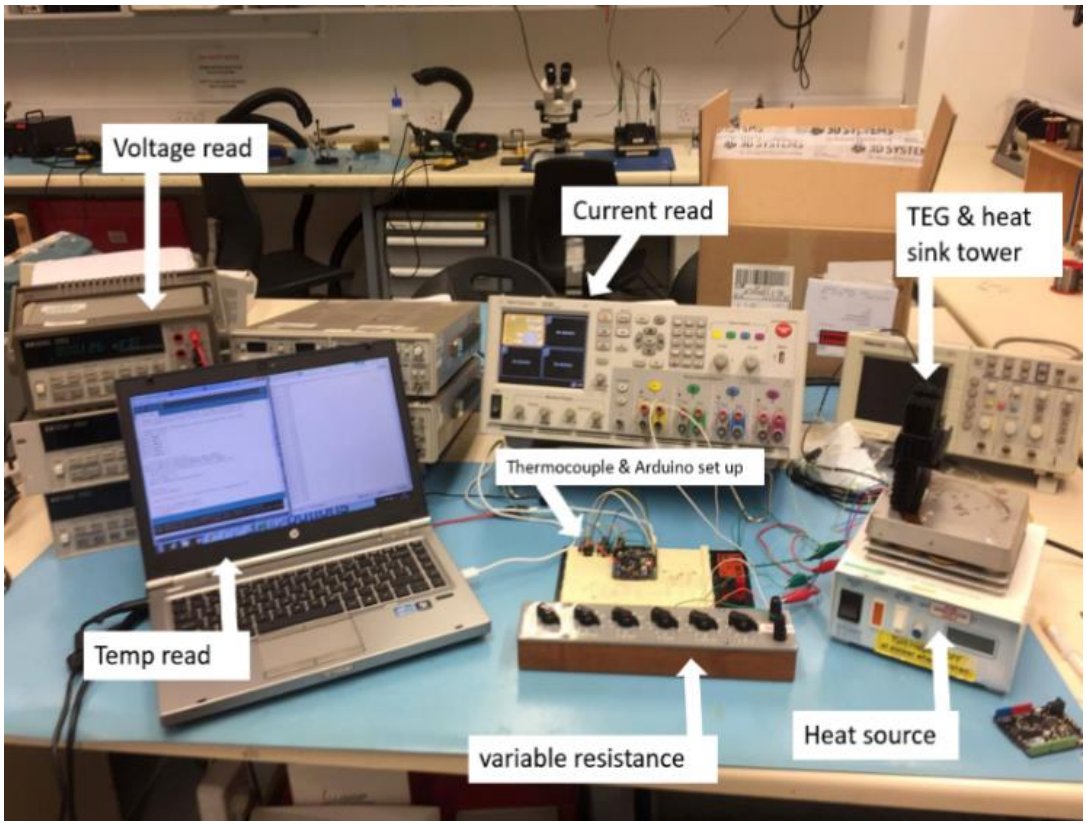


Figure 32: Lab Setup

3.4.2.2 TG12-4-01LS

Due to it being difficult to maintain a constant temperature difference between the two sides of the TEG, the data acquired can vary. The results presented in figure 33 is an I-V curve of a TEG with a temperature difference of 20 degrees Celsius. Compared to the PV cells presented in the previous section, it can be seen that TEGs produce a significantly higher amount of current which allows them to produce more power. However, the voltage generated is far lower than that of a PV cell. The hot plate was not 100% accurate when displaying the temperature and it was also difficult to steady the temperature on the TEG when varying the resistance.

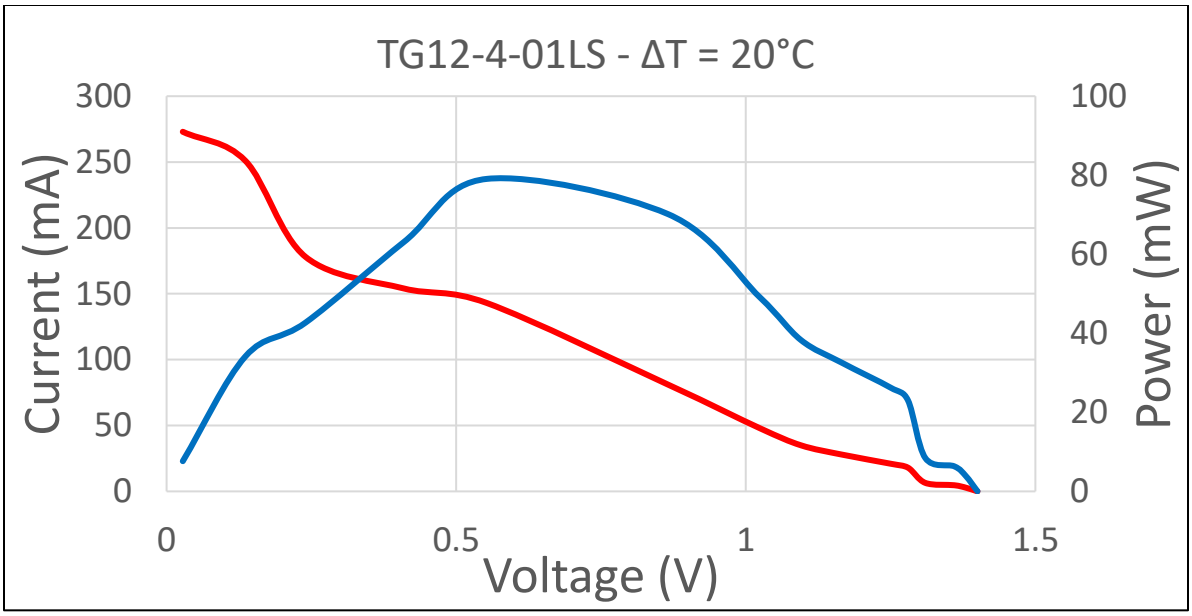


Figure 33: I-V & P-V Curve for TG12-4-01LS

Voltage	***Power***	***Current***
V	mW	mA
0.028	7.644	273
0.136	34.136	251
0.24	42.72	178
0.41	63.14	154
0.553	79.079	143
0.866	70.146	81
1.024	49.152	48
1.095	38.325	35

Voltage	***Power***	***Current***
V	mW	mA
1.165	32.62	28
1.25	26.25	21
1.28	23.04	18
1.31	8.4364	6.44
1.36	6.3376	4.66
1.38	3.8778	2.81
1.4	0.0224	0.016

Table 8: Results from IV curve (TG12-4-01LS)

Once all of the data is characterized for the TEG, the data template can then be completed. The TEG programmed into the simulation tool was characterized for temperature differences of 10, 15 and 20 degrees Celsius. Table 9 shows the data gathered from TG12-4-01LS.

Part Number :	TG12-4-01LS		
Size:	10cm^2		
Voltage	Current	Power	Temperature Difference
V	mA	mW	°C
0.192	64	12.288	10
0.25	103	25.75	15
0.553	143	79.079	20

Table 9: Data Template for TG12-4-01LS

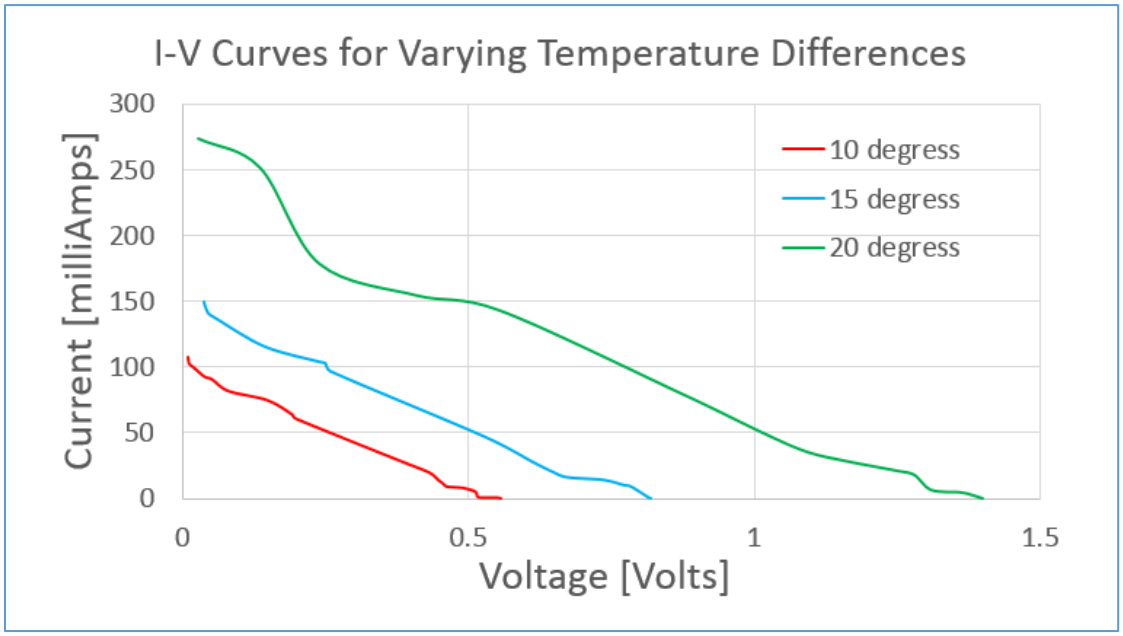


Figure 34: IV Curve for varying temperature differences (TG12-4-01LS)

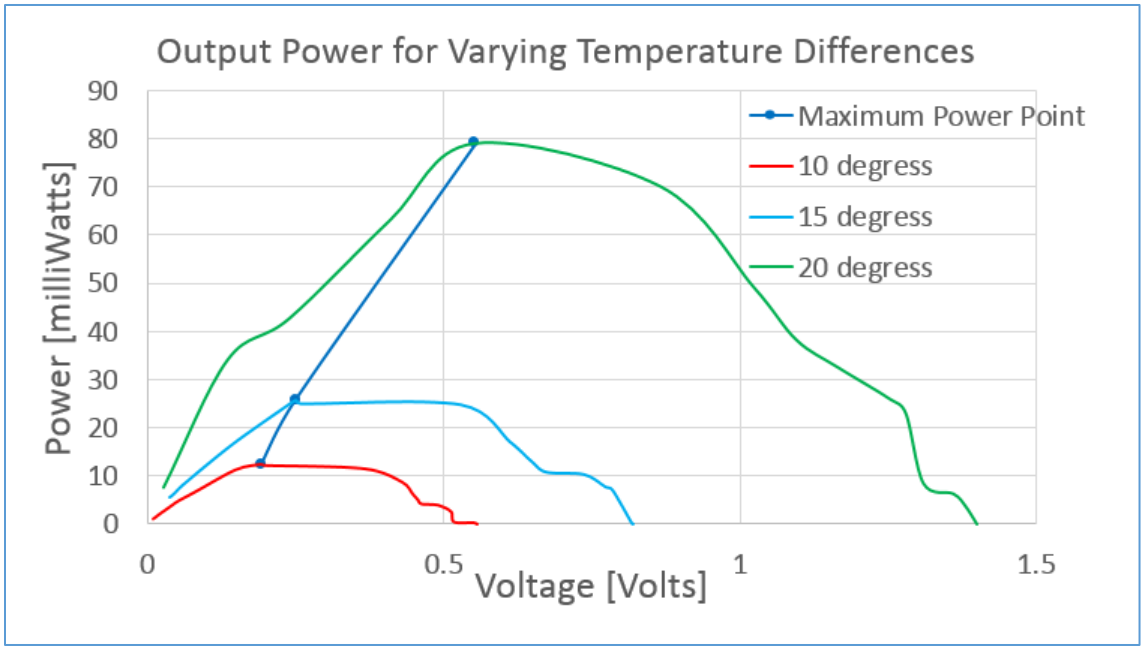


Figure 35: MPP for varying temperature differences

3.4.2.3 MCPE1-12706AC-S

MCPE1-12706AC-S was characterized under the same conditions and test equipment. These graphs and data tables are intended to allow a user to understand how the components are characterized and how the simulation tool handles that data, so when new components are added, the user can appropriately add their data to compare with different components.

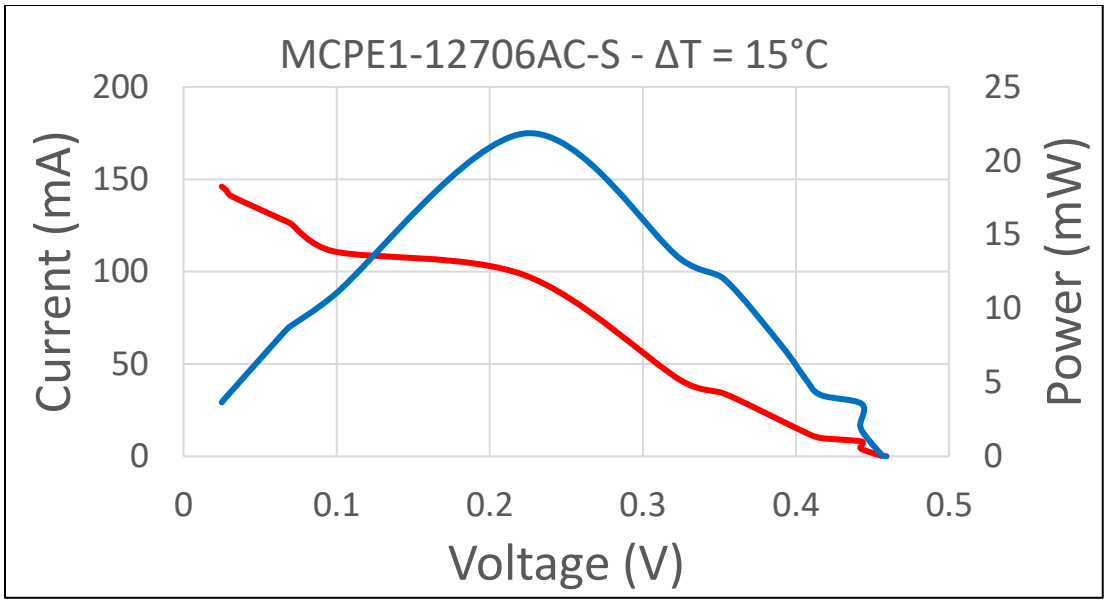


Figure 36: TEG I-V & P-V Curve

Voltage	***Power***	***Current***
V	mW	mA
0.025	3.65	146
0.028	4.032	144
0.031	4.371	141
0.065	8.32	128
0.07	8.82	126
0.098	10.878	111
0.223	21.854	98
0.325	13.325	41
0.353	12.002	34

Voltage	***Power***	***Current***
V	mW	mA
0.391	7.429	19
0.406	5.278	13
0.416	4.16	10
0.443	3.544	8
0.442	2.02878	4.59
0.448	1.04832	2.34
0.457	0.008683	0.019
0.459	0.003672	0.008

Table 10: Results from IV curve (MCPE1-12706AC-S)

3.4.2.4 MPPT for TEG

As previously mentioned in the introduction of this section, the voltage levels are too low to charge a supercapacitor. In the simulation tool, the user has the ability to add multiple TEGs in

series or parallel to boost the device's voltage or current respectively. For example, if 6 x TG12-4-01LS TEGs were used in series at 20°C temperature difference, the resultant output power to the energy storage device would be:

$$TEG_{VOLTAGE} \approx 0.553 * 6 \approx 3.3\,V \tag{15}$$

This would then increase the MPP of the device, using FOCV to:

$$3.3\ V * 143\,mA \approx 471.9\,m\text{W} \tag{16}$$

$$471.9\,mW * 0.96 \approx 453\,m\text{W} \tag{17}$$

Alternatively, if a user wanted to use a boost converter for their system instead of multiple TEGs, their output current would decrease. Using the efficiency equation for DC-DC converters, with an efficiency of 90% at this low voltage level and boosting it to 3.3 V, the simulation tool converts it as follows:

$$\eta \approx \frac{V_{OUT} * I_{OUT}}{V_{IN} * I_{IN}} \tag{18}$$

$$0.9 \approx \frac{3.3 * I_{OUT}}{0.553 * 0.143} \tag{19}$$

$$I_{OUT} \approx 21\,mA \tag{20}$$

When selecting components for an EH-WSN, there are always trade-offs with certain characteristics. This is why a simulation tool such as this can be very useful to accurately find the optimum components for different setups. With a known constant output voltage and current, the power transmitted to the energy storage device is:

$$P_{EH} \approx V_{OUT} * I_{OUT} \approx 69.3\,mW \tag{21}$$

3.5 Energy Storage Unit

3.5.1 Introduction

In this section, the energy storage units used in this simulation tool are explored. The simulation tool encompasses measuring the lifetime of a supercapacitor when used in conjunction with either an AA, AAA or coin cell battery. The research begins by studying the characteristics of a supercapacitor under different charging and discharging conditions. When simulating a supercapacitor, two things need to be taken into account to allow the system to be as accurate as possible, namely leakage current and equivalent series resistance (ESR). These simulations can then be compared to in-lab testing. The supercapacitor tested in this section was from the PowerStor PHB series [78], with a voltage rating of 5 V, a capacitance of 5 F and a leakage current of 25 μA.

3.5.2 Characterization

3.5.2.1 Equivalent Series Resistance

Knowing the ESR value of a supercapacitor at expected operating conditions can help determine the suitability of a supercapacitor for a given WSN. ESR is one of the non-ideal characteristics of a supercapacitor which has a direct impact on the performance of the device and depending on the size of the ESR value, can cause huge problems when dealing with I^2R losses as well as transients.

In an EH application, the supercapacitor needs to take charge from low-power transducers and efficiently convert that stored energy to power a load. Having a supercapacitor with a high ESR will have a negative effect in efficiently converting power as some of that power will be lost to heat in the circuit. The bigger the load transients, the larger the voltage drop on the supercapacitor. If the voltage drop is too big, it could dip below a threshold voltage and no longer maintain power at the load.

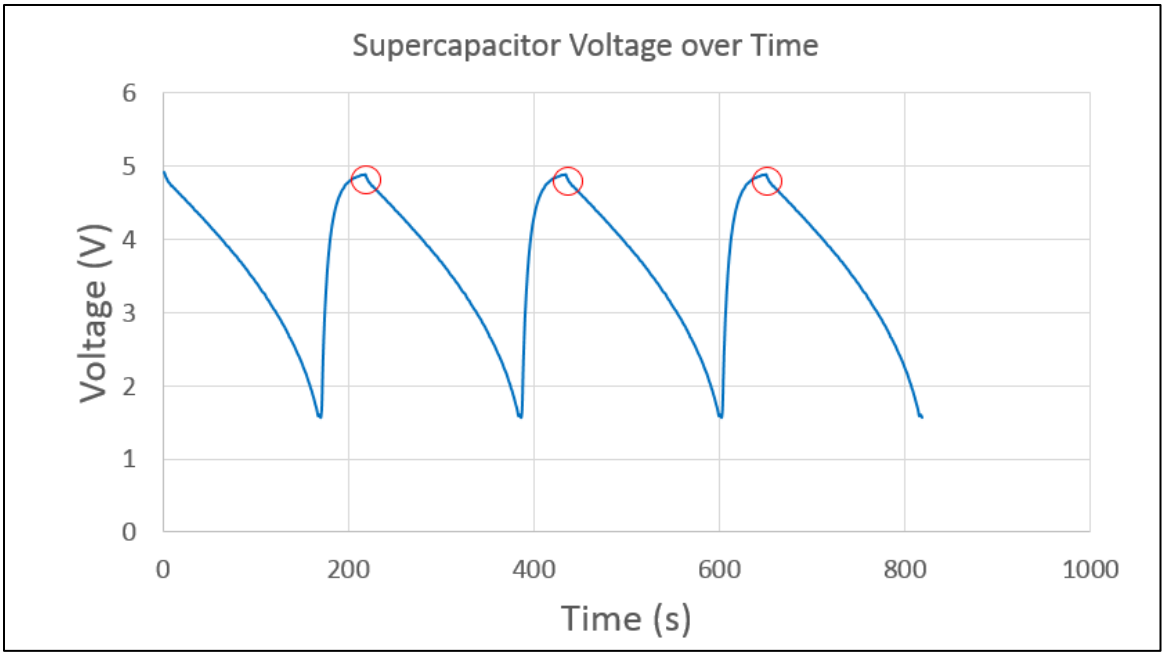


Figure 37: ESR effect on real-world test

The PowerStor supercapacitor was tested to evaluate the ESR value of the device. The supercapacitor was placed in a circuit supplying a load with 67.7mA. For a more detailed description of the test setup and equipment used see section 4. The supercapacitor was also connected to a Bluno V2 board [79] which recorded the voltage level across it and stored that data on a laptop. The supercapacitor, starting from a charged state began to supply 67.7mA until it reached the minimum input voltage level of the DC-DC converter. A switch was implemented to disconnect it from the load and allow it to charge up until it reached 4.89 V and was then reconnected with the load. Figure 37 shows a voltage drop, indicated with the red circles, in the supercapacitor from 4.89 V to 4.8 V due to the load transient of switching from charging to discharging.

$$ESR \approx \frac{Voltage\ Drop}{Current} \approx \frac{4.89-4.8}{0.0675} \approx 1.33\ \Omega \quad (22)$$

$$P_{ESR} \approx I(t)_{SC}^{2} * ESR \quad (23)$$

When deciding which supercapacitor to use when designing an EH-WSN, it is critical to choose a supercapacitor with as low an ESR value as possible. If the voltage drop is too high for a given ESR value, it could result in the voltage in the supercapacitor dropping below a minimum voltage and not being able to provide power to the sensor node.

3.5.2.2 Leakage Current

Another consideration when selecting an energy storage component is its leakage current. Usually this value is included with the data sheet of the component. This value can then be used to calculate the power leakage of the supercapacitor using the following equation where P_{LEAK} is the power leakage and V_{SC} is the voltage in the supercapacitor:

$$P_{LEAK} \approx V(t)_{SC} * I_{LEAKAGE} \quad (24)$$

The supercapacitor described above can be imported into the simulation tool using the data template accompanying the software. The characteristics can be filled out as follows:

Part Number :	PowerStor PHB		
Rated Voltage	Capacitance	ESR	Leakage
V	F	Ω	A
5	5	1.33	0.000025

Table 11: Data Template for PowerStor supercapacitor

3.5.2.3 Charge

Using the values discussed in this section, a simulation model to charge a supercapacitor can be created. Taking into account the initial energy of the supercapacitor, the power being generated by the EH transducer, the leakage power and the ESR power losses, equation 25 can simulate a charging supercapacitor.

$$E(t)_{SC} \approx E(initial)_{SC} + \int_0^t (P_{EH} - P_{LEAK} - P_{ESR})\, dt \quad (25)$$

To test this equation, each energy value was converted to voltage, graphed over time and compared to a real-world test.

A circuit schematic of the test can be seen in figure 38.

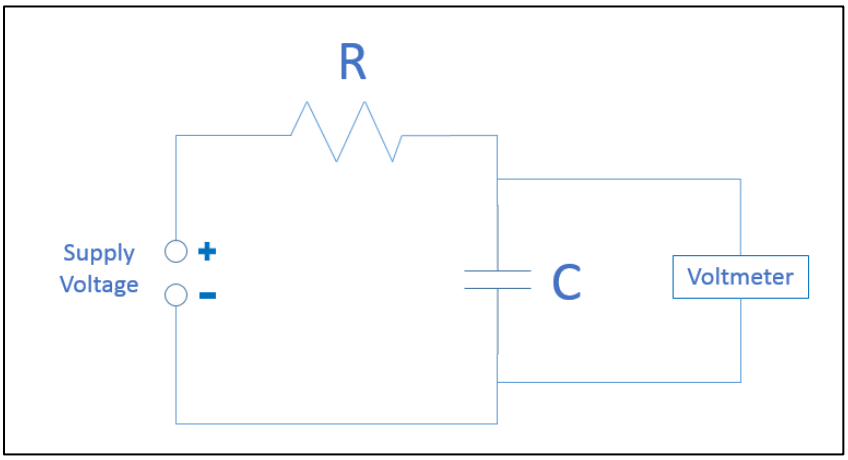


Figure 38: Charge Circuit

To measure the accuracy of this equation, a test was conducted on a supercapacitor and the results were gathered and compared with the simulation tool. Figure 39 shows the real-world test results in comparison to the simulation of a supercapacitor with a rated voltage of 5V, capacitance of 5F, leakage current of 25µA and ESR of 1.33Ω. The supply voltage was 4.9 V and resistance in the circuit was 32.77 Ω.

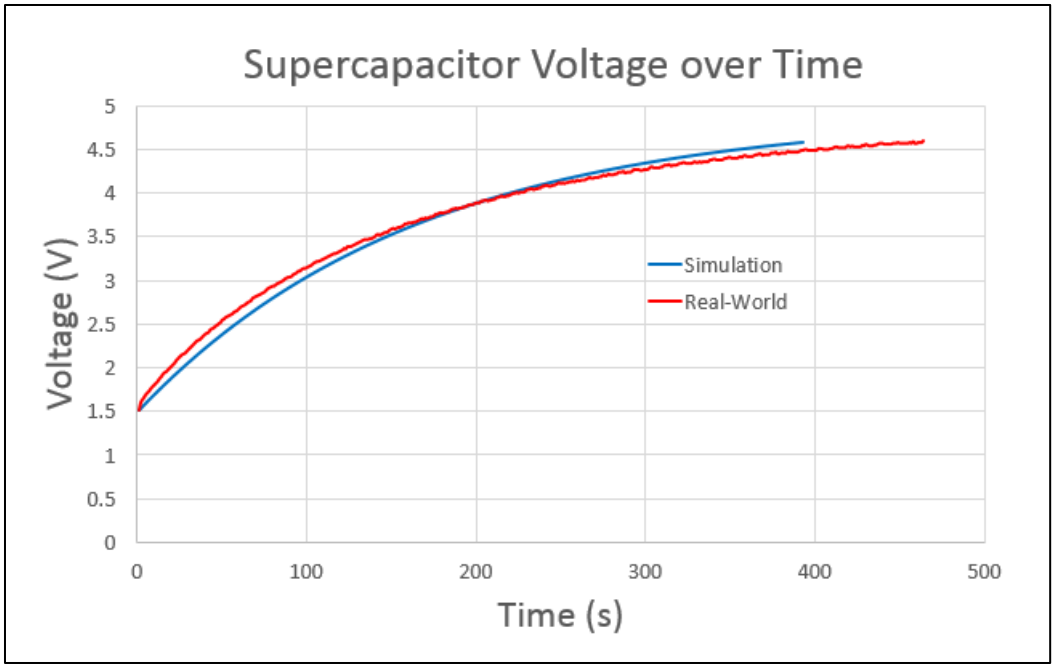


Figure 39: Charge Comparison between Real-World and Simulation

It can be seen from the graph that the simulation shows a highly consistent result with the real-world measurement, however, additional work to the simulation could be made in order to improve the accuracy. An accurate depiction of a real-world supercapacitor is essential to an EH-WSN simulation tool. Section 4 of this thesis will demonstrate the simulation tool's capabilities in simulating a discharging supercapacitor as it powers a WSN.

3.5.2.4 Batteries

Features such as wide input voltage range, low ESR, wide temperature range and large number of charge cycles without degradation, render supercapacitors a more eco-friendly option to power WSN as opposed to batteries. However, their lower energy density and leakage current, means that batteries are still an essential part in many WSN applications. In this simulation tool, these two types of energy storage devices are working together. When ambient energy is available, EH transducers can simultaneously power a WSN and charge a supercapacitor. Once the ambient energy is no longer available and the supercapacitor is depleted, a battery is necessary to maintain constant power to the load. This software includes three types of batteries

at different amp-hour ratings. Batteries can be used with different materials which leads to different ratings, however to keep it simple, the values used in this software are an average value.

Battery Type	Capacity (mAh)
AAA	1000
AA	2000
Coin cell	200

Table 12: Battery Capacity

These batteries have a voltage rating of 1.5 V. If a WSN is rated higher than 1.5 V, additional batteries would be required to power the device, or the use of a boost converter would be implemented.

Throughout the simulation, the battery and supercapacitor are switching back and forth as the primary power source for the WSN. The point at which these two storage devices are switching is completely determined by the user. Once the simulation has run for a 168-hour week, the software adds the total time at which the battery was the primary source. First it calculates the lifetime of the WSN using solely the battery.

$$Battery\ Lifetime \approx \frac{Battery\ Capacity}{Device\ Consumption} * 0.7 \quad (26)$$

The 0.7 value is added to make allowances for external factors which can affect battery life such as temperature, load transients and self-leakage. This value was chosen after surveying multiple online battery calculators [62] [63]. Once complete, the software divides the total capacity lifetime, with the amount of time spent powering the device throughout the week. This gives a total WSN lifetime value using a supercapacitor-battery hybrid to power an EH-WSN.

3.6 Power Management

3.6.1 Introduction

The voltage on the supercapacitor in the device is constantly varying, which means that additional circuitry is required to deliver a steady source. For supercapacitors to become useful in these circuits, a DC-DC converter is required to either increase the voltage of supercapacitor or decrease the voltage to the operating voltage of the sensor node. A boost converter can increase the voltage while a buck converter decreases it. The use of DC-DC converter results in the supercapacitor powering a load with steady voltage.

3.6.2 DC-DC Converter

A DC-to-DC converter is an electronic circuit that converts the voltage level on the input to another on the output. DC-DC converters are essential for EH-WSNs to provide a constant stable voltage at the sensor node, as the voltage in the energy storage unit varies. Low-dropout (LDO) regulators can also be used in these circuits, with the advantage of them being that they produce no switching noise as no switching takes place. The disadvantage of LDOs over switching DC-DC converters is that they can only step down voltage, with the reduction of the input and output voltages being removed as heat. If switching DC-DC converters are used the energy transfer from the supercapacitor to the load can be done with high efficiency. Depending on the type of DC-DC converter, each device has a different range of voltages at which the converter can no longer convert that input voltage to the specified output voltage. The efficiency rating of a DC-DC converter is very important when deciding which converter to use. The efficiency of a DC-DC converter can be defined by this equation:

$$\eta \approx \frac{Voltage_{OUT} * Current_{OUT}}{Voltage_{IN} * Current_{IN}} \quad (27)$$

However, the efficiency can vary as the input voltage varies. The DC-DC converter included in this simulation tool is the TPS63020. Its minimum and maximum threshold input voltages are 1.8 and 5.5 V respectively, with an adjustable output voltage of 1.2 to 5.5 V. It is a buck-boost converter with an operating quiescent current of 25µA. A block diagram of this circuit can be seen in figure 42.

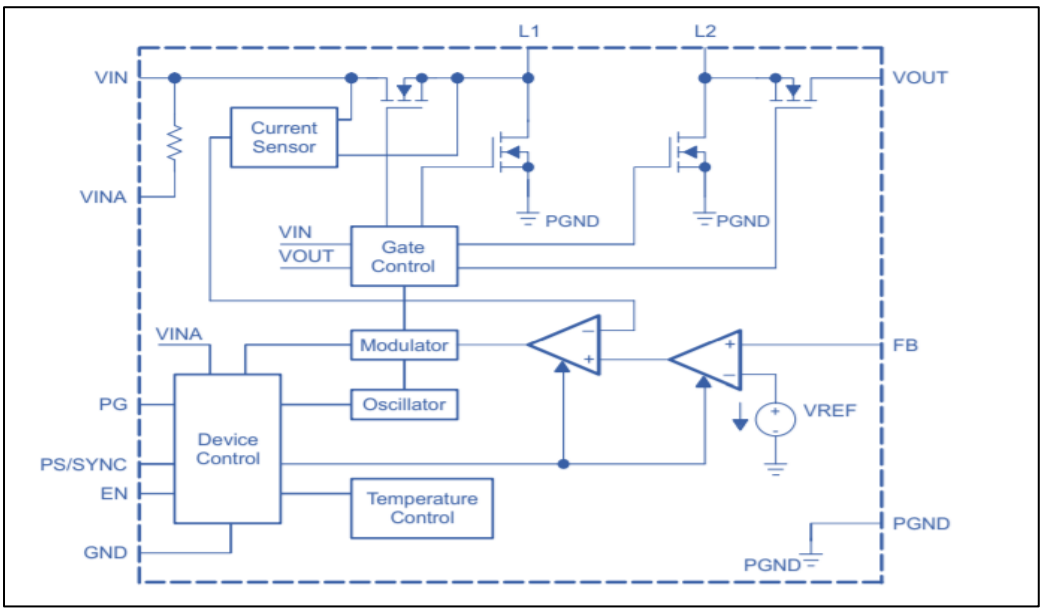


Figure 40: TPS63020 Block Diagram [80]

The varying efficiencies of this converter at different input voltage levels as the output current varies was given in the datasheet as is represented in figure 43.

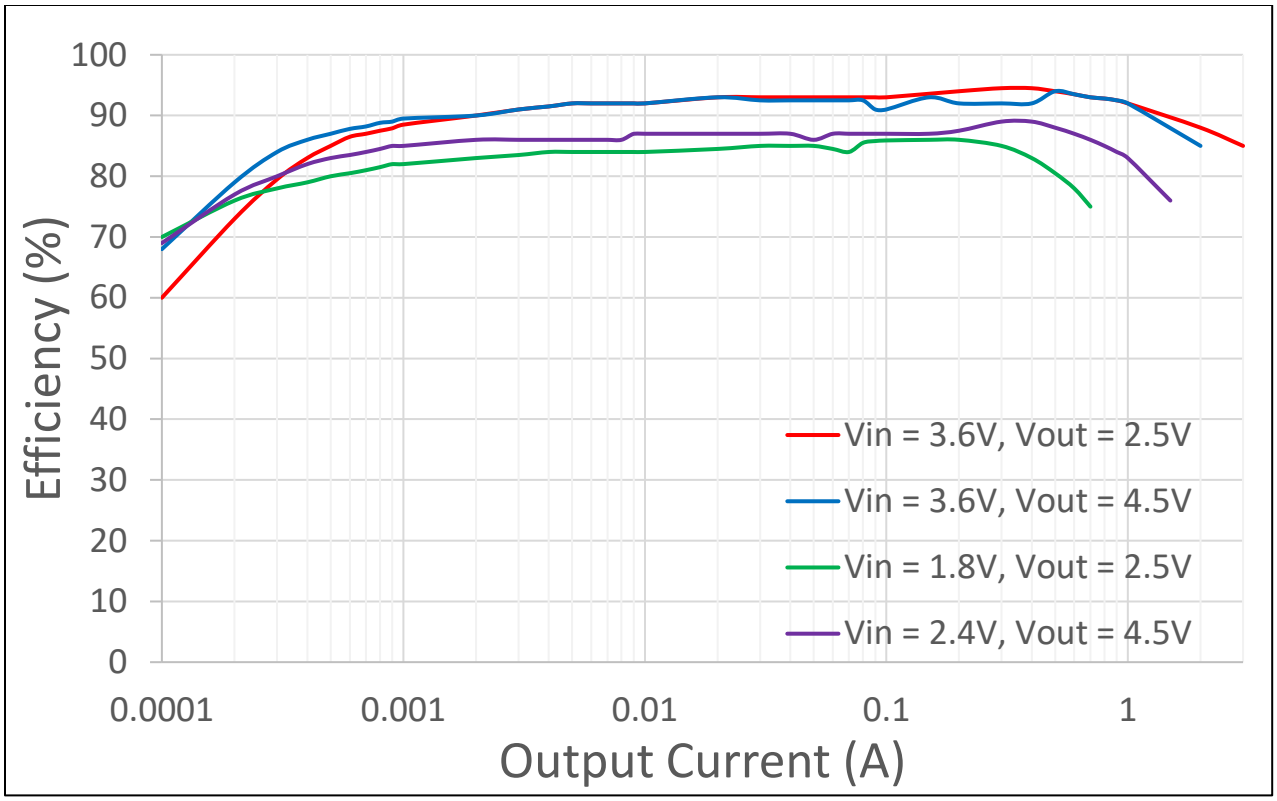


Figure 41: TPS63020 - Efficiency vs. Output Current [80]

This data can be implemented into the software as follows:

Efficiency	Output Current
%	A
60	0.0001
85	0.001
88	0.01
90	0.1
85	1

Table 13: Data Template for TPS63020 Efficiency

The efficiencies in the table above are an average value of the different voltages as importing values for each individual voltage level at each output current would not have large enough effect on the overall simulation to warrant that level of detail into the characteristics.

As the efficiency varies, the maximum output current that the DC-DC converter can provide also varies. These values are required when designing a simulation tool to ensure that the load at the output does not require a current level that exceeds the maximum current output for a given

input voltage. A graph detailing this maximum current was given in the datasheet and represented in figure 44.

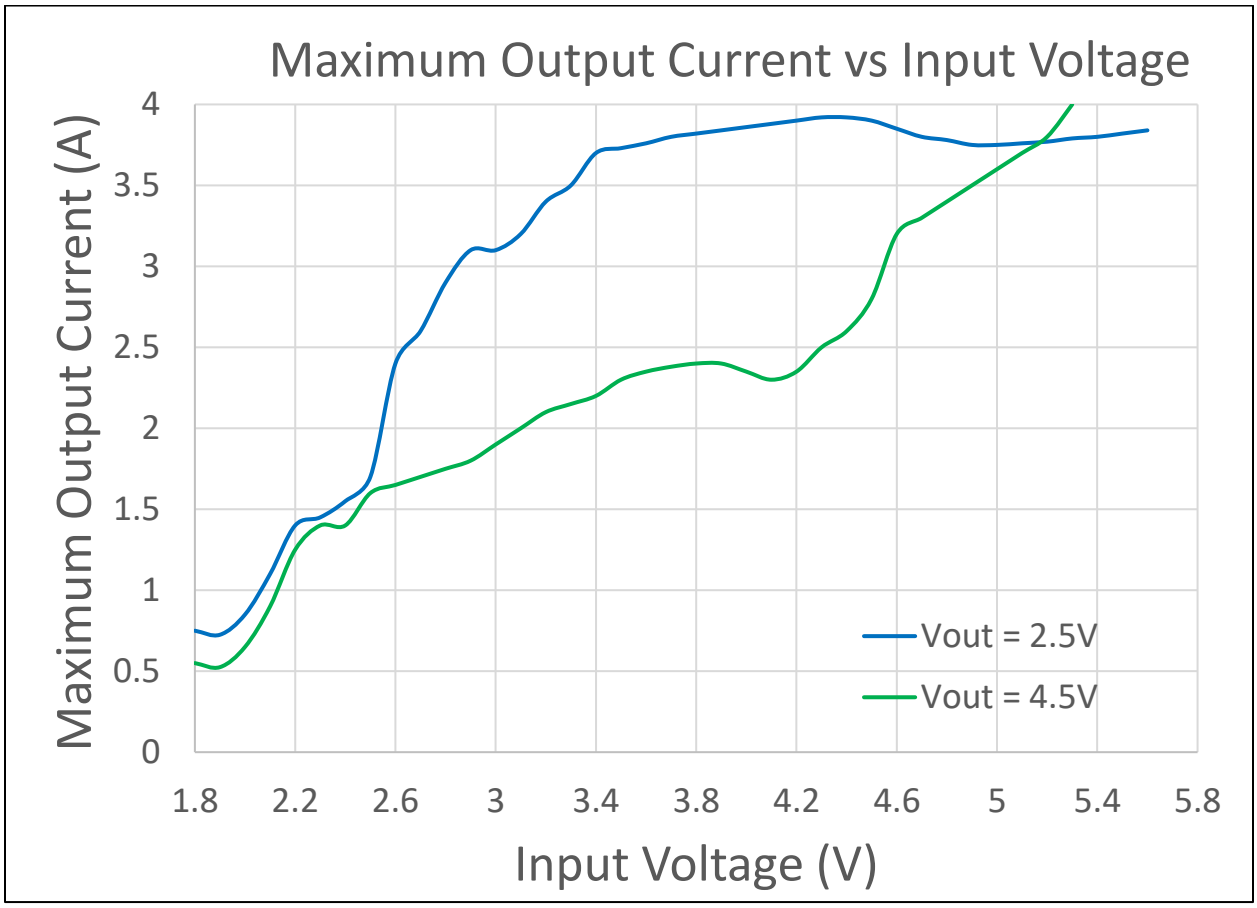


Figure 42: TPS63020 Max Output Current vs. Input Voltage [80]

The maximum and minimum threshold voltage levels can be imported into the system with their corresponding maximum current value in the following table:

Part Number :	TPS63020
Output Voltage :	4.5 V
Input Voltage	Maximum Output Current
V	A
1.8	0.55
2.2	1.25
2.6	1.65
3	1.9
3.4	2.2
3.8	2.4
4.2	2.35
4.6	3.2
5	3.65
5.4	4.2

Table 14: Data Template for TPS63020 [80]

This will allow the simulation tool to determine when to notify the user if their system would stop working if the sensor node was no longer supplied power due to the cutoff point of the DC-DC converter. This is also crucial when factoring in leakage current when the EH is no longer supplying power to the supercapacitor. If a PV cell was being used to harvest energy, long periods where the EH could not harvest the light energy can occur. With the supercapacitor not being supplied power, a power losses over time will occur. This power availability drop due to the leakage current can be calculated using equation 24.

The simulation assumes a linear transfer function when determining leakage to allow for easier functionality when using different supercapacitor types and sizes. In reality a supercapacitor's leakage would be initially high but then taper off after several hours. With PV cells, they cannot convert energy when the lights are off. As DC-DC converters have minimum input voltages, it is important to factor in the voltage drop in the supercapacitor over time when selecting each component. For example, the TPS63020 has a minimum input voltage of 1.8 V. If a supercapacitor had a voltage drop of 0.2 V overnight, the system should allow the supercapacitor to charge when it reaches 2 V. The battery should turn on and power the sensor node, so that when light energy is available again, the supercapacitor can immediately power the sensor node without having to initially charge up to the minimum input voltage of the DC-DC converter.

3.7 Sensor

3.7.1 Introduction

The main goal of this project was to be able to accurately simulate a WSN lifetime for any device. For any user specified device, the simulation will calculate the lifetime of the device using the components specified. This section will look at how the simulation tool takes in sensor node characteristics.

3.7.2 Characterization

A typical WSN sensor node has multiple power requirements for different actions that it must do to ensure data gathering and processing is complete.

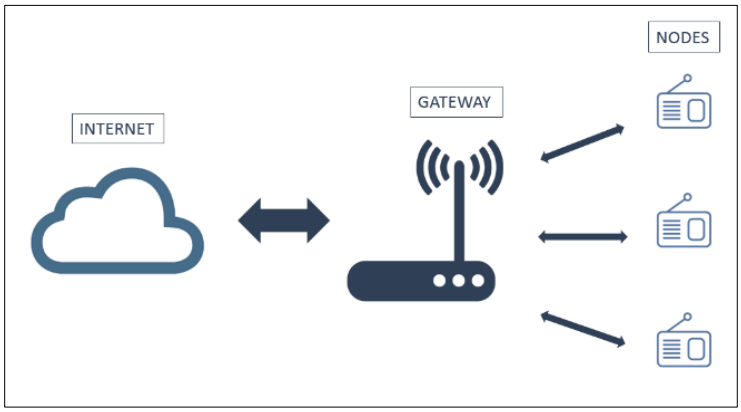


Figure 43: Full WSN

Communicating with a gateway periodically means that each sensor node must have receiving and transmitting capabilities which often have different power requirements. There is also sleep and active modes for different duty cycles. Sometimes the device may need to measure every few seconds as opposed to every minute which drastically changes the current consumption. All of this can be complex and very device specific which makes it difficult to simulate during different modes of operation. Modelling the complex power profile of wireless sensor nodes was beyond the scope of the project, but an area for further research. The approach taken to ensure

that the simulation tool could be used over as wide a range of devices as possible was to take an average power consumption value that is taken over at least one cycle of transmit, sleep and receive. Additions to the software such as these will be discussed in the Future Work section of this thesis.

Equation 28 is used to simulate the operation of an EH-WSN; it combines the power requirements of the node with the operating efficiencies of the DC-DC converter.

$$DC - DC\ converter\ efficiency \approx \frac{Power_{Required\ by\ Sensor}}{Power_{\ From\ SC}} \tag{28}$$

For example, a sensor node that operates at 3.3 V and requires 10mA of current using a DC-DC converter with 90% efficiency results in:

$$Power_{\ From\ SC} \approx P_{WSN} \approx \frac{3.3*0.01}{0.9} \approx 36.67\ mW \tag{29}$$

Every building block of an EH-WSN has been explained, characterized and modelled. Based on those characterizations, the simulation tool can simplify and summarize an energy flow model using the following equation:

$$E(t)_{SC} \approx E(initial)_{SC} + \int_0^t (P_{EH} - P_{WSN} - P_{LEAK} - P_{ESR})\ dt \tag{30}$$

Where $E(t)_{SC}$ is the amount of energy in the supercapacitor at any given time,

$E(initial)_{SC}$ is the initial energy is the supercapacitor at the start of the simulation,

P_{EH}, P_{WSN} and P_{LEAK} are the energy harvesting power, WSN power and the supercapacitor leakage power respectively.

3.8 Summary

This chapter went into detail of each the components used in a EH-WSN and how they are characterized and used in the simulation tool. By adjusting the parameters of the components in the simulation tool, the user can find the optimum power setup for their device. In the next chapter, a comparison between a real-world WSN device and a simulation will be made.

4 Measurement vs. Simulation

4.1 Introduction

In this final chapter, a comparison between the simulation tool and a real-world test will be made. The sensor node used in the real-world simulation was a “LoPy4 Pycom” [81] device. The LoPy4 is a compact quadruple network MicroPython enabled development board with the ability to communicate using Wi-Fi, Bluetooth, Sigfox and LoRa. The device was connected to a supercapacitor, through a DC-DC converter, and a power supply. The supercapacitor was initially fully charged while it powered the device. Once the supercapacitor reached the minimum input voltage of the DC-DC converter, a switch was implemented to begin charging the supercapacitor to a turn-on voltage determined before the test while the LoPy4 device was no longer receiving power from the supercapacitor. While in this test, the device was switched off when the supercapacitor was charging, in a deployable WSN, the device will never lose power as a battery is used to continue powering the load.

4.2 Comparison



Figure 44: LoPy4 Pycom Device [81]

During the test, circuit diagram in figure 47, the LoPy4 was programmed to operate at 90mA. This was achieved by switching off the Wi-Fi, Bluetooth and Sigfox capabilities, leaving the LoRa as the only open communication channel. LoRa (Long-Range) is a low-power wide-area network

technology. This communication protocol enables long-range transmissions with low-power consumption. This device was connected to a supercapacitor which was then connected to a power supply. The goal of this test was to measure the voltage of the supercapacitor as it charged and discharged to compare with a simulated test under the same conditions. The voltage across the supercapacitor was recorded using a Bluno V2.0 board which was connected to a laptop via a USB cable. The voltage data was stored and graphed once the test was complete. The Bluno V2.0 board recorded the voltage over time with a ±0.15V error rate.

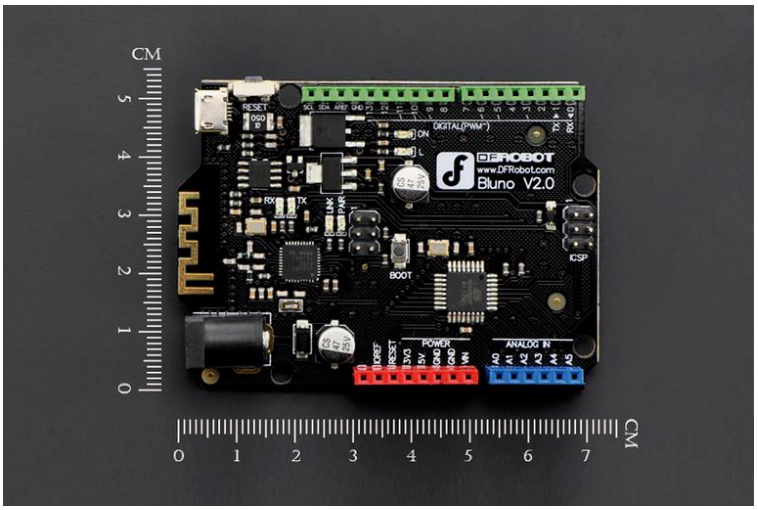


Figure 45: Bluno V2.0 [79]

While in the performed test there was no battery, the test was performed to imitate this circuit where the load was constantly powered. The PowerStor PHB supercapacitor was the same component hardcoded into the simulation which was described in the previous chapter. To mimic a TPS63020, a commercial evaluation board was used, TPS63020evm-487. This evaluation board took the voltage in the supercapacitor and converted it to 3.3 V as required by the LoPy4.

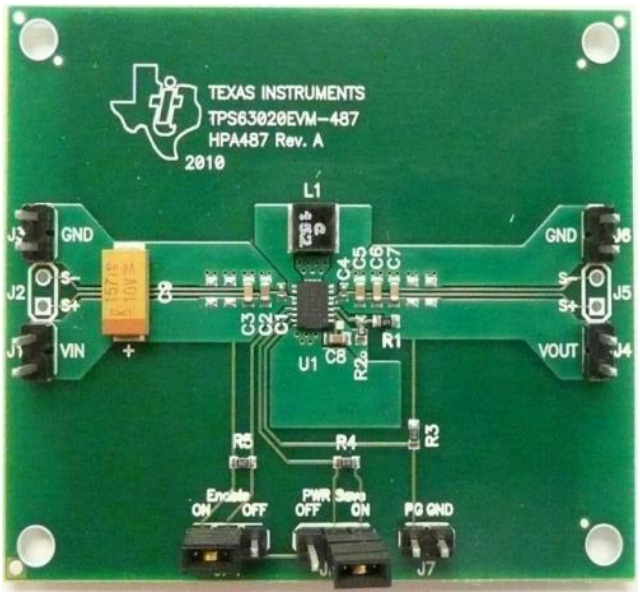


Figure 46: TPS63020evm-487 [82]

The power supply connected to the supercapacitor was set to 5 V with a 32Ω resistor attached. The value for the resistor was chosen after using equation 7 to calculate the time needed to charge the supercapacitor using a 5 V power supply. The desire was to have the charge time of the supercapacitor be similar to the discharge time so as to fit as many data points on to the graph. The circuit diagram for the entire setup can be seen in figure 49 while a picture showing the setup can be seen in figure 48.

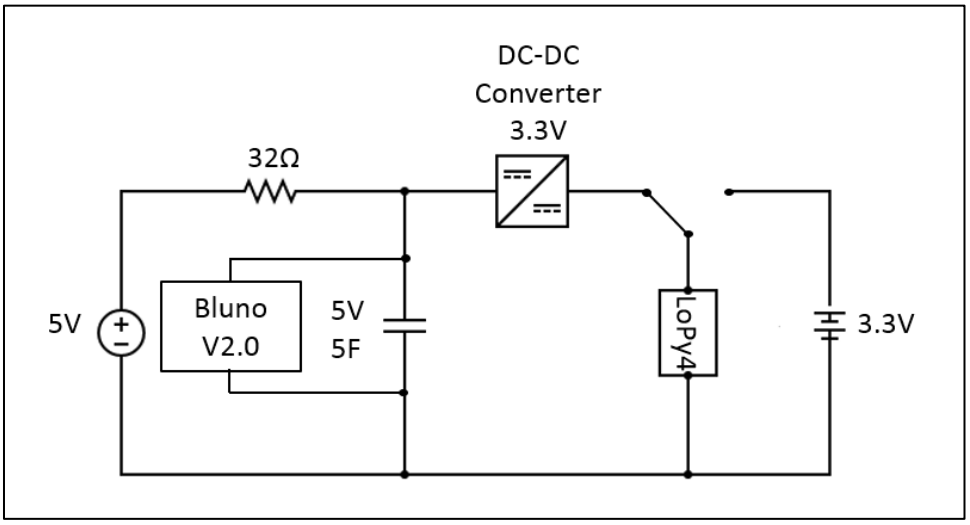


Figure 47: Test Circuit

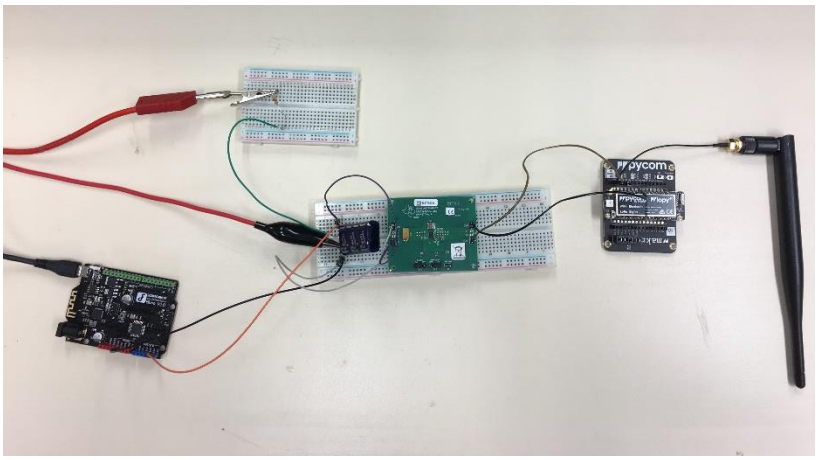


Figure 48: Lab Setup Circuit

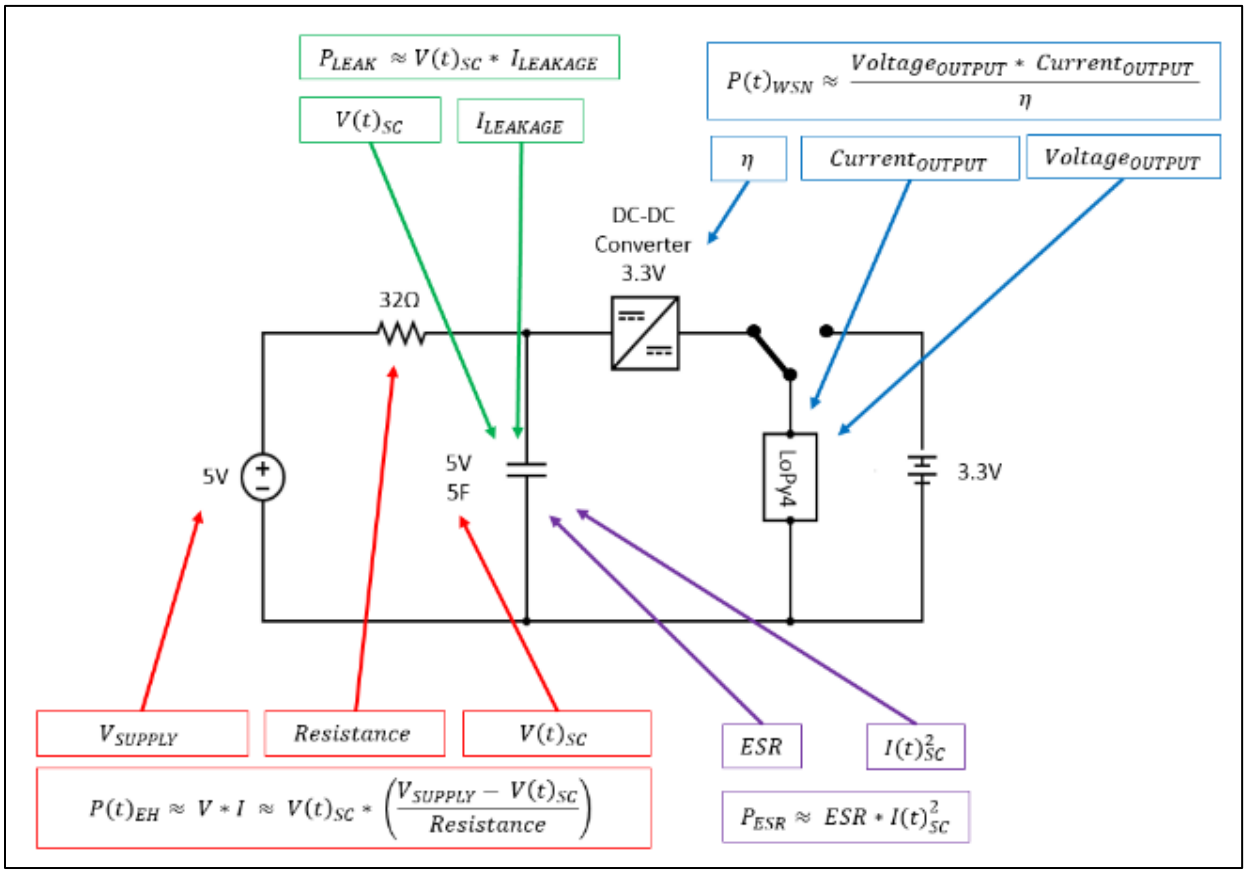


Figure 49: Circuit - Equation Block Diagram

4.3 Governing Energy Equation

Equation 30 is the governing energy equation used in the simulation to describe and predict the results of the real-world test. The following set of equations will show how the different parameters are used in that equation.

Power is a product of current multiplied by voltage. With the voltage constantly varying, so too was the supply current.

$$P(t)_{EH} \approx V * I \approx V(t)_{SC} * I(t)_R \approx V(t)_{SC} * \left(\frac{Supply\ Voltage - V(t)_{SC}}{Resistance}\right) \quad (31)$$

Where $V(t)_{SC}$ is the voltage across the supercapacitor over time.

Using the buck boost evaluation board DC-DC converter, the current and voltage supplied at the input also needed to be calculated. With efficiency losses in the DC-DC converter, more power needs to be supplied than is required by the end sensor node. The LoPy4 was set at 3.3 V consuming 90 mA. Using the efficiency equation for DC-DC converter, with the known voltage across the supercapacitor, the current supplied by the supercapacitor can be acquired.

$$\eta \approx \frac{Voltage_{OUTPUT} * Current_{OUTPUT}}{Voltage_{INPUT} * Current_{INPUT}} \quad (32)$$

However, as discussed previously the efficiency of the DC-DC converter is dependent on the output current and the input voltage. Using the information gathered from the datasheet, the efficiency could be calculated.

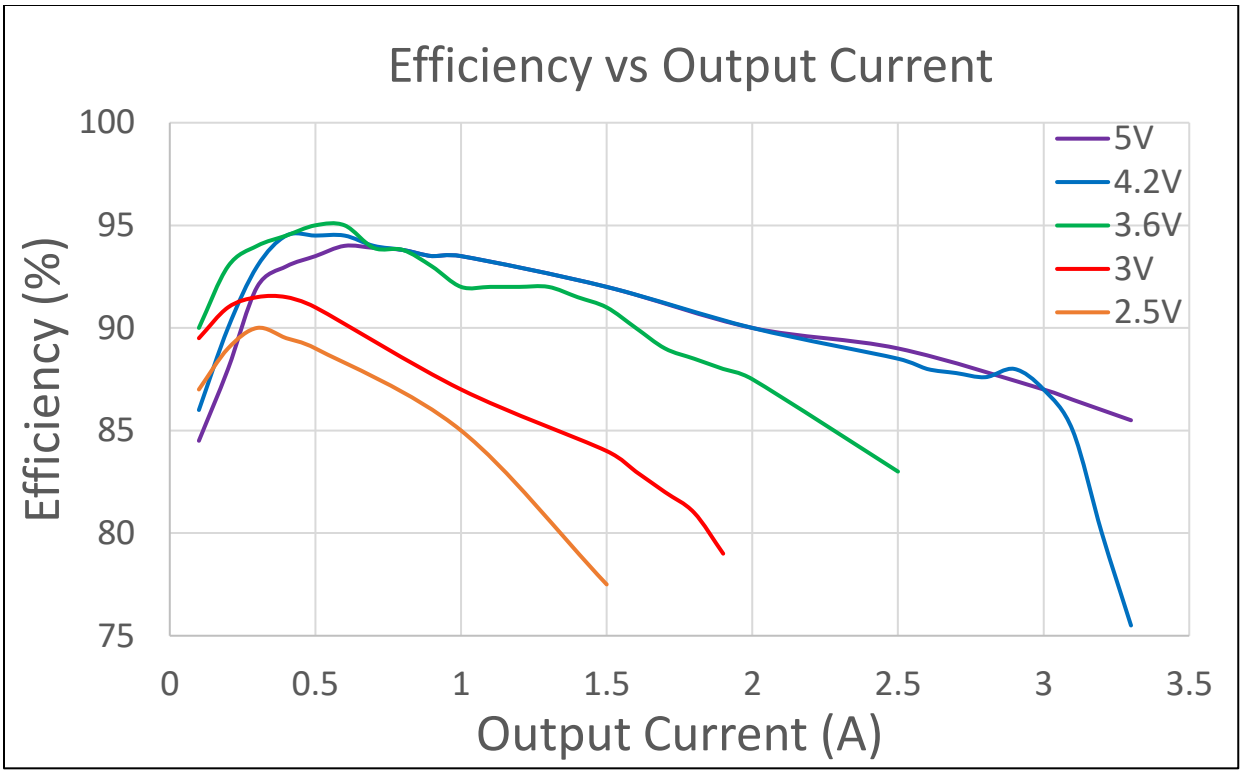


Figure 50: Efficiency vs Output Current for a range of input voltages [82]

At 90 mA with a set output voltage of 3.3 V, the constant WSN power required is 297 mW. As the efficiency of the converter changes, the input power required by the DC-DC converter to maintain 297 mW changes. Using figure 50 a table was made to store the varying efficiencies of the DC-DC converter. This data table is used to maintain accuracy in the simulation by simulating the correct input power required by the LoPy4 as the efficiency of the DC-DC converter changes.

Input Voltage Range (V)	Efficiency (%)
5 – 4.2	84.5
4.2 – 3.6	86
3.6 - 3	90
>3	89.5

Table 15: Efficiency for different Input Voltages

These numbers can then be used to calculate the power supplied by the supercapacitor. Rearranging equation 32,

$$P(t)_{WSN} \approx \frac{Voltage_{OUTPUT} * Current_{OUTPUT}}{\eta} \quad (33)$$

Efficiency (%)	Power Input (mW)
84.5	351.5
86	345.3
90	330
89.5	332

Table 16: Input Power at different efficiencies

From the previous chapter, the leakage current of this supercapacitor is 25 µA. Using equation 24, the leakage power can be calculated.

Power dissipation due to ESR in the supercapacitor can be calculated by multiplying the ESR value by the square of the supercapacitor's operating current as shown in equation 23.

When the supercapacitor has reached its minimum energy availability, the load is disconnected from the DC-DC converter, allowing the supercapacitor to recharge. The "pycom" is switched to receive power from the battery. Using the circuit presented in figure 49, it can be seen that when the load is disconnected, the DC-DC converter still receives current in the form of quiescent current and the supercapacitor continues to have leakage and ESR losses. This change in current is accounted for in equations 34, 35 and 36.

$$P(t)_{EH} \approx V(t)_{SC} * \left(\frac{V_{SUPPLY} - V(t)_{SC}}{Resistance} - I_{DC-DC\ Quiescent}\right) \quad (34)$$

$$P(t)_{WSN} \approx 0 \quad (35)$$

$$P(t)_{ESR} \approx ESR * \left(\frac{V_{supply} - V(t)_{SC}}{Resistance} - I_{DC-DC\ Quiescent} - I_{LEAK}\right)^2 \quad (36)$$

$P(t)_{LEAK}$ during this period is still governed by equation 24.

From there, equation 37 is used to calculate the voltage in the supercapacitor and then graphed over time to allow the user to continually refine the component parameters in the software.

This is done by rearranging equation 6.

$$V(t)_{SC} \approx \sqrt{\frac{2*E(t)_{SC}}{C}} \quad (37)$$

4.4 Results

Using the minimum voltage specifications from the DC-DC converter of 1.52 V, the supercapacitor was disconnected from the load and allowed to recharge once it reached that level. It would then switch back to powering the device once it reached 4.6 V. Using these equations, the results from the simulation were gathered and compared to the real-life test in the following graph.

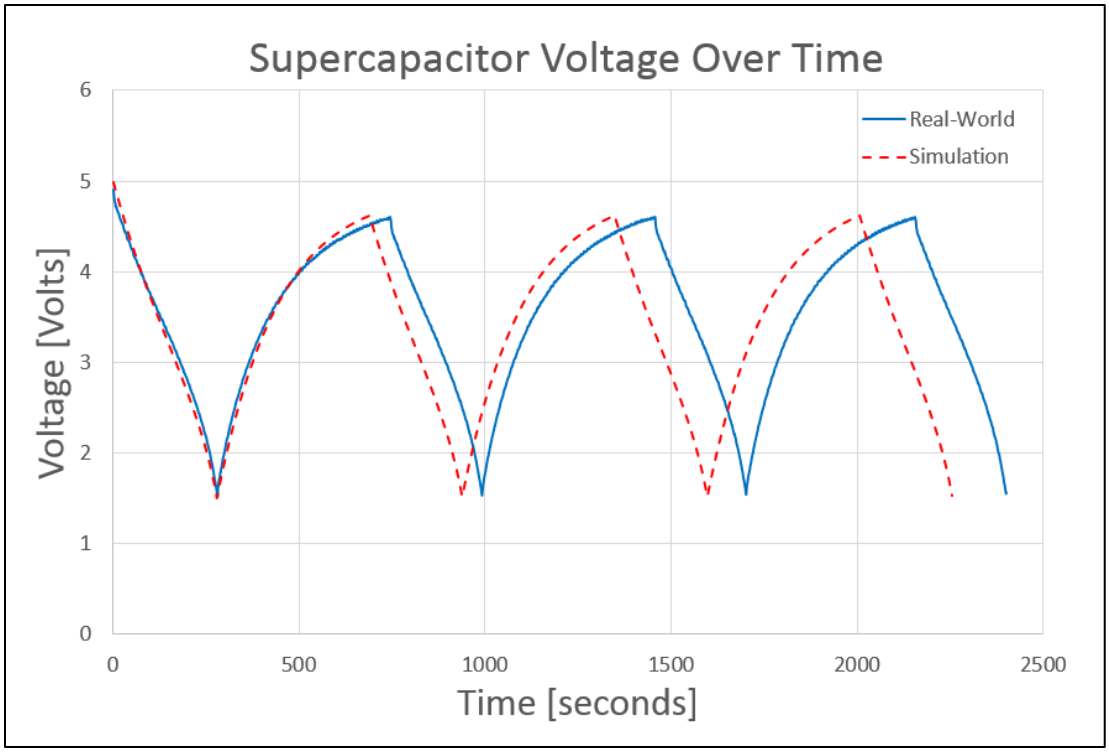


Figure 51: Real-World vs. Simulation

Figure 51 shows the voltage over time in the supercapacitor for both the real-world and the simulated test as it charges and discharges. Based on these results, table 17 and 18 show that the simulation was able to match the supercapacitors discharge profile with 98.9% accuracy while the charge profile predicts with an 89.5% degree of accuracy. In both instances the general shape of the charge/discharge curve looks good except when charging between around 4 and 4.5V which also creates a net error in the predicted time constant that accumulates with each simulated cycle.

Charge Cycle Number	Real-World Time (s)	Simulation Time (s)
1	462	411
2	462	411
3	453	411
Average	459	411

Table 17: Charge Time Comparison

$$Charge\ Accuracy = \frac{Average\ Simulation}{Average\ Real-World} * 100 = \frac{411}{459} * 100 = 89.5\% \quad (38)$$

Discharge Cycle Number	Real-World Time (s)	Simulation Time (s)
1	281	279
2	247	250
3	246	250
4	244	250
Average	254.5	262.25

Table 18: Discharge Time Comparison

$$Discharge\ Accuracy = \frac{Average\ Real-World}{Average\ Simulation} * 100 = \frac{254.5}{257.25} * 100 = 98.9\% \quad (39)$$

4.4 Summary

Taking the exact voltage values from this data and calculating the difference between the simulation and real-world test, it was found that the simulation had a margin of error of ±0.21801V.

With the simulation tool proven to be accurate, what makes it a desirable application for designers and engineers is its ability to run simulations for different component types and sizes. The visualization of this software is presented in the appendix of this thesis and will show how a user can modify already existing components or add new models to the system.

5 Conclusions & Future Work

In this thesis, a simulation tool that predicts the lifetime of energy-harvested wireless sensor networks is presented.

WSN nodes consist of multiple nodes populating a particular region, all coordinating with each other. These systems are designed on an ad hoc basis, to sense, collect and process data. The one thing that is constant in these systems, however, is power. With current battery technology, batteries are unable to last long enough to provide power to a WSN node for the application lifetime of the embedded sensor. EH holds the key to sustainable data collection by making batteries outlive the devices they power.

Based on the comparison between a real-world scenario and the simulation data, the software can potentially predict the lifetime of a wireless sensor network with a high degree of accuracy. However, there is a noticeable margin of error in the results. This is likely to be due to a combination of reasons that need further work, but the following should be noted. Firstly, as mentioned, a Bluno V2 board was used to measure the voltage in the “Real-World” test which had a margin of error of ±0.15V. Also, while the resistor was measured to be exactly 32.77 Ω, the capacitance of the supercapacitor was taken from the datasheet as the rated capacitance. Some simplifying assumptions were used for charging such as taking all of the current from the resistor to be entering the supercapacitor when in reality a small percentage will go into the DC-DC converter, acting in quiescent/no load mode. Correspondingly, it is approximated that when the supercapacitor is discharging that all of the source current for the DC-DC converter comes from the supercapacitor. However, over a given cycle these approximations should more or less ‘balance out’ but cause a small net approximation error.

With the implementation of a standardised way of characterising components, this simulation tool provides a much faster method for finding the optimum power setup for a particular application.

For future work, more in-depth analysis of the real-life charging and discharging currents should be undertaken via metrology and closer interaction with the supercapacitor vendor to understand device behaviour particularly in the 4-4.5V charging region. In particular the previously mentioned approximation error assumptions need to be validated and their magnitude assessed. The DC-DC converter will also be in 'no load' rather than quiescent operation so its characteristics in this mode need to be characterised. This should lead to more accurate calculations in future iterations of the model. The way that the software is setup allows for this, as each component has its own separate function, allowing for individual component improvements to the system as a whole.

Another addition to this project could be that this tool be made available online where every component added to the system can be available for everyone to use, increasing the adoption of WSN solutions and giving end users methodology to determine and optimise battery life. A Horizon 2020 project titled EnABLES [64] is currently integrating key European research infrastructures in powering the IoT. One of their goals is to create a standardized way of characterising components so they can become inter-operable. The models of the components in this simulation tool will be available with the software, with the goal of expanding the library of components as the simulation tool gets used.

With all objectives accomplished and providing additional insight into where this project could be enhanced, it can be concluded that this project was successful in creating a modelling and simulation tool for IoT edge devices.

Appendix

The main page of the GUI where all of the different components can be selected is presented in figure 52. This is where the user can select each component and see the results of each simulation.

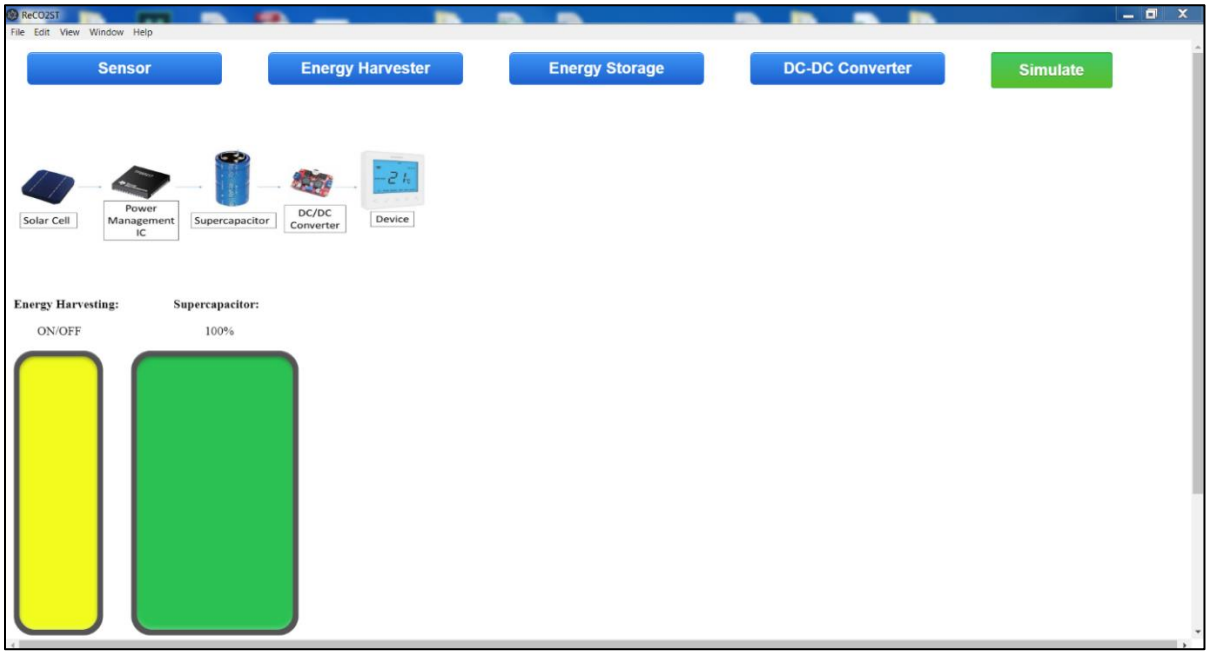


Figure 52: ReCO2ST GUI

The buttons at the top of the page allow the user to navigate to the different sections and select each component. Each button will open a separate window where the user can select and modify each component.

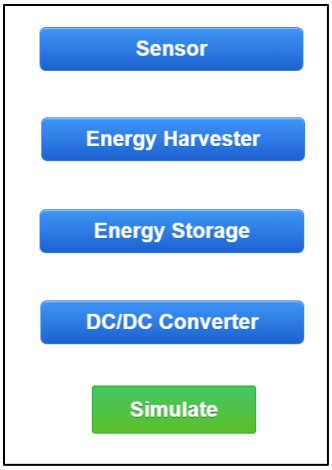


Figure 53: ReCO2ST GUI buttons

Figure 54 shows the requirements for adding a sensor node to the simulation. Once the sensor window opens, the user can select the operating voltage and average operating current of the sensor node being simulated. Once that data is entered, the values are stored until the user is ready to run the simulation.

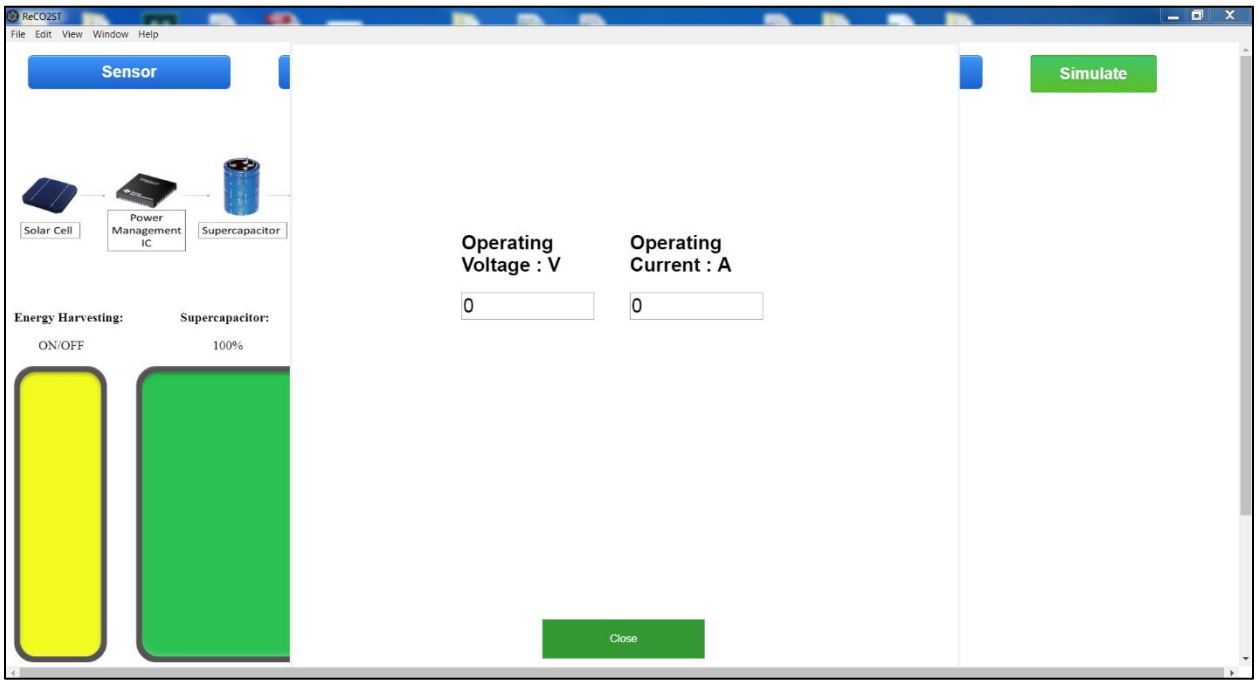


Figure 54: Select Device Load

When selecting the EH, the user has two options, PV or TEG. Once selected, additional dropdown menus open up allowing for further modification to the EH device.

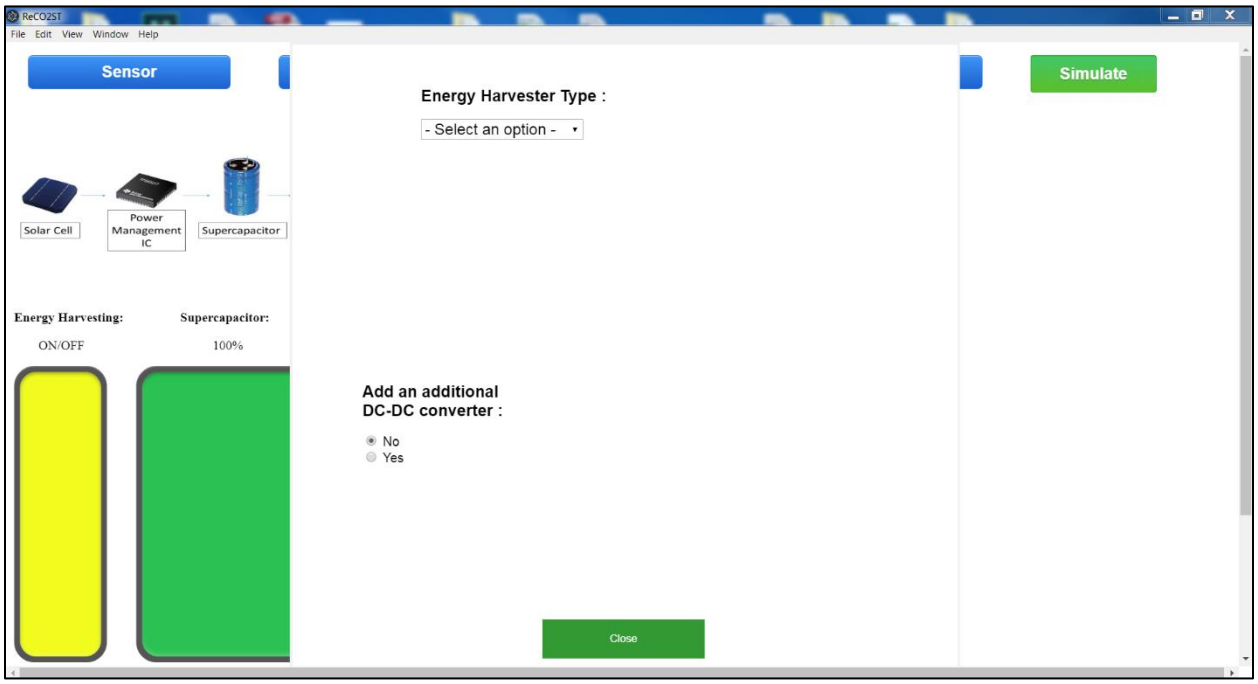


Figure 55: Select Energy Harvesting Device

Figure 56 shows the full data requirements for simulating an EH transducer, as well as the ambient energy available throughout the simulation. The user can select the component model, the size of the component and the ambient light levels. For TEGs the user can select the temperature difference between the two sides.

Also, if the user requires an additional DC-DC converter from the EH transducer to the supercapacitor, it can be selected here.

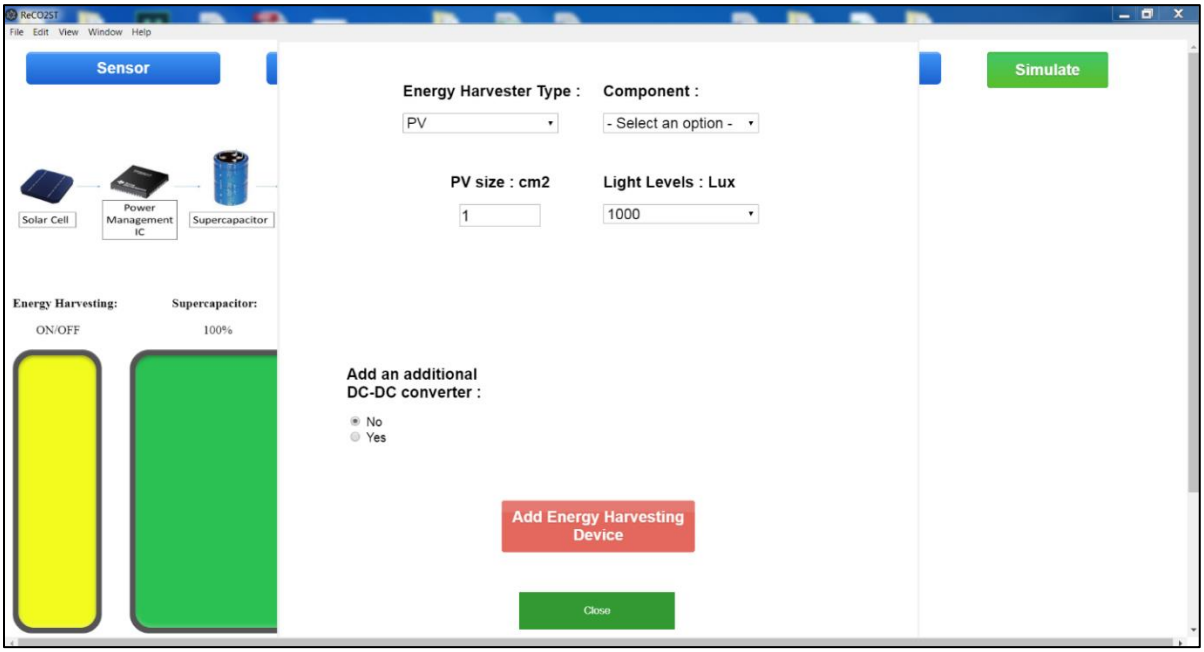


Figure 56: Select Energy Harvesting Conditions

Figure 57 shows the ES section. The user must input all of these values, including which battery is being used in the simulation to power the device. Once the supercapacitor characteristics are chosen, the user must then decide the turn-on voltage and the minimum voltage of the supercapacitor. These values can have a significant effect on the simulation.

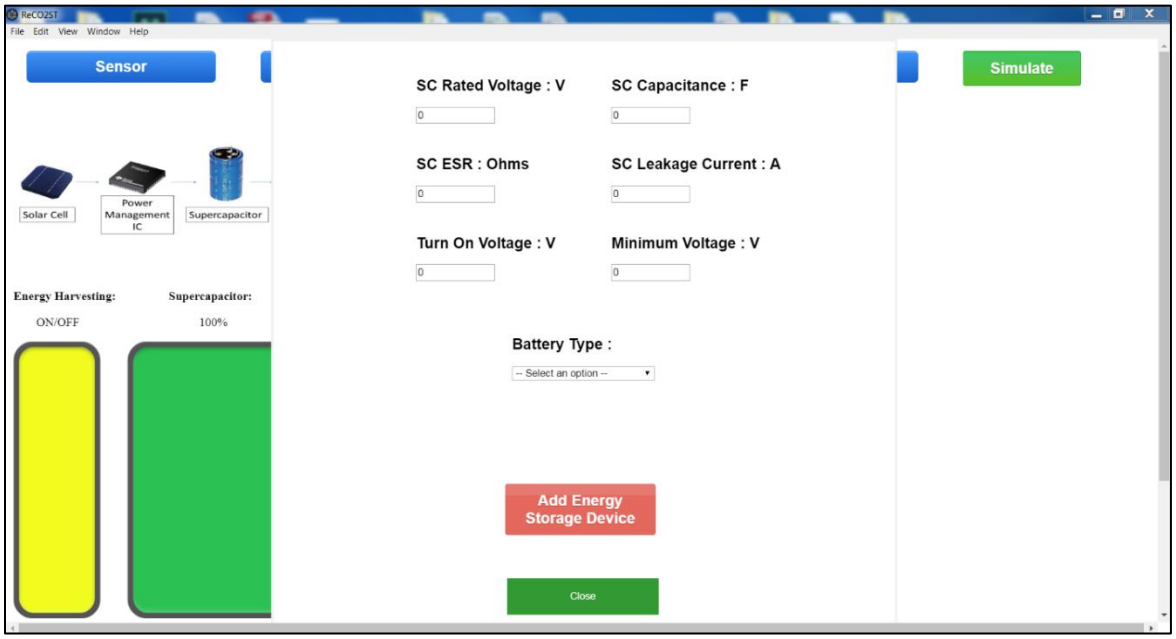


Figure 57: Select Energy Storage Devices

The final section in the GUI is the DC-DC converter. Depending on the operating voltage required by the sensor node, multiple options are available to the user. For this section a drop down menu containing hard-coded models can be selected.

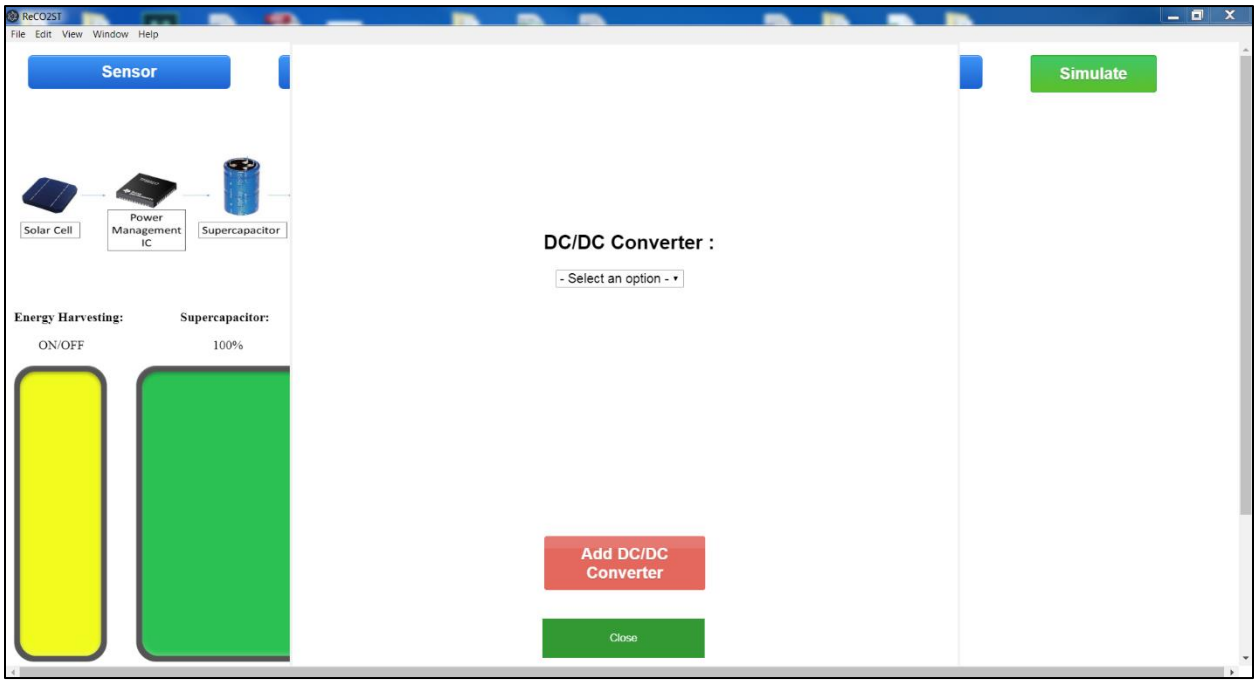


Figure 58: Select DC-DC Converter

For each section, if a user wishes to use a component not listed in the simulation, they must press the “Add a component” button in each section and navigate to the file containing that components data. However, new components must follow the template provided with this software to allow it to be compatible.

Figure 59 shows the user what is happening in the live simulation over 1 week, whether the sensor is receiving power or not, as well as the voltage level in the supercapacitor.

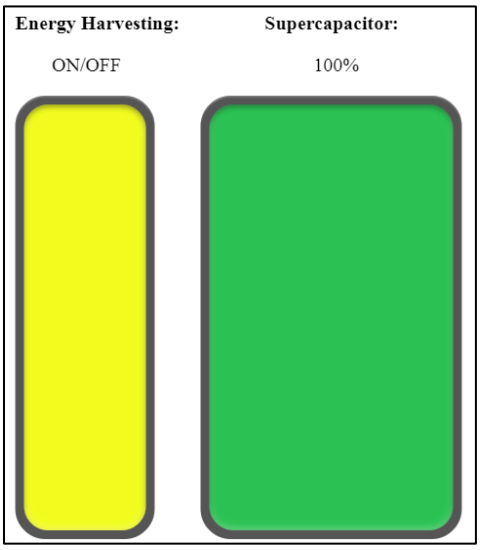


Figure 59: Dynamic Simulation Conditions

Once the simulation is complete, the software calculates and compares the lifetime of the device using solely batteries with the lifetime of the device utilizing EH methods to extend the battery lifetime.

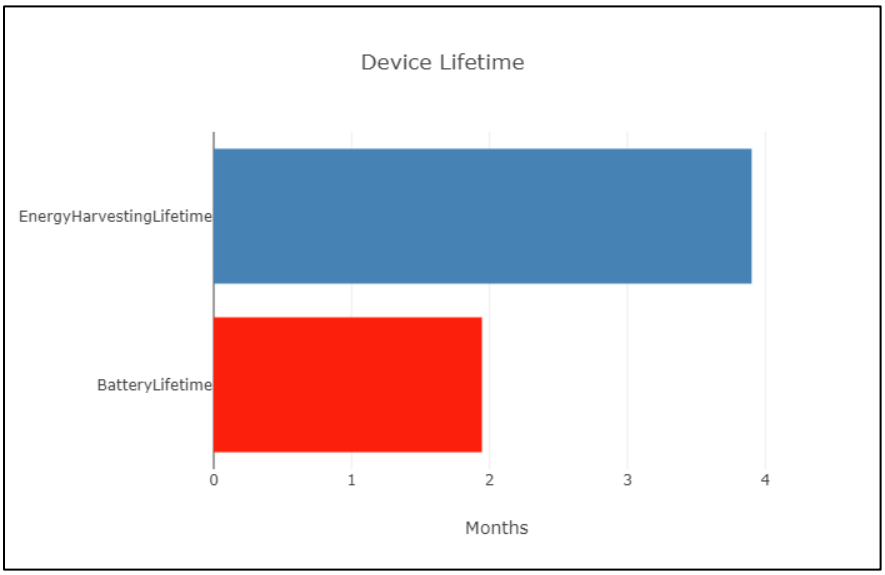


Figure 60: Battery vs. EH Lifetime

Figure 61 and 62 notify the user if the device is being powered by EH or if it is being powered by the battery. As the simulation is running, one of these images will always be shown thereby informing the user when the WSN is receiving power from ambient energies or battery power.

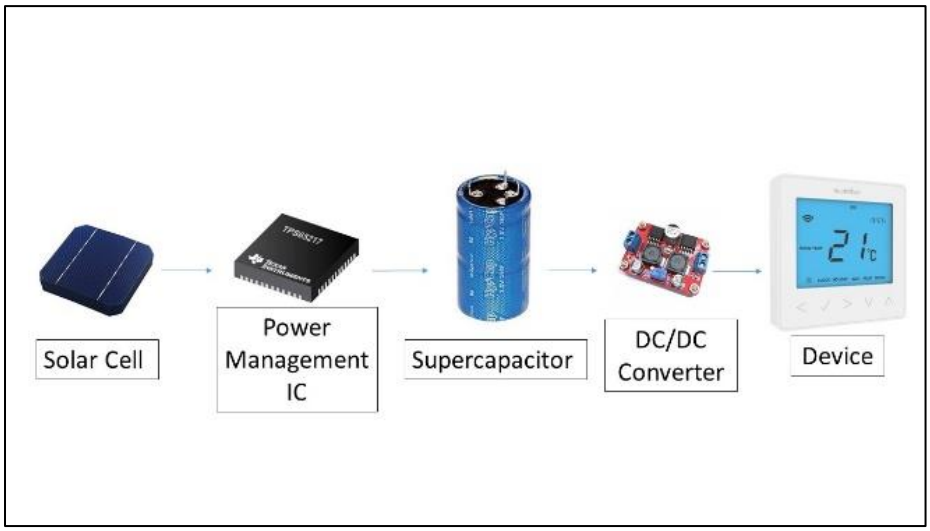


Figure 61: Using EH Indicator

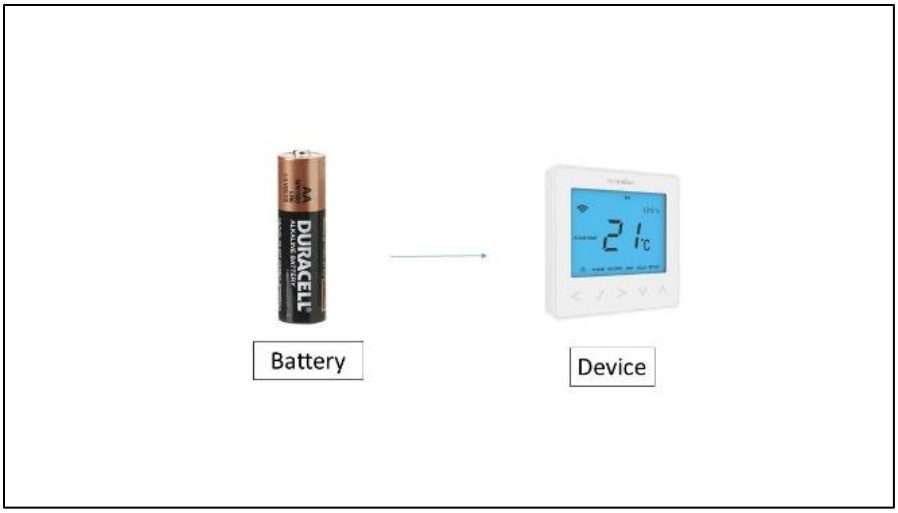


Figure 62: Using Battery Indicator

Figure 63 shows the 1-week simulation in progress. The lifetime comparison, simulation parameters and the 1-week simulation can all be seen. This simulation shows the user the voltage level in the supercapacitor at every hour. The top left image shows the user that the WSN is receiving battery power. The device lifetime is already calculated in the top right of the image. The dynamic graph at the bottom of the image shows the voltage in the supercapacitor over time.



Figure 63: Dynamic Simulation

The dynamic graph is shown so that a user can know when the WSN is dropping below the minimum voltage and can better understand which component needs to be changed in order to optimize the set-up of the WSN.

For more granular detail of the simulation, an additional graph is presented showing the voltage level in the supercapacitor at every second throughout the week, as well as every parameter selected by the user.

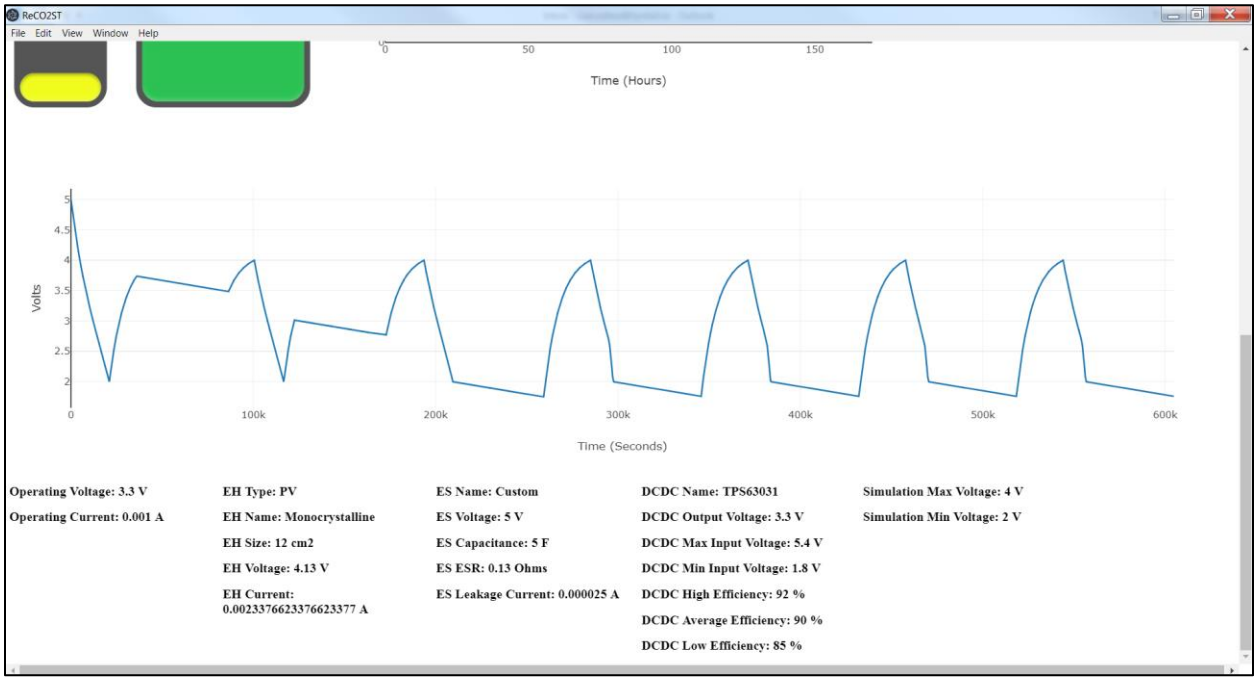


Figure 64: Simulation Results

References

[1] SEAI. *Nearly Zero Energy Building Standard [Online]. Available at:* https://www.seai.ie/sustainable-solutions/nearly-zero-energy-buildi-1/ [Accessed 11th June 2019].

[2] U.S. Department of Energy. *Buildings Energy Data Book*. [Online] 2011. Available from: https://ieer.org/wp/wp-content/uploads/2012/03/DOE-2011-Buildings-Energy-DataBook-BEDB.pdf [Accessed: May 11th 2019].

[3] European Commission. Energy performance of b*uildings*. [Online] 2014. Available from: https://ec.europa.eu/energy/en/topics/energy-efficiency/energy-performance-of-buildings/overview [Accessed: May 11th 2019].

[4] Statista. Internet of Things (IoT) connected devices installed base worldwide from 2015 to 2025 (in billions) [*Online]. Available at:* https://www.statista.com/statistics/471264/iot-number-of-connected-devices-worldwide/ [Accessed 11th June 2019].

[5] EPA. *Sustainable Material Management [Online]. Available at:* https://www.epa.gov/smm [Accessed 5th June 2019].

[6] National Renewable Energy Laboratory. Best Research-Cell Efficiency Chart. [Online]. Available from: https://www.nrel.gov/PV/cell-efficiency.html [Accessed 21st May 2019].

[7] Live Science. How Do Solar Panels Work? [Online]. Available from: https://www.livescience.com/41995-how-do-solar-panels-work.html [Accessed 21st May 2019].

[8] SunLink PV. Crystalline Cells. [Online]. Available from: http://www.sunlinkPV.com/products/PVcell.html [Accessed 26th May 2019].

[9] American Society of Mechanical Engineers. Using Waste Engine Heat in Automobile Engines. [Online]. Available from: https://www.asme.org/topics-resources/content/using-waste-engine-heat-in-automobile-engines [Accessed 26th June 2019].

[10] Makerlab Electronics. Thermoelectric Power Generator TEG Module. [Online]. Available from: https://www.makerlab-electronics.com/product/thermoelectric-power-generator-module-teg-sp1848-27145/ [Accessed 26th May 2019].

[11] Nicholas Gekakis et al. [2015]. Modeling of Supercapacitors as an Energy Buffer for Cyber-Physical Systems. [Online]. Available at: https://www.researchgate.net/publication/265784892_Modeling_of_Supercapacitors_as_an_Energy_Buffer_for_Cyber-Physical_Systems [Accessed 6th June 2019].

[12] Power System Design. Using supercapacitors in energy harvesting [Online]. Available from: https://www.powersystemsdesign.com/articles/using-supercapacitors-in-energy-harvesting/18/11098 [Accessed 28th May 2019].

[13] Singh, S.K.; Paulus, R.; Jaiswal, A.K.; Kumar, M. Analysis of energy model and Performance of IEEE 802.15.4 WSNs under Different Duty Cycle. J. Electron. Commun. Eng. 2014, 9, 48–54.

[14] S. Mahlknecht. Energy-self-sufficient wireless sensor networks for the home and building environment. Master Dissertation, Fakultat fur Elektrotechnik, Technischen Universitat Wien, Vienna, 2004, [Accessed 6th June 2019].

[15] R. Hahn and H. Reichl. Batteries and power supplies for wearable and ubiquitous computing. In Wearable Computers, 1999. Digest of Papers. The Third International Symposium on, pages 168{169. IEEE, 1999.

[16] G. Mao, B. Fidan, and B. Anderson. Wireless sensor network localization techniques. Computer Networks, 51(10):2529{2553, 2007, [Accessed 30th April 2021].

[17] X. Zhao, T. Qian, G. Mei, C. Kwan, R. Zane, C. Walsh, T. Paing, and Z. Popovic. Active health monitoring of an aircraft wing with an embedded piezoelectric sensor/actuator network: part i: Wireless approaches. Smart Materials and Structures, 16(4):1218, 2007, [Accessed 30th April 2021].

[18] A. Bodensohn, R. Falsett, M. Haueis, and M. Pulvermuller. Autonomous sensor systems for car applications. Advanced Microsystems for Automotive Applications 2004, pages 225{232, 2004, [Accessed 30th April 2021].

[19] A. Baggio. Wireless sensor networks in precision agriculture. In ACM Workshop on Real-World Wireless Sensor Networks (REALWSN 2005), Stockholm, Sweden, 2005, [Accessed 30th April 2021].

[20] G. Werner-Allen, P. Swieskowski, and M. Welsh. Motelab: A wireless sensor network test bed. In Proceedings of the 4th international symposium on Information processing in sensor networks, page 68. IEEE Press, 2005, [Accessed 30th April 2021].

[21] K. Lahiri, A. Raghunathan, and S. Dey, “Battery-driven system design: a new frontier in low power design”, in Proc. IEEE International Conference on VLSI Design, pp. 261–267, 2002, [Accessed 30th April 2021].

[22] V. Raghunathan, C. Schurgers, S. Park, and M. Srivastava, “Energy aware wireless micro sensor networks”, IEEE Signal Processing Magazine, vol. 19, issue 2, pp. 40–50, March 2002, [Accessed 30th April 2021].

[23] J. Polastre, J. Hill, and D. Culler, “Versatile low power media access for wireless sensor networks”, Proc. ACM International Conference on Embedded Networked Sensor Systems, pp. 95–107, 2004, [Accessed 30th April 2021].

[24] Prauzek M., Konecny J., Borova M., Janosova K., Hlavica J., Musilek P. Energy Harvesting Sources, Storage Devices and System Topologies for Environmental Wireless Sensor Networks: A Review. Sensors. 2018; 18:2446. Doi: 10.3390/s18082446, [Accessed 30th April 2021].

[25] Ulrich Stutenbaeumer and Belayneh Mesfin. Equivalent model of monocrystalline, polycrystalline and amorphous silicon solar cells. Renewable Energy 18 [Online] 1999; 501-512. Available from: https://www.sciencedirect.com/science/article/pii/S0960148198008131 [Accessed 20th May 2019].

[26] Lahcen El Mentally, Abdelllah Amghar, Hassan Sahsah. [2017]. Comparison between HC, FOCV and TG MPPT algorithms for PV solar systems using buck converter. [Online]. 2017 International Conference on Wireless Technologies, Embedded and Intelligent Systems (WITS). Available at: https://ieeexplore.ieee.org/document/7934609 [Accessed 6th June 2019].

[27] Manel Hlaili and Hfaiedh Mechergui, “Comparison of Different MPPT Algorithms with a Proposed One Using a Power Estimator for Grid Connected PV Systems,” International Journal of Photo energy, vol. 2016, Article ID 1728398, 10 pages, 2016. https://doi.org/10.1155/2016/1728398 [Accessed 17th June 2019].

[28] R. Faranda, S. Leva, V. Maugeri, “MPPT techniques for PV systems: energetic and cost comparison.” Proceedings of IEEE Power and Energy Society General Meeting- Conversion and Delivery of Electrical Energy in the 21st Century, 2008, pp-1-6.

[29] Nedumgatt, J.J.; Jayakrishnan, K.B.; Umashankar, S.; Vijayakumar, D.; Kothari, D.P. Perturb and observe MPPT algorithm for solar PV systems-modeling and simulation. In Proceedings of the 2011 Annual IEEE India Conference, Hyderabad, India, 16–18 December 2011; pp. 1–6.

[30] M. Kamran, M. Mudassar, M. R. Fazal, M. U. Asghar, M. Bilal, and R. Asghar, "Implementation of improved Perturb & Observe MPPT technique with confined search space for a standalone photovoltaic system," Journal of King Saud University - Engineering Sciences, 2018/06/18/ 2018.

[31] V. Raghunathan, S. Ganeriwal, and M. Srivastava. Emerging techniques for long lived wireless sensor networks. Communications Magazine, IEEE, 44(4):108{114, 2006, [Accessed 30th April 2021].

[32] P. Das, Maximum power tracking based open circuit voltage method for PV system, Energy Procedia 90 (2016) 2–13, [Accessed 30th April 2021].

[33] Baimel, D.; Tapuchi, S.; Levron, Y.; Belikov, J. [2019]. Improved Fractional Open Circuit Voltage MPPT Methods for PV Systems. Electronics 2019, 8, 321, [Accessed 30th April 2021].

[34] Esram, T., Chapman, P.: 'Comparison of photovoltaic array maximum power point tracking techniques', IEEE Trans. Energy Convers., 2007, 22, (2), pp. 439–449, [Accessed 30th April 2021].

[35] Hedi Trabelsi, Hafedh Abid "MPPT controllers for PV array panel connected to Grid" 1 18th international conference on Sciences and Techniques of Automatic control & computer engineering - STA'2017, Monastir,Tunisia,December21-23,2017, [Accessed 30th April 2021].

[36] Jawad Ahmad. [2010]. A Fractional Open Circuit Voltage Based Maximum Power Point Tracker for Photovoltaic Arrays. [Online]. 2010 2nd International Conference on Software Technology and Engineering. Available at: https://ieeexplore.ieee.org/document/5608868 [Accessed 10th June 2019].

[37] Greenmatch. 7 Different Types of Solar Panels Explained. Weblog. [Online] Available from: https://www.greenmatch.co.uk/blog/2015/09/types-of-solar-panels [Accessed 19th May 2019].

[38] Tech Target. *Seebeck effect*. [Online]. Available from: https://searchnetworking.techtarget.com/definition/Seebeck-effect [Accessed 3rd April 2019].

[39] Wang, Wensi, Victor Cionca, Ningning Wang, Mike Hayes, Brendan O'Flynn, and Cian O'Mathuna. "Thermoelectric energy harvesting for building energy management wireless sensor networks." International journal of distributed sensor networks 9, no. 6 (2013): 232438, [Accessed 30th April 2021].

[40] J. Gruber and S. Mathis. Efficient Boost Converter for Thermoelectric Energy Harvesting. Industrial Electronics. [Online]. 2017. pp 642-645. Doi: 10.5162/sensor2017/P3.6, [Accessed 30th April 2021].

[41] Analog Devices. Ultralow Voltage Step-Up Converter and Power Manager. LTC3108 datasheet, 2019, [Accessed 30th April 2021].

[42] R.-Y. Kim and J.-S. Lai, "A seamless mode transfer maximum power point tracking controller for thermoelectric generator applications.," IEEE Trans. Power Electron., vol. 23, no. 5, pp. 2310–2318, Sep. 2008, [Accessed 30th April 2021].

[43] L. Chen, D. Cao, H. Yi, and F. Z. Peng. (2008, Jun.). Modeling and power conditioning for thermoelectric generation. In Proc. IEEE Power Electron. Spec. Conf., pp. 1098–1103. [Online]. Available: http://ieeexplore.ieee.org/lpdocs/epic03/wrapper.htm?arnumber=4592076 [Accessed 17th May 2019].

[44] Montecucco, A.; Knox, A.R. Maximum Power Point Tracking Converter Based on the Open-Circuit Voltage Method for Thermoelectric Generators. IEEE Trans. Power Electron. 2015, 30, 828–839, [Accessed 30th April 2021].

[45] Alex S. Weddell et al. [2011]. Accurate Supercapacitor Modeling for Energy Harvesting Wireless Sensor Nodes. *Transactions on circuit and systems – II: Express Briefs* [Online]. Volume 58, Issue 12, Pages 911-915. Available at: https://ieeexplore.ieee.org/document/6093951 [Accessed 13th May 2019].

[46] A.G. Pandolfo and A.F. Hollenkamp. Carbon properties and their role in supercapacitors. Journal of Power Sources, 157(1):11{27, 2006, [Accessed 30th April 2021].

[47] M. Winter and R.J. Brodd. What are batteries, fuel cells, and supercapacitors? ChemInform, 35(50): no {no, 2004, [Accessed 30th April 2021].

[48] P. Sharma and T.S. Bhatti. A review on electrochemical double-layer capacitors. Energy Conversion and Management, 51(12):2901{2912, 2010, [Accessed 30th April 2021].

[49] Anthony Green and Christophe Jehoulet. The Non-battery Battery – The Potential Role of Supercapacitors in Standby Power Applications. BATCON 2002, Florida, USA, April 2002, [Accessed 30th April 2021].

[50] C. Farcas, D. Petreus, I. Ciocan, and N. Palaghita, "Modeling and simulation of supercapacitors," in 15th International Symposium for Design and Technology of Electronics Packages, (SIITME), Sept. 2009, pp. 195 –200, [Accessed 30th April 2021].

[51] W. Wang, "Energy harvesting system design and optimization for wireless sensor networks," Ph.D. dissertation, Univ. College Cork, Cork, Ireland, 2014, [Accessed 30th April 2021].

[52] Elshrkawey, M., Elsherif, S.M., M.E., 2018. An Enhancement Approach for Reducing the Energy Consumption in Wireless Sensor Networks. J. King Saud Univ. Comput. Inf. Sci. 30 (2), 259-267, [Accessed 30th April 2021].

[53] Maman Abdurohman. Improving reliability of wireless sensor network (WSN) using network coding multipath routing. ComTech: Computer, Mathematics and Engineering Applications, 8(3):121–126, 2017, [Accessed 30th April 2021].

[54] Ongaro, F., Saggini, S., Mattavelli, P.: 'Li-ion battery-supercapacitor hybrid storage system for a long lifetime, photovoltaic-based wireless sensor network', IEEE Trans. Power Electron., 2012, 27, (9), pp. 3944–3952, [Accessed 30th April 2021].

[55] Wang, Wensi & Wang, Ningning & Vinco, Alessandro & Siddique, Muhammad & Hayes, Mike & O'Flynn, Brendan & O'Mathuna, Cian. (2013). Super-capacitor and Thin Film Battery Hybrid Energy Storage for Energy Harvesting Applications. Journal of Physics Conference Series. 476. 2105-. 10.1088/1742-6596/476/1/012105 [Accessed 30th April 2021].

[56] Texas Instruments. Ultra-Low-Power DC/DC Converters for Battery-Powered and Energy-Harvesting Applications. SLYT593B, 2016, [Accessed 30th April 2021].

[57] Harsh Sundani, Haoyue Li, Vijay K. Devabhaktuni, Mansoor Alam, & Prabir Bhattacharya "Wireless Sensor Network Simulators A Survey and Comparisons" International Journal Of Computer Networks, Volume (2), Issue (5), pp 249-265, 2011, [Accessed 30th April 2021].

[58] Yunus Emre Yağan, Kadir Vardar, Mehmet Ali Ebeo, "Modeling and Simulation of PV Systems", IOSR Journal of Electrical and Electronics Engineering (IOSR-JEEE) e-ISSN: 2278-1676,p-ISSN: 2320-3331, Volume 13, Issue 2 Ver. III (Mar. – Apr. 2018), PP 01-11, [Accessed 30th April 2021].

[59] A. Korotkov, V. Loboda, A. Feldhoff, and D. Groeneveld, "Simulation of Thermoelectric Generators and Its Results Experimental Verification," Proc. IEEE International Symposium on Signals, Circuits and Systems (ISSCS 2017), 13-14 July 2017, Iasi, Romania, 2017, [Accessed 30th April 2021].

[60] Cericola D, Ruch PW, Kötz R, Novák P, Wokaun A. Simulation of a supercapacitor/Li-ion battery hybrid for pulsed applications. J Power Sources 2010; 195(9):2731–6, [Accessed 30th April 2021].

[61] IERC. RoWBUsT Project Success. [Online]. Available from: http://www.ierc.ie/news/rowbust-project-success/ [Accessed 17th December 2019].

[62] Farnell. Battery Life Calculator & Conversion Formula. [Online]. Available from: https://il.farnell.com/battery-life-calculator?ICID=lp-calc-battery-life-WF1529210 [Accessed 17th December 2019].

[63] Arduino. MKR1000 Battery Life. [Online]. Available from: https://www.arduino.cc/en/Tutorial/MKR1000BatteryLife [Accessed 17th December 2019].

[64] Enables. European Infrastructure Powering the Internet of Things. [Online]. Available from: http://www.enables-project.eu/home/ [Accessed 17th December 2019].

[65] Maxwell. Low-cost high-energy density pc series ultracapacitors. In PC270 series www.maxwell.com/products/ultracapacitors/docs/datasheetpc10-1003996.pdf, 2009 [Accessed 12th August 2019].

[66] Cap-XX. Pc series ultracapacitors. In High Temperature Surface-mount Supercapacitor www.tecategroup.com/ultracapacitors-supercapacitors/, 2010 [Accessed 12th August 2019].

[67] Infinite Power Solutions. Thinergy thin film battery product: Mec202. In www.digikey.com/product-detail/en/MEC202-22P, 2009 [Accessed 13th August 2019].

[68] Energizer. Ca5l li-ion battery. In 1120mAh cell phone battery www.farnell.com/energizer/ca5l, 2010 [Accessed 14th August 2019].

[69] Tadiran battery gmbh. In Tadiran Rechargeable Lithium-Ion Battery For Wireless Sensor Networks TLI series battery, product newsletter: www.sourcetech411.com/2013/07/, 2009 [Accessed 20th August 2019].

[70] S. Sundresh, Wooyoung Kim and G. Agha, "SENS: a sensor, environment and network simulator," *37th Annual Simulation Symposium, 2004. Proceedings.*, 2004, pp. 221-228, doi: 10.1109/SIMSYM.2004.1299486 [Accessed 20th August 2019].

[71] Ngo, Khoa & Huynh, Trong & Huynh, De. (2018). Simulation Wireless Sensor Networks in Castalia. 39-44. 10.1145/3193063.3193066 [Accessed 20th August 2019].

[72] Chen, Gilbert & Branch, Joel & Pflug, Michael & Zhu, Lijuan & Szymanski, Boleslaw. (2006). Sense: A Wireless Sensor Network Simulator. 10.1007/0-387-23466-7_13 [Accessed 25th August 2019].

[73] Institude for Software Intergrated System. Jprowler. Available online: http://www.isis.vanderbilt.edu/Projects/nest/jprowler/ (accessed on 02 December 2019) [Accessed 25th August 2019].

[74] ANYSOLAR. IXOLAR™ High Efficiency SolarMD. https://ixapps.ixys.com/DataSheet/SLMD600H10L_Nov16.pdf [Accessed 25th August 2019].

[75] Panasonic. Amorphous Silicon Solar Cells Amorphous Photosensors. https://panasonic.co.jp/ls/psam/en/products/pdf/Catalog_Amorton_ENG.pdf [Accessed 26th August 2019].

[76] Marlow Industries. Technical Data Sheet for TG12-4. https://cdn2.hubspot.net/hubfs/547732/Data_Sheets/TG12-4.pdf [Accessed 27th August 2019].

[77] Peltier Cooler. Technical Data Sheet for MCPE1-12706AC-S. http://www.farnell.com/datasheets/3178964.pdf [Accessed 27th August 2019].

[78] PowerStor. PHB Supercapacitors Cylindrical pack. https://www.mouser.ie/datasheet/2/87/eaton-phb-supercapacitors-cylindrical-pack-data-sh-1608775.pdf [Accessed 27th August 2019].

[79] DFROBOT. Technical Data Sheet for Bluno SKU: DFR0267. https://media.digikey.com/pdf/Data%20Sheets/DFRobot%20PDFs/DFR0267_Web.pdf [Accessed 27th September 2019].

[80] Texas Instruments. TPS6302x High Efficiency Single Inductor Buck-boost Converter with 4-A Switches. https://www.ti.com/lit/ds/symlink/tps63020.pdf?HQS=dis-mous-null-mousermode-dsf-pf-null-wwe&ts=1619784186090&ref_url=https%253A%252F%252Fwww.mouser.ie%252F [Accessed 28th September 2019].

[81] LoPy4. Technical Data Sheet for LoPy4. http://www.farnell.com/datasheets/2571934.pdf [Accessed 28th September 2019].

[82] Texas Instruments. Technical Data Sheet for TPS63020EVM-487. https://www.ti.com/lit/ug/slvu365/slvu365.pdf?ts=1619784955246&ref_url=https%253A%252F%252Fwww.google.com%252F [Accessed 29th September 2019].